

**A STUDY OF DRYING CHAMBER INTEGRATED WITH SOLAR  
COLLECTOR USING COMPUTATIONAL FLUID DYNAMICS**



**UNIVERSITI TEKNIKAL MALAYSIA MELAKA**

**A STUDY OF DRYING CHAMBER INTEGRATED WITH SOLAR COLLECTOR  
USING COMPUTATIONAL FLUID DYNAMICS**

**WONG SHIN FHUI**



**UNIVERSITI TEKNIKAL MALAYSIA MELAKA**

**2020**

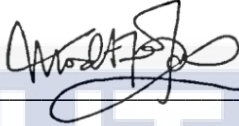
## DECLARATION

I declare that this project report entitled “A study of drying chamber integrated with solar collector using Computational Fluid Dynamics” is the result of my own work except as cited in the references.

 Signature :   
Name : WONG SHIN FHUI  
Date : 26 JUNE 2020   
UNIVERSITI TEKNIKAL MALAYSIA MELAKA

## APPROVAL

I hereby declare that I have read this project and in my opinion this report is sufficient in terms of scope and quality for the award of the degree of Bachelor of Mechanical Engineering.

Signature :   
Supervisor's Name : DR MOHD AFZANIZAM BIN MOHD ROSLI  
Date : 26 JUNE 2020

اونيورسيتي تيكنيكل مليسيا ملاك

UNIVERSITI TEKNIKAL MALAYSIA MELAKA

## DEDICATION

To my beloved mother and father for the endless support.



## ABSTRACT

Drying chamber integrated with solar collector has been introduced as one of the new advanced technologies and environment friendly process for drying agriculture products. To propose a proper drying chamber integrated with solar collector for specific products, uniform distribution of velocity and temperature in the chamber need to be considered. Computational Fluid Dynamics (CFD) Ansys Fluent 16.0 software is used to study and analyse the air flow and temperature distribution pattern within the drying chamber in order to reduce experimental time and avoid high cost. A validation results of a journal studying indirect solar food dryer is carried out using CFD. The validation is done by comparing the data experiment from the study journal with the data obtained from the CFD simulation. The results show that the maximum mean temperature difference on the symmetry plane of solar drier between the CFD Simulation in study journal and CFD validation is found to be 2.3 K. The CFD simulation shows high agreement with the results in study journal which shows that the CFD simulation's setting are correct and acceptable. With the purpose of improve the uniformity of airflow and temperature distribution in the drying chamber integrated with solar collector, three parameters are evaluated in this research which improve the weakness of the solar collector integrated drying chamber in the journal studied. The purpose of this study project is to investigate the performance of velocity and temperature distribution in drying chamber integrated with solar collector using three-dimensional (3D) CFD simulation in transient state condition. It was found that Parameter 3 (b) shows more uniform air flow velocity and temperature distribution with mean velocity 0.08m/s and mean temperature distribution 320.4K as compared to others design.

## ABSTRAK

*Ruang pengering yang disatukan dengan pengumpul suria telah diperkenalkan sebagai salah satu teknologi canggih dan proses mesra alam baru untuk pengeringan produk pertanian. Untuk mengusulkan ruang pengeringan yang tepat yang disatukan dengan pengumpul suria untuk produk tertentu, pengagihan kecepatan dan suhu yang seragam di dalam ruang perlu dipertimbangkan. Perisian Perkomputeran Dinamik Bendalir (CFD) Ansys Fluent 16.0 digunakan untuk mengkaji dan menganalisis aliran udara dan corak taburan suhu di dalam ruang pengeringan untuk mengurangkan masa eksperimen dan mengelakkan kos yang tinggi. Hasil pengesahan jurnal yang mengkaji pengering makanan suria tidak langsung dilakukan menggunakan CFD. Pengesahan dilakukan dengan membandingkan eksperimen data dari jurnal kajian dengan data yang diperoleh dari simulasi CFD. Hasil kajian menunjukkan bahawa perbezaan suhu maksimum pada satah simetri suria kering antara Simulasi CFD dalam jurnal kajian dan pengesahan CFD didapati 2.3 K. Simulasi CFD menunjukkan persetujuan yang tinggi dengan hasil dalam jurnal kajian yang menunjukkan bahawa CFD tetapan simulasi betul dan boleh diterima. Dengan tujuan meningkatkan keseragaman aliran udara dan pengedaran suhu di ruang pengering yang disatukan dengan pemungut suria, tiga parameter dinilai dalam penyelidikan ini yang memperbaiki kelemahan ruang pengering terpadu pengumpul suria dalam jurnal yang dikaji. Tujuan projek kajian ini adalah untuk mengkaji prestasi penyaluran halaju dan suhu di ruang pengeringan yang disatukan dengan pengumpul suria menggunakan simulasi CFD tiga dimensi (3D) dalam keadaan sementara. Didapati bahawa Reka Bentuk 3 (b) menunjukkan halaju aliran udara dan taburan suhu yang lebih seragam dengan halaju min 0.08m / s dan taburan suhu rata-rata 320.4K berbanding dengan reka bentuk yang lain.*

## ACKNOWLEDGEMENTS

First and foremost, I would like to express my great appreciation to all who provided me the chances to complete my final year project and this report. This report which taken 2 semesters does help me to apply my knowledge in thermal fluids field and also trained my project management skill.

Moreover, a deepest gratitude to my final year project's supervisor, Dr. Mohd Afzanizam Bin Mohd Rosli for providing me passion guidance, expertise knowledge and stimulating advices along the project. I have received a lot of helps and encouragement from him whenever I am facing challenges in software simulating and writing report in this project. Dr. Afzanizam also patiently explained all the knowledge which beneficial a lot to me. His patience and organized plan are essential factors that lead to the successful of this project.

I would also like to show my highest appreciation to Dr. Abdul Rafeq bin Saleman and Dr. Mohamad Shukri bin Zakaria as my examiners for all the encouragement, support, and advices upon the completion of this project. Besides that, a special thanks to En. Hairul Nizam Bin Daud, the laboratory assistant of Computer-Aided Engineering Studio for assisting me in using the laboratory. The co-operation provided is highly appreciated. Million thanks to Universiti Teknikal Malaysia Melaka (UTeM) for providing me the chance to have this final year project. Furthermore, I would like to thank all my friends for providing me ideas and suggestions in software simulation in my project.

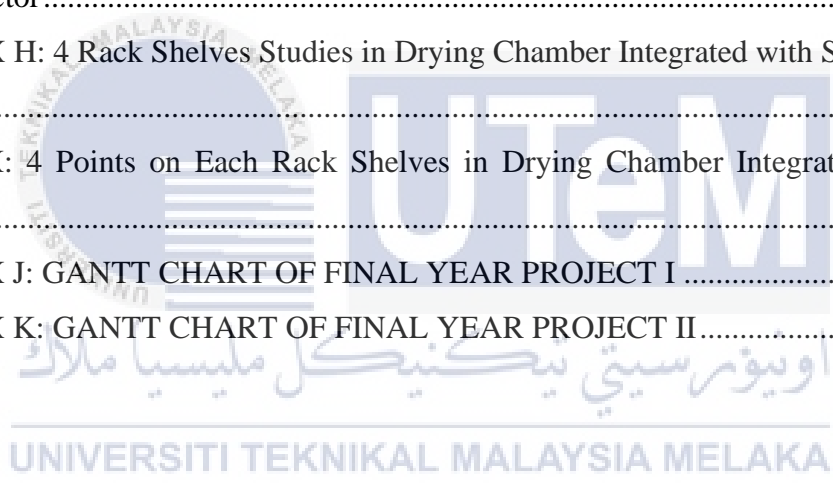
Last but not least, many thanks to my parents' endless gratitude for their sacrifices, encouragement and patience as I have faced all the challenges throughout this project.

## TABLE OF CONTENT

DECLARATION	
APPROVAL	
DEDICATION	
ABSTRACT .....	i
ABSTRAK .....	ii
ACKNOWLEDGEMENTS .....	iii
TABLE OF CONTENT .....	iv
LIST OF TABLES .....	vii
LIST OF FIGURES .....	ix
LIST OF ABBEREVATIONS .....	xiii
LIST OF SYMBOLS.....	xiv
CHAPTER 1 .....	1
INTRODUCTION.....	1
1.1 Background of Study .....	1
1.2 Problem Statement.....	6
1.3 Objectives .....	7
1.4 Scopes of Project .....	7
1.5 General Methodology .....	8
CHAPTER 2.....	10
LITERATURE REVIEW.....	10
2.1 Definition of Drying .....	10
2.2 Heat and Mass Transfer Mode.....	11
2.3 Thermal Emissivity and Radiative Heat Transfer.....	13
2.4 Parameters Affecting Drying Rates .....	16
2.5 Method of Drying .....	18
2.5.1 Traditional Drying (Open Drying).....	20
2.5.2 Industrial Drying (Drying Chamber Integrated with Solar Collector).....	22
2.5.3 Comparison Between the Different Design of Drying Chamber Integrated with Solar Collector .....	25
2.6 Computational Fluid Dynamics .....	30
2.6.1 Benefit of CFD.....	32
2.6.2 Basic Governing Equations for CFD Simulation.....	33

CHAPTER 3.....	34
METHODOLOGY.....	34
3.1 Introduction.....	34
3.2 Literature Review .....	36
3.3 Computational Fluid Dynamics (CFD) Simulation Process.....	36
3.4 Pre-processing of CFD Simulation.....	37
3.4.1 Geometry Creating.....	37
3.4.2 Domain Tags .....	42
3.4.3 Meshing.....	43
3.5 Solver of CFD Simulation .....	45
3.5.1 Properties Materials .....	46
3.5.2 Boundary Conditions .....	46
3.5.3 Turbulence Modelling.....	47
3.5.4 Solution.....	47
3.6 Post-processing of CFD Simulation .....	47
CHAPTER 4.....	48
RESULT ANALYSIS AND DISCUSSION.....	48
4.1 Introduction.....	48
4.2 Results of Convergence Solution.....	48
4.3 CFD Simulation Verification and Validation Results.....	53
4.3.1 CFD Simulation Verification Results .....	53
4.3.2 CFD Simulation Validation Results.....	59
4.4 CFD Modelling on Drying Chamber integrated with Solar Collector.....	61
4.4.1 Modified Design on Solar Collector .....	61
4.4.2 Parameter 1: Different Air Inlet Area .....	62
4.4.3 Parameter 2: Different Gap Size Between Each Rack Shelves.....	66
4.4.4 Parameter 3: Difference Tilt Angle of Solar Collector .....	70
4.5 The Best Configurations of the Trays.....	74
CHAPTER 5.....	75
CONCLUSION AND RECOMMENDATIONS .....	75
5.1 Conclusion .....	75
5.2 Recommendation for Future Work.....	76
REFERENCES .....	77

APPENDIX A: Full 3D Schematic Diagram of Solar Collector Integrated with Solar Collector .....	86
APPENDIX B: Full 3D Schematic Diagram of Solar Collector Integrated with Solar Collector .....	87
APPENDIX C: 3D Drawing of Modified Design on Solar Collector.....	88
APPENDIX D: Parameter considered in Drying Chamber Integrated with Solar Collector at different air inlet area (a), (b), (c).....	89
APPENDIX E: Parameter considered in Drying Chamber Integrated with Solar Collector at different gap size (a), (b), (c).....	90
APPENDIX F: Parameter considered in Drying Chamber Integrated with Solar Collector at Different Solar Collector Angle (a), (b), (c).....	91
APPENDIX G: 8 Points on the Symmetry Plane within Drying Chamber Integrated with Solar Collector.....	92
APPENDIX H: 4 Rack Shelves Studies in Drying Chamber Integrated with Solar Collector .....	93
APPENDIX I: 4 Points on Each Rack Shelves in Drying Chamber Integrated with Solar Collector .....	94
APPENDIX J: GANTT CHART OF FINAL YEAR PROJECT I .....	95
APPENDIX K: GANTT CHART OF FINAL YEAR PROJECT II.....	96



## LIST OF TABLES

TABLE	TITLE	PAGE
2.1	Surface properties involved in radiative heat transfer	15
2.2	Previous study in drying chamber	26
3.1	Geometrical parameters and dimension of solar drier	39
3.2	Geometrical parameters considered in the drying chamber integrated with solar collector	40
3.3	Parameters of grid independence test for drying chamber integrated with solar collector from journal	44
3.4	Mesh sizing parameters	45
3.5	The properties of material used in CFD simulation	46
3.6	Boundary conditions set-up	46
3.7	Run calculation of the drying chamber integrated with solar collector in the simulation	47
4.1	Comparison data results of temperature distributions on four rack shelves between the experiment and CFD modelling from journal and CFD simulation.	59
4.2	Comparison data results of temperature distributions on symmetry plane between the experiment and CFD modelling from journal and CFD simulation.	60
4.3	Temperature distributions on the symmetry plane of the modified enhancement on solar collector	61
4.4	Velocity distributions on four rack shelves of modified design of solar collector	61
4.5	Temperature distributions on parameter 1 at different air inlet area (a), (b), (c)	64

4.6	Velocity distributions on parameter 1 different air inlet area (a), (b), (c)	64
4.7	Temperature Distributions on parameter 2 at different gap size (a), (b), (c)	68
4.8	Velocity Distributions on parameter 2 at different gap size (a), (b), (c)	68
4.9	Temperature Distributions on parameter 3 at different tilt angle of solar collector (a), (b), (c)	72
4.10	Velocity Distributions parameter 3 at different tilt angle of solar collector (a), (b), (c)	72



## LIST OF FIGURES

FIGURE	TITLE	PAGE
1.1	Indirect active solar dryer	3
1.2	Behaviour of any parameter as predicted from a two-fluid transient simulation	5
2.1	Convective drying of a fruit example	12
2.2	The absorption, reflection, and transmission of incident radiation by a semitransparent material	14
2.3	a) Drying curves of apple slices at different air temperatures and velocities of $v=0.6\text{m/s}$ ; b) Drying curves of apple slices at different air temperatures and velocities of $v=1.2\text{m/s}$ ; c) Drying curves of apple slices at different air temperatures and velocities of $v=1.8\text{m/s}$	17
2.4	Method of drying	19
2.5	Open sun drying	21
2.6	Typical solar air collector	22
2.7	a) Contour plot of total velocity distribution flow in solar drying chamber on the symmetry plane; b) Air flow velocity distribution on the four rack shelves in 3D	25
2.8	Solar dryer	26
2.9	Schematic drawing of indirect cabinet model	27
2.10	Assembled biomass stove heat exchanger system	28
2.11	Side-view diagram of dryer	39
3.1	Flow chart of the methodology	35
3.2	Steps in fluid flow (fluent)	36
3.3	Computational flow domain for CFD simulation	37

3.4	Full 3D schematic representation of various components of the solar drier in Ansys software	38
3.5	3D Drawing of modified design on solar collector	38
3.6	(a) Front view of drying chamber integrated with solar collector from journal (b) Front view of modified design on solar collector	39
3.7	Parameter considered at different (a) air inlet area, (b) gap size between each rack shelves, (c) tilting angle of solar collector	41
3.8	Domain Tags and Names Selection of the drying chamber integrated with solar collector from The Journal	42
3.9	Domain Tags and Names Selection of the Enhance Solar Collector	43
3.10	Meshing of drying chamber integrated with solar collector	44
4.1	Convergence Solution for Validation Design in Journal	49
4.2	Convergence Solution for Modified Design of Solar Collector	49
4.3	Convergence Solution for Parameter 1 at Different Air Inlet Area (a), (b), (c)	50
4.4	Convergence Solution of Parameter 2 at Different Gap Size between Rack Shelves (d), (e), (f)	51
4.5	Convergence Solution of Parameter 3 at Different Tilt Angle of Solar Collector Angle (g), (h), (i)	52
4.6	Validated results of contour profile of total velocity distribution on the symmetry plane of the solar dryer	53
4.7	Validated results of contour profile of air flow velocity distribution on the four rack shelves in 3D representation	53
4.8	Comparison of the result of simulation velocity and CFD simulation velocity from the journal and simulation	54
4.9	Validated results of contour profile of temperature distribution on the four rack shelves	55
4.10	Comparison of the result of simulation temperature on four points on each of the rack shelves from the journal and simulation	56
4.11	Validated results of contour profile of temperature distribution on the symmetry plane dividing the two halves of the drying chamber	57

4.12	Comparison of the result of simulation temperature on the symmetry plane of the drying chamber from the journal and simulation	57
4.13	The analysis of streamline by using ANSYS Fluent	58
4.14	Contour Plot of Modified Design of Solar Collector	61
4.15	Contour Plot of temperature distribution on parameter 1 of Drying Chamber Integrated with Solar Collector at different air inlet area (a), (b), (c)	62
4.16	Contour plot of velocity distribution on parameter 1 of drying chamber integrated with solar collector at different air inlet area (a), (b), (c)	63
4.17	Predicted temperature by CFD simulation of parameter 1 against 8 points located on the symmetry plane.	64
4.18	Predicted air velocity by CFD simulation of parameter 1 against the four shelves rack on the symmetry plane	65
4.19	Contour plot of temperature distribution on parameter 2 of drying chamber integrated with solar collector at different gap size (a), (b), (c)	66
4.20	Contour plot of velocity distribution on parameter 2 of drying chamber integrated with solar collector at different gap size (a), (b), (c)	67
4.21	Predicted temperature by CFD simulation of parameter 2 against 8 points located on the symmetry plane.	68
4.22	Predicted air velocity by CFD simulation of parameter 2 against the four shelves rack on the symmetry plane.	69
4.23	Contour Plot of temperature distribution on parameter 3 of Drying Chamber Integrated with Solar Collector at different Angle (a), (b), (c)	70
4.24	Contour Plot of velocity distribution on parameter 3 of Drying Chamber Integrated with Solar Collector at different tilt angle of solar collector (a), (b), (c)	71

4.25	Predicted Temperature by CFD Simulation of parameter 3 against 8 points located on the symmetry plane.	72
4.26	Predicted Air Velocity by CFD Simulation of parameter 3 against the four shelves rack on the symmetry plane.	73
4.27	Propose Design for The Best Performance in Term Uniformity Distribution	74



## LIST OF ABBEREVATIONS

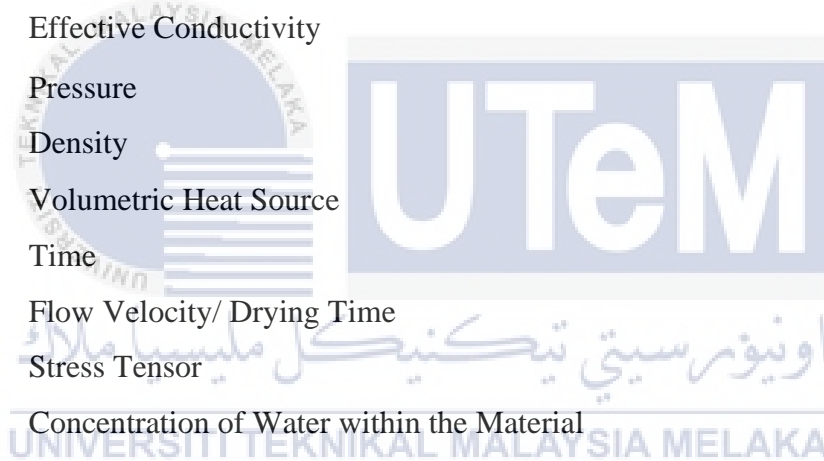
2 D	2-Dimensional
3 D	3-Dimensional
ANSYS	Analysis System
CAD	Computer-Aided Design
CFD	Computational Fluid Dynamics
CFX	Computational Fluid Xerography
ETSC	Evacuated Tube Solar Collectors
LPG	Liquefied Petroleum Gas or Liquid Petroleum Gas
UV	Ultraviolet

اونيورسيتي تيكنيكل مليسيا ملاك

UNIVERSITI TEKNIKAL MALAYSIA MELAKA

## LIST OF SYMBOLS

$C$	Concentration of Water within the Material
$C_p$	Specific Heat Capacity
$D$	Diffusion Coefficient of the Material
$E$	Total Enthalpy
$\vec{F}$	Momentum Sink Term
$g$	Gravity
$k_{eff}$	Effective Conductivity
$p$	Pressure
$\rho$	Density
$S_h$	Volumetric Heat Source
$t$	Time
$v$	Flow Velocity/ Drying Time
$\vec{\tau}$	Stress Tensor
$\rho$	Concentration of Water within the Material



## CHAPTER 1

### INTRODUCTION

#### 1.1 Background of Study

Drying is a widely used process in industrial area to reduce moisture or removing water from a product or material, with a consequent weight reduction by evaporating from the product (Oluwasanmi and Obayopo, 2019; Al-Busoul, M. 2017). There are various sources that can supplied for food drying process, which is fossil fuel, natural gas and solar. Nowadays, due to certain reasons such as speedy exhaustion of natural fuel resources, environmental damages and increasing fossil fuel costs, solar energy is being given much attention in food drying process (Misha et al. 2019 and Demissie et al., 2019). This is because solar energy is abundant available and renewable around the world (Al-Neama et al., 2018). Drying process is important in industrial process in order to preserves the foods for longer period (Al-Busoul, M. 2017 and Al-Neama et al., 2018). It uses to dry various food products, for instance fruits, vegetables, meats, and fishes (Al-Busoul, M. 2017). Free excess water will cause the food materials corrupt if there is no drying process. Therefore, drying process plays an important role to removing the free water from food or agricultural products so as to extend shelf life of food, make them easier for packing, retailing and transport (Iranmanesh et al., 2019).

Open sun drying is considered as a traditional method of drying that had practice widely around the world. Open sun drying dries foods directly under the sun where exposed to the open air without any shielding or cover. This will eventually lead to low hygiene level of the dried product (Iranmanesh et al., 2019). Solar drying also facing some natural

limitation such as rainy weather, winds, moisture and dusts that will fail or interrupting the drying process (Alqadhi et al., 2017) Also, the food products may be contaminated by dust, pollutant, rodents, insects or other animals. Thus, the drying process should be done in closed systems which provided shielding and covers to the food products, in order to maintain its best quality and hygiene (Al-Neama et al., 2018). In the early 1980s, high power, electrical dryers were introduced to the market (Gavelin, 1982). The purpose of drying chamber is to supply the heat to foods by convection and conduction from the surrounding air more than that available under ambient conditions at temperatures above the foods, or conduction from heated surfaces in contact with the foods in a closed system (Aissa et al., 2014). Electrical drying chamber has brought a lot of advantages to industry instead of using open sun drying process as it can cover the food from being polluted during the drying process. However, various electrical drying chamber in the industries also have some limitations such as those drying systems in the market require the use of electricity to motorize fan or pump in the drying chamber. Thus, it will increase the consumption of energy and also increase the cost on electricity. Nowadays, the device of drying chamber integrated with solar collector has been designed to conquer the disadvantage of traditional open sun drying and also the electrical drying chamber.

Drying chamber integrated with solar collector is a device that absorbs the incoming solar radiation, converts it into heat and transfer the heat to fluid such as air, water or oil flowing through the solar collector (Kalagirou, 2014). There are many advantages of using drying chamber integrated with solar collector such as fastening the drying speed due to the possibility of continuous batch operation (Abdullah et al.2020 and Dina et al.2015). As the food is in a separate and covered chamber, foods can be protected from animals, insects, and insect larvae. Thus, it has better dried product quality and hygiene due to controlled drying environment (Sotocinal, 1992). In addition, the food is not subject to direct radiation that can

be harmful to some foods, particularly those that are UV-sensitive. The low capital and utility costs make solar drying attractive in poorer countries (Kerr, 2013). Besides that, drying chamber integrated with solar collector was operated in two drying modes, which is daytime and night time. In the daytime, the foods are dried inside the drying chamber by using hot air flow from the solar collector. At the same time, the solar collector is heated using direct solar energy in order to store the heat and release the moisture. Whereas at the night time, the solar collector is placed inside the drying chamber along with foods and the drying chamber was isolated from the ambient air. Thus, the drying process will be continued, although the temperature is relatively low. The meaning of continuous term here is that during sunshine hours and off-sunshine hours which is rainy day and also night time, the drying process is uninterrupted (Dina et al., 2015).

The main components in the solar collector integrated drying chamber including solar flat plat air collector, drying chamber, drying trays, centrifugal type blower, chimney, inlet, and outlet as shown in Figure 1.1.

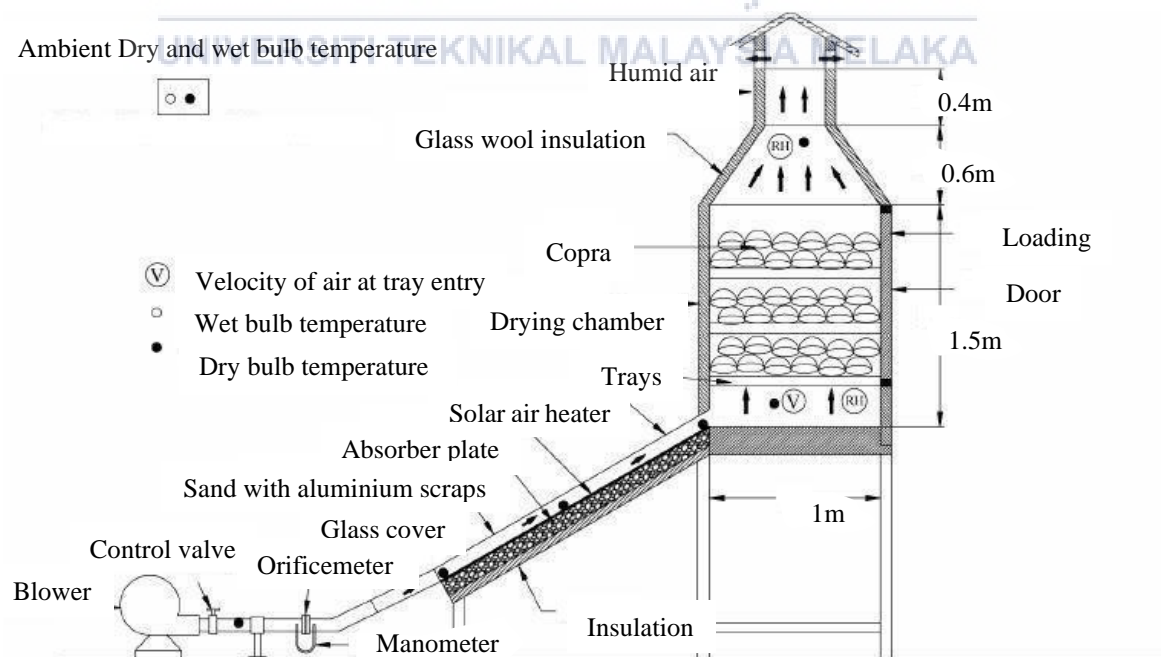


Figure 1.1 Indirect active solar dryer (Al-Neama and Farkas 2018).

In solar dryers, the radiant energy from sun penetrates on a glass cover and is collected on flat plate air collector, which heats air moving pass through it as shown in Figure 1.1. Air moves in by natural convection or may force in by blower or powered fan. (Kerr, 2013). When heat is added, the drying rate will increases based on the selected air velocity and drying temperature (Jayas and Sohkansanj, 1989). The function of a chimney is used to control the residency period of drying air in the drying chamber, increase overall efficiency of the dryer and maintain the optimum temperature inside the chamber with a better circulation of air. This component in drying chamber can prevent the excessive increase of temperature inside the chamber and adverse effects on the quality of the dried product (Aissa et al., 2014). Generally, the drying rate for solar collector drying chamber will be faster than direct sun drying (Kerr, 2013).

However, there are some problems that may encounter by using drying chamber, the problems are over drying and quick drying of food. Over drying on food will cause increase in energy value or cost. Fast drying will prevent the chemical processes started throughout the fermentation to be completed and thus reduces the dry matter of food (Arinze et al., 1996; Ndukwu, 2009). Therefore, correct prediction of the drying time is incredibly vital. Drying rate and drying consistent have the strong relationship with the drying temperature and air velocity. This is incredibly vital as these are the factors that lead to the good drying rate process (Ndukwu, 2009).

Computational fluid dynamics (CFD) is known as a of fluid mechanics that use numerical analysis and algorithm to solve and analyze the problem that involve fluid flows. CFD provides a qualitative and sometimes even quantitative prediction of fluid flows by means of mathematical modeling, numerical methods and also software tools (Ambesange and Kusekar, 2017). Recently, it has been used in multitudes of food drying applications, because of its promising design and modeling tool as a substitute to pricey experimental

trials. The technique is successfully utilizing in predicting distribution of air flow and temperature distribution within drying chambers. It is also used to predict drying uniformity of a new design of the commercial tray dryer for agricultural products by analyzing temperature and velocity distribution. The usefulness of CFD for performance assessment of food processing applications is highlighted by predicting the air velocity field for drying chamber (Demissie et al., 2018).

The CFD simulations consist two method either steady or transient state as shown in Figure 1.2. From an initial condition, the simulation goes through an early stage which is transient state, and finally reaches the steady state regime. Owing to the fact of flow instabilities, the risers cannot consider in the real steady state conditions (Christian and Fernando, 2009).

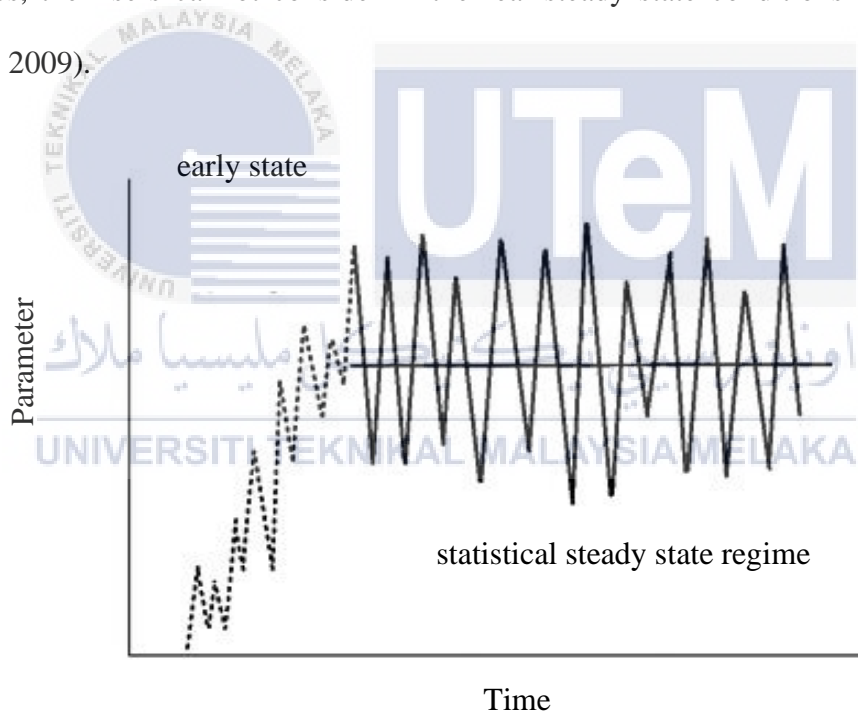


Figure 1.2: Behaviour of any parameter as predicted from a two-fluid transient simulation (Christian and Fernando, 2009)

The transient state is basically between the beginning of the event and the steady state. It refers to a process, which variables are changing in a particular time period. Basically, the transient period is a processed duration which shows unstable changes in variable, which also known as unsteady state (Chegg.com, 2009). However, steady state is the state that

established after a certain time in the system. It computes the fully developed solution that does not change in time. This study will be focused on the pattern of the air stream in the dryer (Cyprien, 2013). In this project, the transient heat transfer phenomenon within a solar collector integrated drying chamber was simulated and the flow of the drying air was two-dimensional axisymmetric fluid domain.

## 1.2 Problem Statement

Traditional method of direct sun exposing food drying have been used widely around the world since ancient times to dry plants, seeds, fruit, fish, wood, and other agricultural products for the purpose of longer preservation. It is simple to operate and has low labor cost. However, this method has numerous shortcomings such as products spoiling due to climate variation and cannot conduct during night time. The drying process is restricted based on the rainy weather, winds and moistures. High relative humidity and cloudy periods will result in slow drying rate and increase the growth of bacteria and fungi. Besides, possibility of product damage can occur due to contamination by pollutant, dirt, dust and eaten by birds, animals, insect, etc. Therefore, the drying process should develop in closed systems to ensure more hygiene of the products. However, various drying chamber in the industries also have some limitations such as those drying systems in the market require the use of electrical to motorize fan or pump in the drying chamber. Thus, it will increase the consumption of energy and also increase the cost on electricity. Today, the design of drying chamber integrated with solar collector has been use in the industry area as it has the greater energy efficiency, good yields even with less sunlight and diffuse light. However, the geometry and arrangement of tray in the drying chamber integrated with solar collector will also affect the rate of drying. Factors such as the inlet area, gap size between rack shelves as well as the tilt angle of solar collector will affect the uniformity of air flow in the drying chamber integrated with solar collector. Simulation of the system using Computational Fluid

Dynamics (CFD) software will be used to predict the best condition of air flow, temperature and velocity distribution through the drying chamber integrated with solar collector. Simulation of the system using Computational Fluid Dynamics (CFD) software is used in the research instead of developing a drying chamber model experiment. This is because it is costly to create a prototypes and physical test. Moreover, the measurement of drying parameters in the drying chamber integrated with solar collector is difficult as a lot of sensors and data loggers have to installed in many positions. It will lead to time consuming, especially in a large-scale dryer. Therefore, CFD software is the best option in this research.

### 1.3 Objectives

The objectives of this project are as follows:

- i To propose a design of drying chamber integrated solar collector.
- ii To investigate the temperature and velocity distribution uniformity in the drying chamber integrated solar collector using Computational Fluid Dynamics (CFD) simulation.
- iii To investigate the temperature and velocity distribution on each level of shelf trays within the drying chamber.

### 1.4 Scopes of Project

The scopes of this project are:

- i Verification and validation results of existing solar collector drying chamber from publish journal.
- ii Computational Fluid Dynamics (CFD) simulation will be carried out by using ANSYS Fluid Flow Fluent 16.0.

- iii The parameters consideration of the drying chamber integrated with solar collector focus on the inlet area, gap size between trays as well as the tilt angle of solar collector.
- iv Simulation is in transient state condition and the geometries of drying chamber integrated solar collector in the form of 3D.

## 1.5 General Methodology

The actions that need to be carried out to achieve the objectives in this project are listed below.

### 1. Introduction

Start the project planning and study the background of the project. Discuss the topic with supervisor to get more understanding on the topic.

### 2. Literature review

Searching related journals, articles, or any materials regarding the project and will be reviewed in the report.

### 3. Model Geometry Design in 2D/ 3D

The geometry of solar collector drying chamber sketched in the form of 3D.

### 4. Apply Boundary/ Fluid Conditions

The boundary condition of inlet and outlet of dryer are studied.

### 5. CFD Simulation

Simulation of the computational Fluid Dynamics (CFD) will be conducted to predict the temperature and velocity distribution in the drying chamber

### 6. Validation and Analysis

Validation on the results of journal will be carried out. Analysis will be presented on the optimization of solar collector dryer by predicting the

airflow distribution, temperature, and velocity profiles throughout the dryer.

After that, the comparison of CFD results with experimental results will be done.

7. Improve the existing design of the dryer

Consider different parameter to improve the existing dryer to enhance drying ability. The boundary condition of inlet and outlet of dryer are applied in the CFD simulation.

8. Optimization Design of the dryer

Validate the redesign drying chamber integrated with solar collector. The simulation will be carried out by using ANSYS CFD simulation. Simulation of the computational Fluid Dynamics (CFD) will be conducted to predict the temperature and velocity distribution in the drying chamber.

9. Report writing

A report consisting discussion and conclusion on this study will be written at the end of the project.

## CHAPTER 2

### LITERATURE REVIEW

#### 2.1 Definition of Drying

Drying or dehydration of materials is defined as the process of removing water or moisture content by evaporating it from the interior of the material to the surface. The purpose of this process is to obtain dry effect on the object (Ambesange & Kusekar, 2017, Sabarez and Food, 2016). In drying process, the latent heat of vaporization will be supplied to increase vapor pressure over the product. In this process, airflow is an important element that required to remove vapor away from the product (Mat, Sohif, et al., 2018).

Drying is one of the major preservation methods which has been widely utilized in the world since ancient time (Al-Busoul, M., 2017). It is one of the oldest techniques utilized by humankind to reduce the water content inside the food stuffs with the purpose of prevent microbial growth. It will help to improve the shelf life of the product and longer storage period, encourage in reduces wastes and cost of transportation to dispose spoiled foods (Zoukit et al.,2008).

The large demands of the drying industry have pushed constantly the development of new technologies and equipment which related to drying process. In the last decades, considerable efforts have been devoted to understanding the changes that occur in the drying operations, aiming to develop different ways to prevent undesirable quality losses of the drying products. Those efforts on researching better drying process not only benefiting food industry area, but on the contrary, it expands to industries such as bio-chemical, pharmaceutical and agricultural sectors (Miguel et al., 2018).

### **Short summary:**

Drying is a process of removing water content in an object. It is a major preservation method which has been utilized in the world since ancient time which can help to improve the product's shelf life and storage durability. A lot of effort on researching the new technologies of better drying process has not only beneficially food industry area but also bio-chemical, pharmaceutical, and agricultural sectors.

## **2.2 Heat and Mass Transfer Mode**

Drying method can be classified into 4 different types based on the type of energy used for the drying process, they are radiation, conduction, convection, and excitation. The most direct drying method is radiation, which uses infrared energy, such as sunlight, to heat the material. Vacuum dryer and direct solar dryers are example of drying through radiation. Secondly, the most used drying method, which is convection, transfer heat through warm air to the material and moisture inside the product will be evaporated. Thirdly, drying through conduction utilized the heated surface to conduct heat to the material and induce evaporation of the moisture. The fourth drying method, excitation drying method heat the material through polarized molecules to absorb the energy (Samantha, 2016). Excitation can be utilized to quickly dry liquids, pastes or milled material and maintaining the material quality (Cano and Barta, 2006).

Comparing to direct solar drying method, indirect solar drying method uses convective drying method to dry the materials. The heated and low moisture air is used to transfer heat to the material and evaporation happens at the surface of the material (Belessiotis and Delyannis, 2011; Cano and Barta, 2006). After that, the moisture in the material diffuse to the surface as the material continuing to dry. Figure 2.1 illustrate the

process of convective drying of a fruit example. Solid arrow in Figure 2.1 indicate heat transfer and dotted arrow indicate mass transfer.

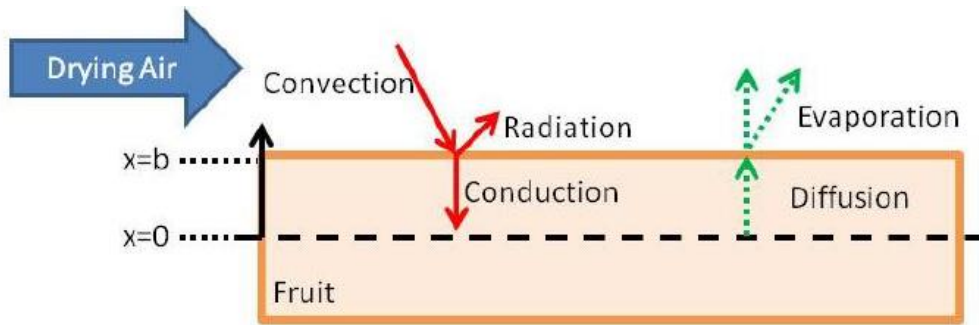


Figure 2.1: Convective drying of a fruit example (Samantha, 2016).

The interaction between heat-and-mass transfer in the drying material and the transfer to the drying air flow are important factors to be consider in a complete drying process (Lamnatou, 2009). Many researches developed the drying kinetics of different types of food are developed in order to predict the drying curves for food material. These models focus on falling drying rate period where the diffusion of moisture in the material is the governing process instead of the constant rate period where moisture evaporation at the surface is driving the system (Samantha, 2016).

Mass transfer operation of drying involving the removal of water from a material by evaporation (Zoukit et al., 2018). Water or moisture is expected to diffuse through the surface of the material and evaporate. One of the most common utilized models in the study of mass transfer mode is Fick's Second Law of Diffusion. Equation (2.1) express the model, it considered concentration of water within the material and diffusion coefficient of the material.

$$\frac{\partial C}{\partial t} = D \left( \frac{\partial^2 C}{\partial x^2} \right) \quad (2.1)$$

where,

$C$  = concentration of water within the material;

$D$  = diffusion coefficient of the material

The diffusion coefficient of the material typically determines by empirical method and it normally not constant as dependent on temperature and moisture content. Many theoretical models had been developed based on Fick's Second Law of Diffusion (Karim, 2005; Dissa et al., 2008; Yesilata and Aktacir, 2009). Those models adapting the shrinkage of the material into consideration in their model.

Drying methods that involving heat transfer mode are radiation, conduction and convection which are transferring heat from a medium, either vacuum, air or through any contacted surface to the material and realize the evaporation of moisture in drying material. Heat transfer within the material can be similarly based on Fourier's Law (Bergman, 2011). Models often assume the food material is in thermodynamic equilibrium with the drying air. Due to it reaches equilibrium much faster than the moisture part of the model, this assumption is often true and was confirmed through preliminary modeling (Samantha, 2016).

**Short summary:**

Drying methods that involving heat transfer mode are radiation, conduction and convection which are transferring heat from a medium. Besides that, mass transfer operation of drying is involving diffusion and the removal of water from a material by evaporation.

### **2.3 Thermal Emissivity and Radiative Heat Transfer**

Radiative heat transfer is difference from thermal conduction and convection. Radiative heat transfer requires no medium to transfer heat as it can be travel easily through a vacuum (Gedeon, M, 2018). Everything around us are keep emits radiation all the time, everything is frequently exposed by radiation from multi-direction over a range of wavelength. Radiation flux incident on a surface or body is called irradiation and denoted by  $G$  (Cengel, Y.A, 1998). Figure 2.2 shows the absorption, reflection, and transmission of an incident radiation by a semitransparent material. Once a radiation strikes over a surface,

some of the radiation is absorbed, some of it is reflected and the remaining part is transmitted through the material.

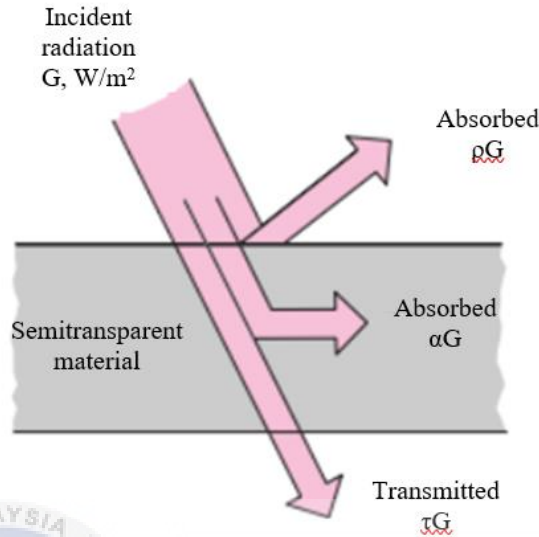


Figure 2.2: The absorption, reflection, and transmission of incident radiation by a semitransparent material (Cengel, Y.A, 1998)

The absorptivity, reflectivity and transmissivity formula are shown in Eq (2.2), Eq (2.3) and Eq (2.4) below. Absorptivity,  $\alpha$  is define as the fraction of irradiation absorbed by a surface, reflectivity,  $\rho$  is the fraction reflected by a surface, last, transmissivity,  $\tau$  is the fraction transmitted by a surface (Cengel, Y.A, 1998).

Absorptivity: 
$$\alpha = \frac{\text{Absorbed radiation}}{\text{Incident radiation}} = \frac{G_{abs}}{G}, 0 \leq \alpha \leq 1 \quad (2.2)$$

Reflectivity: 
$$\rho = \frac{\text{Reflected radiation}}{\text{Incident radiation}} = \frac{G_{ref}}{G}, 0 \leq \rho \leq 1 \quad (2.3)$$

Transmissivity: 
$$\tau = \frac{\text{Transmitted radiation}}{\text{Incident radiation}} = \frac{G_{tr}}{G}, 0 \leq \tau \leq 1 \quad (2.4)$$

Where,

$G$  = The radiation of energy incident on the surface

$G_{abs}$  = Absorbed portions of radiation energy

$G_{ref}$  = Reflected portions of radiation energy

$G_{tr}$  = Transmitted portions of radiation energy

According to the First Law of Thermodynamics, Rudolf Clausius states that heat is a form of energy that cannot be created nor destroyed. However, energy can only be transferred from one point to another or transformed from one form to another (Lucas, J, 2015). Therefore, the sum of the absorbed, reflected, and transmitted radiation energy must be equal to incident radiation (Cengel, Y.A, 1998) as shown in Eq (2.5) below.

$$G_{abs} + G_{ref} + G_{tr} = G \quad (2.5)$$

Dividing each term of this relation by G yields to Eq (2.6)

$$\alpha + \rho + \tau = 1 \quad (2.6)$$

For opaque surface,  $\tau$  will be equal to 0, this will yield to Eq (2.7)

$$\alpha + \rho = 1 \quad (2.7)$$

Table 2.1 shows the properties of surface which involved in radiative heat transfer. Each of the parameters in table below is a number from ranges from 0 to 1. A blackbody is a hypothetical perfect absorption of all radiation that strike on it, with no reflecting power. (Gedeon, M, 2018). It has exactly zero reflectivity and transmissivity for all wavelengths, absorptivity is 1 at all wavelength and total emissivity is also 1.

UNIVERSITI TEKNIKAL MALAYSIA MELAKA

Table 2.1: Surface Properties Involved in Radiative Heat Transfer. (Gedeon, M, 2018).

	Absorptivity ( $\alpha_\lambda$ )	Reflectivity ( $\rho_\lambda$ )	Transmissivity ( $\tau_\lambda$ )	Emissivity ( $\epsilon_\lambda$ )
Perfect Absorption	1	0	0	0-1
Perfect Reflection	0	1	0	0-1
Perfect Transparency	0	0	1	0-1
Black Body	1 (at all $\lambda$ )	0 (at all $\lambda$ )	0 (at all $\lambda$ )	1 (total)
Gray Body	0-1	0-1	0-1	0-1 (same for all $\lambda$ )

### Short summary:

Blackbody is perfect absorption body with no reflecting power. It has precisely 0 reflectivity and transmissivity at all wavelengths, 1 absorptivity at all wavelength. For blackbody,  $\tau$  and  $\rho$  will be equal to 0, therefore  $\alpha$  will be equal to 1.

## 2.4 Parameters Affecting Drying Rates

Drying essentially contains of two basic and simultaneous processes. The two fundamental and simultaneous process is heat transfer and mass transfer. The heat transferred through liquid and liquid evaporate, and mass is transferred as a vapor or liquid from the surface of product (Chabane et al., 2019). A good drying process should take into several consideration as shown in the list below.

### a. Temperature

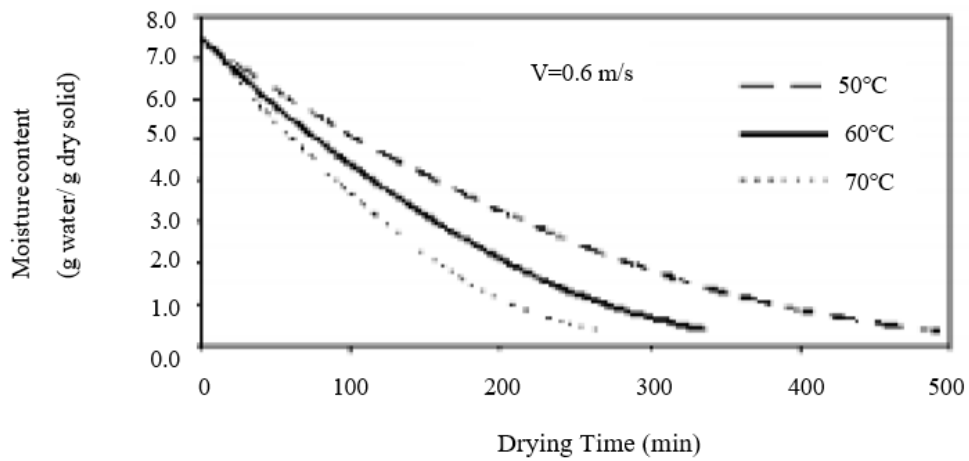
Caparanga (2017) has conducted a study to evaluate the drying kinetics of starch from arrowroot effects from air temperature and velocity. From the experiment conduct, Caparanga state that, at higher temperatures, the drying time for the samples to dehydrate were shorter. (Caparanga, A. R et al., 2017).

### b. Air Velocity

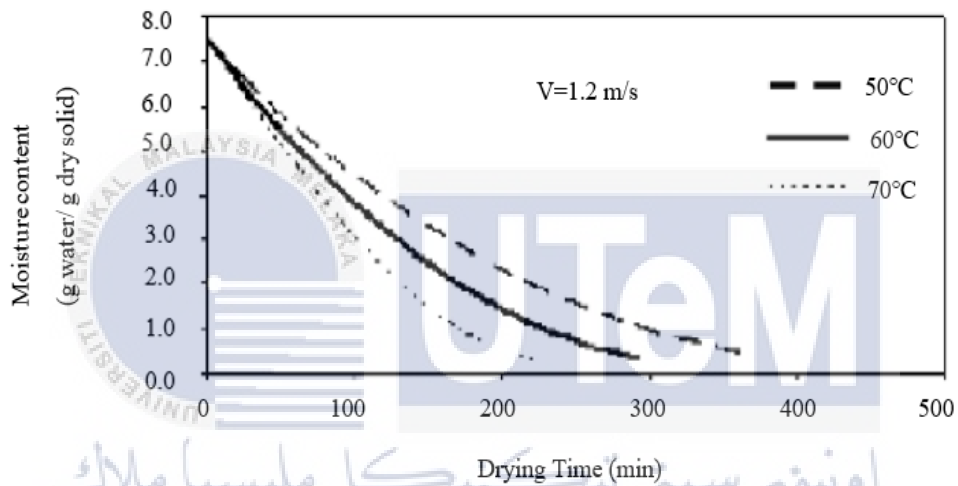
Air velocity is one of the parameters that affect the drying rates (Caparanga, A. R et al., 2017; Sotocinal, 1992). However, it has only little or insignificant effect to the drying time and drying rate (Caparanga, A. R et al., 2017).

### c. Relative Humidity

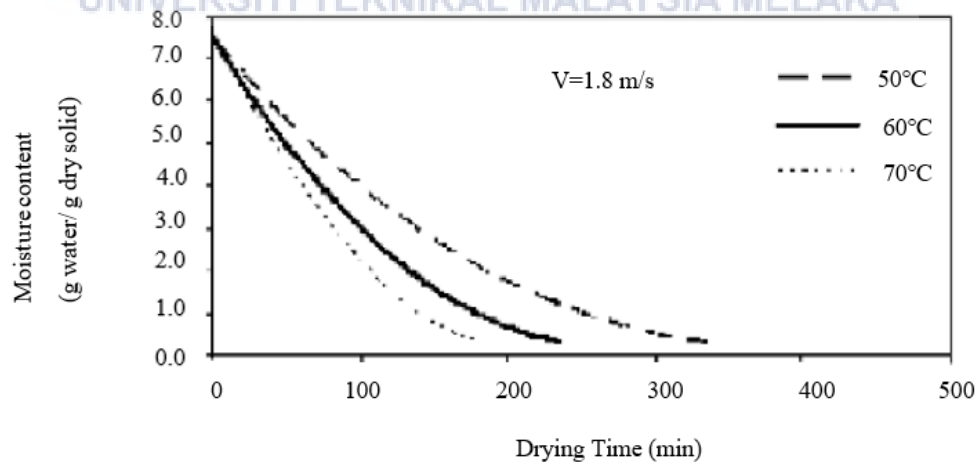
Relative humidity is one of the important things which should be take into consideration which will be affect the drying rates (Sotocinal, 1992; Seiedlou, S, 2010). Seiedlou, S (2010) has conducted a research on the mathematical modeling and determination quality parameter on convective drying of apple. From the experiment conducted, the graft of moisture content against drying time with different air temperatures and velocities were plot as shown in Figure 2.3 (Seiedlou, S, 2010). It can be clearly seen that the drying time of the product will be decrease when the air velocity increase. Besides that, the moisture content in the food product will decrease faster with the increase of drying temperature.



(a)  $v=0.6$  m/s



(b)  $v=1.2$  m/s



(c)  $v=1.8$  m/s

Figure 2.3: Drying curves of apple slices at different air temperatures and velocities (a), (b), (c) (Seiedlou, S, 2010).

### **Short summary:**

There are several parameters that will affecting the drying rates of a product which is temperature, air velocity and relative humidity. The drying time of a product will decrease when air velocity increase. Moreover, the moisture content in the food will also decrease with the increase of drying temperature.

## **2.5 Method of Drying**

There are different types of method of drying using the solar energy. Solar dryer systems can be categorized into two, which is direct and indirect dryers. Direct dryers mean the product or material to be dried absorb the radiated solar directly, meanwhile in indirect dryers, air is heated by solar radiation which then flows through the space containing the product. Meanwhile, a separate solar collector is installed in indirect solar dryers to absorbs solar radiation, converts it into thermal energy and heating up the flowing air that supplies into the chamber. (Tarigan, 2018, p. 149).

Direct dryers which has simpler and more direct procedures, such as exposing the products or materials under the sun, is widely utilized in traditional drying. Meanwhile for indirect solar dryers are mostly utilized in industries drying as required higher level of research and development of equipment. Some general methods of drying are shown in Figure 2.4 below.

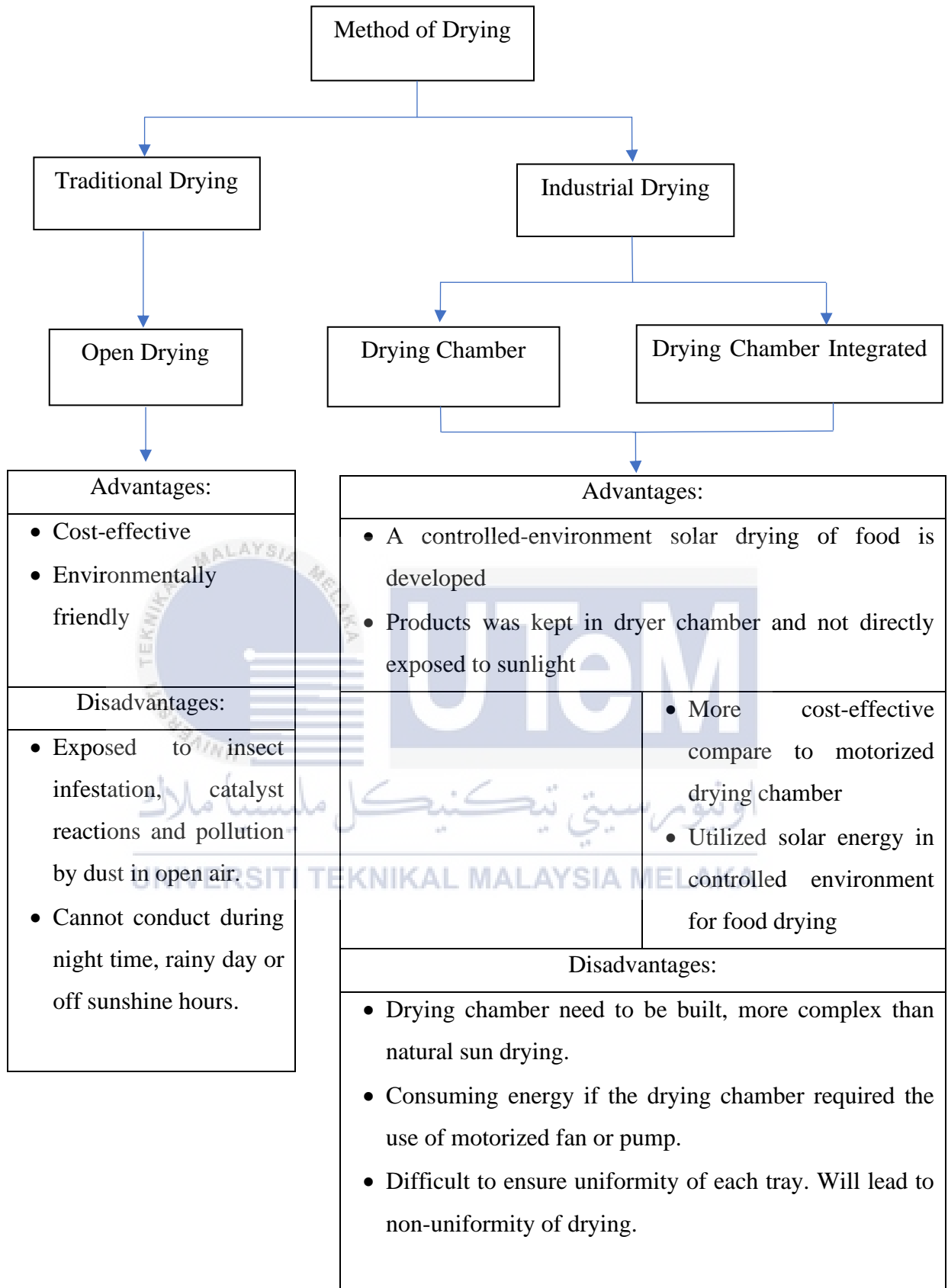


Figure 2.4: Method of drying

### **Short summary:**

There are different types of drying method using solar energy which can categorized into direct and indirect dryers. Direct dryers mean the product or material to be dried absorb the radiated solar directly, meanwhile in indirect dryers, air is heated by solar radiation which then flows through the space containing the product.

#### **2.5.1 Traditional Drying (Open Drying)**

Open sun drying has the advantages of cost-effective and environmentally friendly method for drying agricultural products and it is widely used worldwide (Tarigan, 2018). Natural direct sun drying is the oldest method that use for food preservation (Jackis et al, 2015). It enables agricultural products or foods preserved for long periods. Solar drying process can achieve higher product quality with longer storage period and minimize the post-harvest losses.

Various drying methods are used for drying different types of food product. In general, farmers utilized solar drying to have their products dried fast, efficiently, economically, with the requirement of good condition and correct environmental fashion. In agricultural industry, drying of seeds using solar energy prevents germinations and growth of fungi and bacteria (Ambesange & Kusekar, 2017). Figure 2.5 shows the schematic diagram of open sun drying.

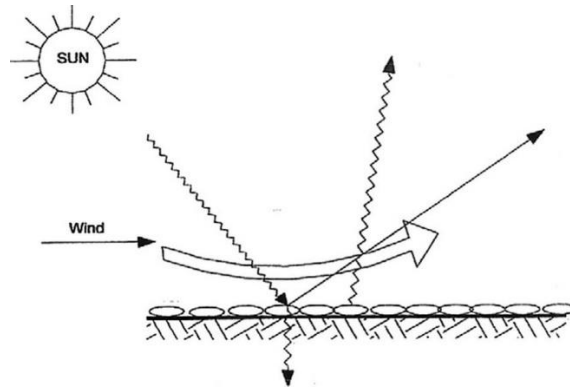


Figure 2.5: Open sun drying (Prakash, 2013)

However, ancient sun drying has several shortcomings such as insect infestation, catalyst reactions and pollution by dust in open air. Besides, sun drying takes longer time to succeed in the required wet content (Reddy et al., 2018). The substitute of open sun drying will be using drying equipment. Even though, most farmers cannot afford to import high-priced drying equipment, such as drying chamber which is either electrically or diesel-engine driven (Tarigan, 2018, p. 149). Those purchase will cause extra financial burdens of maintenance, fuel, electricity, and other running expenses in addition to environmental problems such as air pollution (Zoukit et al., 2018; Tarigan, 2018). Last but not least, open sun drying will required a large operational space for this process to occur (Zoukit et al., 2018). Hence, researchers and academician are continuously developing and researching on a more effectively drying method.

**Short summary:**

Open sun drying is cost-effective and environmentally friendly method for drying food. However, open sun drying has its own disadvantages which mainly will lead to low hygiene level of the dried product. Besides, it will take longer time to dry the wet contain in the food. However, drying equipment has been designed to overcome the disadvantage of traditional

open sun drying. Even though, this drying equipment, such as electrical drying chambers are usually expensive which will cause additional financial burdens of electricity or others running expenses. Hence, researchers are continuously developing and researching on a more effectively drying method to solve this problem.

### 2.5.2 Industrial Drying (Drying Chamber Integrated with Solar Collector)

As the limitation and the concern of disadvantages brought by traditional solar drying which is exposing to open air and directly under sunlight, industry has made some effort to improve the methods. In order to reduce spoilage, solar dryer as an apparatus for solar food drying in controlled environment had been developed. The utilization of solar dryer is very economic as well as effective for domestic users due to the low cost and mostly portable. The cost of operation in the solar dryer is zero as well as environment friendly as they are green energy products. Hence, for domestic utilization purpose, the solar dryers are preferable to other mechanical- and electronic type solar dryers (Jain et al., 2018).

Solar collectors are heat converter that transform solar radiation energy to internal energy of the transport medium. Figure 2.6 shows the typical solar air collector. This solar collector consists of an absorber, thermal insulation, glass plate, air vent and its housing.

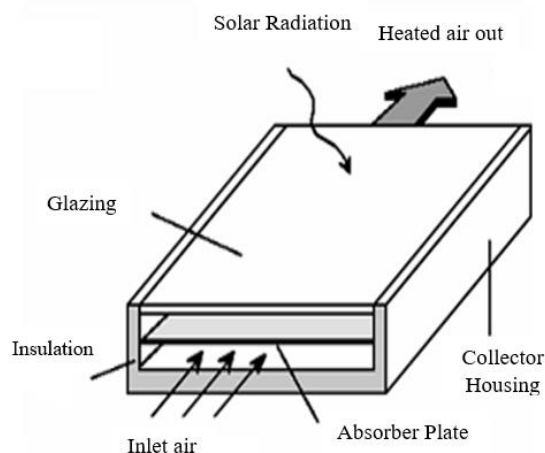


Figure 2.6: Typical solar air collector (Ikem, Ibeh and John, 2017)

Solar collector is the major components of any solar system which absorbing solar radiation that will converts it into heat energy and transfers the heat to a fluid flowing through the collector. The collected solar energy will be carried from the circulating fluid either directly to the hot water or space conditioning equipment, or to a thermal energy storage tank, where it can be used during night or on cloudy days (Nicolas et al., 2017).

There are mainly classified into two types of solar collectors, which are non-concentrating type and concentrating type. A non-concentrating collector was designed with same area for absorbing and intercepting solar radiation. Meanwhile a sun-tracking concentrating solar collector normally has concave reflecting surfaces that enable the sun's beam radiation to intercept and focus into a smaller receiving area, thus increasing the radiation flux. Concentrating collectors usually used for high-temperature applications. On the other hand, a solar collector can also be easily distinguished by knowing the type of heat transfer liquid used; either water, non-freezing liquid, air, or heat transfer oil, and whether they are covered or uncovered.

Among the flat collectors which are connected with the drying chamber, evacuated tube solar collectors (ETSC) has higher efficient which allow the combination with other collectors with lower maintenance or cost together with higher outlet fluid temperature related to flat plate collectors (Kalogirou, 2003). ETSC has several advantages such as higher performance over the year particularly during days with lower solar radiation, as a result of its tubular absorber. Besides, it has advantages of low convection heat lost, needless to stop the whole system when one tube is damaged and also working in inappropriate weather condition (Sharafeldin and Grof, 2018). Several studies have been implemented in the aim of increase the efficiency of ETSC such as implementing nanofluid, manipulating the shape of the absorber tubes, finding the optimal tilt-angles of all-glass over the tubes and etc. (Iranmanesh et al, 2019).

Indirect solar drying represents a promising alternative that should substitute sun drying to overcome the increasing demand for healthy and low-cost natural food. Indirect solar drying prevents direct exposure of food products to solar rays and contamination, which greatly improved the hygiene level of the food products (Zoukit et al., 2018). In indirect solar dryers, the latent heat of vaporization is supplied to drying chamber from the solar collector, the solar collector absorbs the solar energy raising the temperature of the air within the collector while lowering its relative humidity. The hot air then flows by convection through the drying chamber and exit through the chimney by thermo-siphoning effect. Distribution of the air flow across the drying chamber is key in determining the efficiency and uniformity of the dried product (Nicolas et al., 2017).

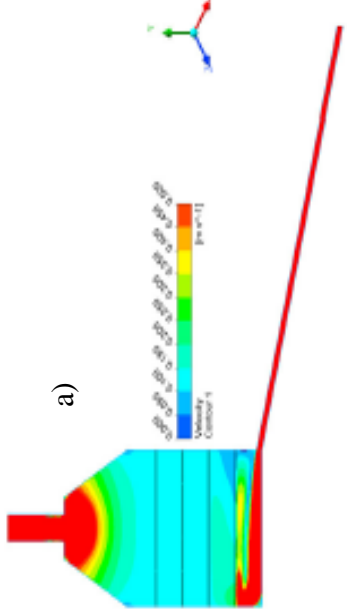
Furthermore, most solar dryers make use of the tray systems in the drying chamber making trays an important part of the drying bed. Due to the simple design and capability to dry products at high volume of the tray dryers, it widely used in a variety of applications to dry products at high volume. The greatest drawback of the tray dryer is uneven drying due to the poor airflow distribution in the drying chamber. By studying the airflow distribution analysis methodology, suitable design approach could be used to improve tray dryer performance, increase quality of dried product, and produce uniform drying (Zoukit et al., 2018).

**Short summary:**

Drying chamber integrated with solar collector are designed to solve the limitation brought by traditional solar drying. In indirect solar dryers, the solar collector absorbs the solar energy, then raising the temperature of the air within the collector. Afterwards, the hot air will then flow by convection through the drying chamber and exit through the chimney by thermo-siphoning effect.

### 2.5.3 Comparison Between the Different Design of Drying Chamber Integrated with Solar Collector

Table 2.2: Previous study in drying chamber

No	Simulation	Condition	Product	Boundary condition	Author	Findings
1	ANSYS Fluent 18.1 3D	Transient Heat Transfer	Fruits	<ul style="list-style-type: none"> <li>Steady operating temperature 315K.</li> <li>The food to be dried with this temperature in 35 minutes.</li> </ul>	Demissie et al., 2018	<ul style="list-style-type: none"> <li>Indirect solar food dryer</li> <li>Bottom shelf rack is subjected to rather high velocity 0.14m/s, and 0.12 m/s for others.</li> <li>Low temperature distribution at higher shelf rack.</li> </ul>
<p>Design:</p>  <p>Figure 2.7: a) Contour plot of total velocity distribution flow in solar drying chamber on the symmetry plane; b) Air flow velocity distribution on the four rack shelves in 3D.</p>						
<p>Advantages:</p> <ul style="list-style-type: none"> <li>The outlet of the dryer is designed in a truncated pyramid geometry, the additional heating of the drying air can exit at the outlet.</li> <li>The precipitation of condensed water would be minimized.</li> </ul> <p>Disadvantages:</p> <ul style="list-style-type: none"> <li>Difficult to ensure uniformity of each tray. Will lead to non-uniformity of drying.</li> </ul>						

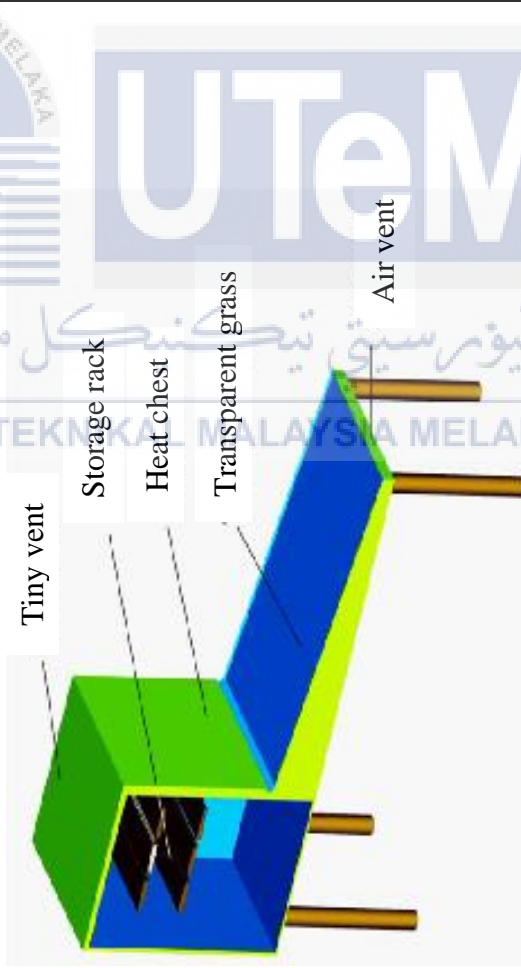
2	ANSYS Fluent Version 6.2 2D & 3D	Steady State	Pineapples (anasas comosus)	<p>Inlet:</p> <ul style="list-style-type: none"> <li>· Temperature- 308 Kelvin</li> <li>· Velocity of Air: 1 m/s</li> </ul>	Ambesange, and Kusekar, 2017	<ul style="list-style-type: none"> <li>· Natural convection solar dryer</li> <li>· Heat transfer is increase with the increase of temperature.</li> </ul>
<p>Design:</p>  <p>The image shows a 3D CAD model of a solar dryer. It consists of a green rectangular base with a black interior. A blue rectangular tray is mounted on top of the base. A green rectangular rack is positioned inside the tray. A yellow rectangular chest is located at the front of the tray. A transparent green surface is attached to the top of the tray. A small blue vent is located at the front of the tray. A larger blue vent is located at the back of the tray. The entire unit is supported by four wooden legs. Labels with dashed lines point to the following components: Tiny vent, Storage rack, Heat chest, Transparent grass, and Air vent.</p>				<p>Advantages:</p> <ul style="list-style-type: none"> <li>· Simple concept, easy to manufacture and operate.</li> <li>· Cheap, used for many domestic and commercial applications like space heating, crop drying and wood seasoning.</li> </ul> <p>Disadvantages:</p> <ul style="list-style-type: none"> <li>· The glass cover used will poses little interference to incoming solar energy.</li> </ul>		

Figure 2.8: Solar dryer

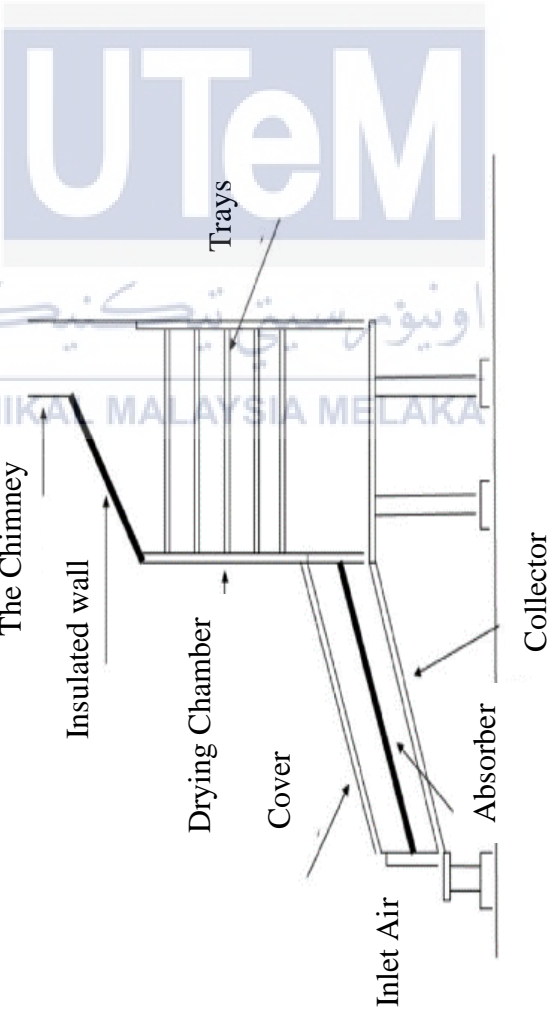
3	CFD in 2D	Transient Heat Transfer	Grape Initial humidity: 80% - 85%	<p>Inlet:</p> <ul style="list-style-type: none"> <li>Temperature- 25 Degree Celsius</li> <li>Velocity of Air: 0.11 m/s</li> <li>Mass flow rate: 0.040 kg/s</li> </ul>	Ghaffari, A., & Mehdi pour, R., 2015	<ul style="list-style-type: none"> <li>Temperature raise of 43°C with a uniform rate.</li> <li>Highest temperature reaches 68°C.</li> <li>From experimental result, final humidity of the product dropping from 82% to 18%.</li> </ul> <p>Air temperature moving out at outlet is 47°C</p>
<p><b>Design:</b></p>  <p><b>Advantages:</b></p> <ul style="list-style-type: none"> <li>Baffles design in this dryer used as an efficient remedy. It will increase the efficiency and better use for time and energy.</li> </ul>						

Figure 2.9: Schematic drawing of indirect cabinet model

4	ANSYS CFX- 12.1 In 3D	Steady State	Maize	<p>Inlet:</p> <ul style="list-style-type: none"> <li>Temperature- 70 Degree Celsius</li> <li>Velocity of Air: 1 m/s with turbulent intensity 5%</li> <li>solar radiation modeling with radiation flux of 900 W/m<sup>2</sup>.</li> </ul>	Aukah et.al., 2015	<ul style="list-style-type: none"> <li>Hybrid Solar Biomass Dryer</li> <li>Uniform temperature distribution</li> <li>Temperature profile of exit air proved that the exhaust air is recirculated without temperature drop.</li> <li>Highest temperature of 384.4 K observed at side walls of the dryer.</li> <li>Minimum air velocity= 1.55m/s</li> </ul>
<p>Drying chamber</p> <p>Solar</p> 				<p>Advantages:</p> <ul style="list-style-type: none"> <li>Uniform temperature distribution and velocity of airflow due to additional heating of air by solar radiation through the UV cover sheet</li> <li>The additional biomass stove- heat exchanger system allows the continuous drying process at night and also wet seasons.</li> </ul>		

Figure 2.10: Assembled biomass stove heat exchanger system

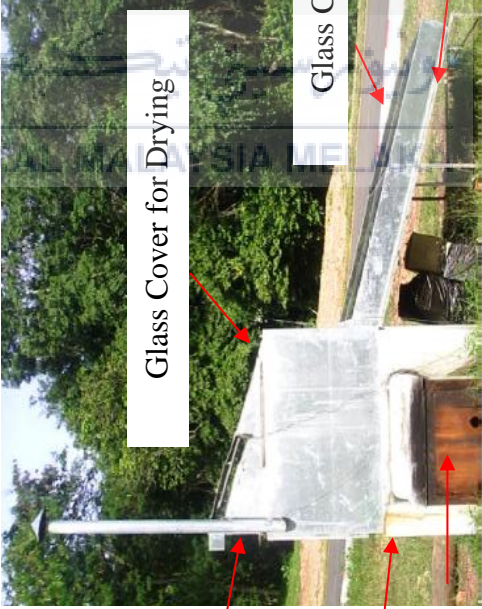
5	FloVent 5.2 -3D	Steady State & Transient	agriculture products (coffee cherries)	Wall temperature was set at 110°C	Tarigan, E. (2018)	<ul style="list-style-type: none"> <li>· Average drying air temperature in the drying chamber of 56 °C.</li> </ul>
<p>Design:</p>  <p>The diagram shows a side view of a solar dryer. It features a white base with a wooden door on the right. A transparent glass cover is mounted on top, supported by a metal frame. Labels with red arrows point to various parts: 'Ventilation' at the top left, 'Thermal' at the bottom left, 'Space for' at the bottom right, 'Glass Cover for Drying' on the top left of the cover, 'Glass Cover for Solar' on the top right of the cover, and 'Insulato' at the bottom right of the base.</p>				<p>Advantages:</p> <ul style="list-style-type: none"> <li>· Able to operate in solar energy mode, back-up heater mode, combination of solar energy and back-up heater mode.</li> <li>· Viability of solar dryer was improved when the source of heat is combined from both solar energy and stored heat in the brick.</li> </ul> <p>Disadvantages:</p> <ul style="list-style-type: none"> <li>· Less flexible usage as it was designed intended for use by individual farmer accordingly.</li> </ul>		

Figure 2.11: Side-view diagram of dryer

## 2.6 Computational Fluid Dynamics

Computational Fluid Dynamics (CFD) is a branch of fluid mechanics that utilizes the mathematical modelling and numerical simulation algorithms to examine and solve the problems that comprise flow of any fluid. Computers have been used to make calculations which are essential to simulate the interaction of the fluid with surfaces defined by the boundary conditions (Jain et al., 2018). Typically, CFD method was used to analysis the thermal performance and optimization of solar dryers such as using CFD for designing new solar cabinet dryer, simulation and validation of vanilla drying process in an indirect solar dryer, analysis of innovative design of solar-biomass hybrid dryer, predicting temperature distribution within the solar drying chamber, simulation of a solar agricultural dryer with thermal storage system simulation transient heat transfer in solar dryers (Iranmanesh et al., 2019). CFD is also used as a tool to predict the airflow distribution and investigate the flow pattern of the air in the drying chamber (Suhaimi et al., 2013).

Recently, computational fluid dynamics (CFD) is being utilized in myriads of solar food drier design efforts, proving itself to be a promising design and modeling tool as a substitute to costly experimental trials (Amanlou and Zomorodian, 2010; Darabi et al., 2015; Norton et al., 2013; Tegenaw et al., 2017). CFD was used and successfully predicting distribution of flow velocity and temperature within drying chambers (Norton and Sun, 2006; Rek et al., 2012). It is also used to predict drying uniformity of a new design of a commercial tray dryer for agricultural products by analyzing temperature and velocity profiles (Misha et al., 2013). The usefulness of CFD for performance assessment of food processing applications is highlighted by predicting the air velocity field for meat dryers (Mirade, 2003). Another field of application of this technique is for designing novel heating devices for infusion fluids in vitrectomy (Mauro et al., 2018; Petros et al., 2019).

In drying operations, CFD numerical simulations are widely utilized and used to significantly cutting down experimentation times without incurring costs. Besides that, CFD simulations are highly correlated with experimental data and therefore it provides reliable and verifiable information (Amanlou and Zomorodian, 2010). The application of CFD to drying processes can help improve the quality of the products, maintaining product uniformity and optimize the drying operation and energy consumption during operation (Defraeye, 2014). A study published by Amanlou and Zomorodian (2010) addressed the problem of non-uniformity in drying operations. They studied the airflow in different geometries of a convective cabinet dryer using CFD and found high correlations with the experimental data of the process. Similarly, studies conducted by Margaris and Ghiaus (2006) showed that experimental investigations in conjunction with CFD numerical simulation can predict configurations that optimize the drying spaces in convective tray dryers to obtain more uniform air flows. Studies by Mathioulakis et al. (1998) extended the application of CFD simulations to industrial facilities and helping to obtain a better understanding of the problems associated with products dried with poor uniformity in a 5-ton industrial dryer.

**Short summary:**

Computational Fluid Dynamics (CFD) is a branch of fluid mechanics that used to solve the problems that comprise flow of any fluid. CFD method was used to analysis the thermal performance and optimization of solar dryers such as to predict the temperature distribution and investigate the flow pattern of the air in the drying chamber.

### 2.6.1 Benefit of CFD

CFD software might be used in solar drying field on the way to predict air velocities and temperature distribution which is in manually will require a lot of sensors. Besides, the CFD may be used as a drying optimization tool to improve the design and to predict the drying time. CFD simulated a dryer which was designed to dry fruits and vegetables, consist of heat exchanger to enhance the heated air supplied from LPG gas burner. Centrifugal fan was located inside the dryer chamber to force the air movement.

Thanks to the rapid development of computing power nowadays, the application of CFD can be a valuable tool for engineering analysis and design of solving complex fluid flow, addressing heat and mass transfer phenomena, aiding in the better design of tray dryers and produce high quality of dried product. The capability of CFD simulation in solving equations for the conservation of mass, momentum, and energy was widely utilized using numerical methods to predict the temperature, velocity, and pressure profiles in the drying chamber (Suhaimi et al., 2013).

#### **Short summary:**

CFD software might use to predict air flow velocities and temperature distribution in a drying chamber. Besides, CFD also used as a drying optimization tool to improve the design and to predict the drying time. CFD are significantly cutting down experimentation times and also experimental trial costs.

## 2.6.2 Basic Governing Equations for CFD Simulation

The airflow field and temporal temperature distribution within the flow domain are modeled and simulated from mass, momentum, and energy conservation equations, as shown in Eq (2.8), Eq (2.9) and Eq (2.10). For a symmetric 3D flow domain, the resulting transient flow and heat transfer equations were written in an inertial (non-accelerating) Cartesian coordinate frame  $(x, y, z)$  (Demissie et al, 2018).

Continuity equations:

$$\frac{\partial \rho}{\partial t} + \nabla \cdot (\rho \vec{v}) = 0 \quad (2.8)$$

Momentum conservation equations:

$$\frac{\partial}{\partial t} (\rho \vec{v}) + \nabla \cdot (\rho \vec{v} \vec{v}) = -\nabla p + \nabla \cdot (\vec{\tau}) + \rho \vec{g} + \vec{F} \quad (2.9)$$

Energy conservation equations:

$$\frac{\partial}{\partial t} (\rho E) + \nabla \cdot (\vec{v} (pE + p)) = \nabla \cdot (k_{eff} \nabla T) + S_h \quad (2.10)$$

Where,

$\rho (kg/m^3)$  = density

$\vec{v} (g/sec)$  = flow velocity

$g (m/sec^2)$  = gravity

$\vec{\tau} (Pa)$  = stress tensor

$S_h (Pa/Sec)$  = volumetric heat source

$\vec{F} (Pa)$  = momentum sink term

$E (m^2/sec^2)$  = total enthalpy

$p (Pa)$  = pressure

$k_{eff} (J/mK)$  = effective conductivity

$t (sec)$  = time

### Short summary:

CFD is capable to simulate air temperature and velocity by governing equation for the conservation of mass, momentum, and energy using numerical methods.

## CHAPTER 3

### METHODOLOGY

#### 3.1 Introduction

This chapter describe the methodology used in this project to study the simulation performance in the drying chamber integrated with solar collector. The detail flow chart of methodology for this project is shown in Figure 3.1. Geometry, meshing, setup, and solution of the drying chamber integrated with solar collector will be illustrated in this chapter.

First and foremost, number of journals, articles and papers regarding to the project are searching to obtain relevant information which is related to the study of drying chamber integrated with solar collector. Different design of drying chamber integrated with solar collector are studied to obtain their working principles and also advantages. Besides, the parameters that affecting the drying rates also has been studies in Chapter 2.

After the studies with the different design of drying chamber integrated with solar collected, a journal studying indirect solar food dryer by using Computational Fluid Dynamics (CFD) (Demissie et al., 2019) had been selected to validate this project. The software ANSYS Fluent 16.0 had been chosen for generating geometry and meshing of the drying chamber integrated with solar collector.

Next, the drying chamber integrated with solar collector from journal is being modified for a better drying rate with uniform air temperature distribution. Last but not least, CFD simulation will visualize the results and analyse streamlines, contour and plots of the solar collector drying chamber. Gantt chart for the completion of this project will be attached at Appendix J and Appendix K.

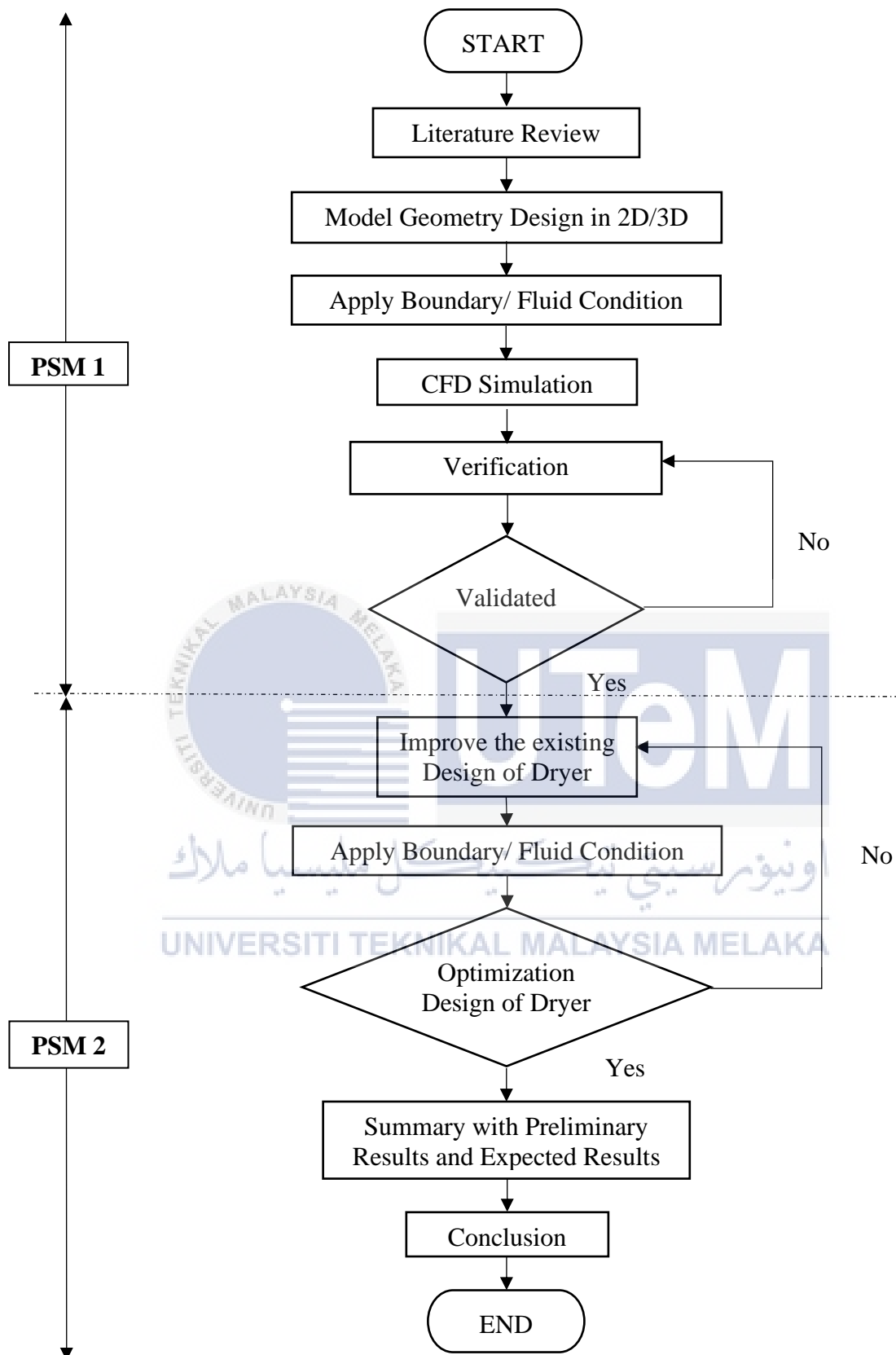


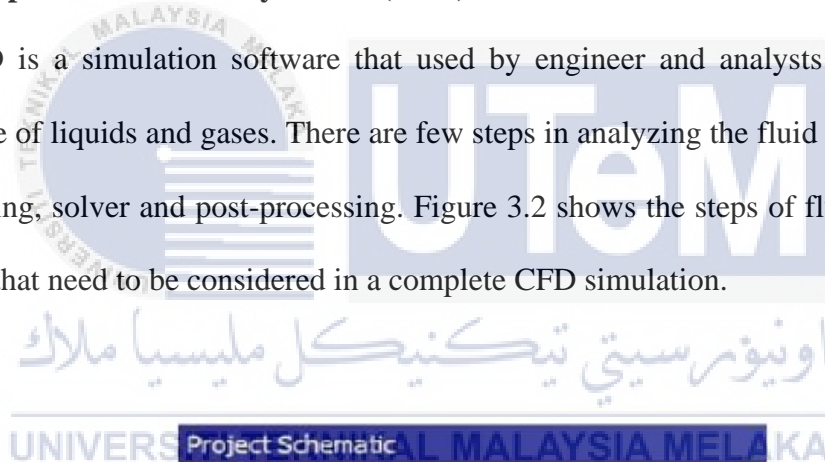
Figure 3.1: Flow Chart of the Methodology

### 3.2 Literature Review

First and foremost, the problem of fluid flow in solar drier is identified this study. Numbers of research studies, review papers and theoretical articles from previous researcher are studied and analyzed to obtain evaluative review. Through the studies, the existing design of drying chamber integrated with solar collector as well as their advantages and disadvantages are identified. In this study, the performance of drying chamber integrated with solar collector was simulated by using three- dimensional (3D) CFD simulation in transient state condition.

### 3.3 Computational Fluid Dynamics (CFD) Simulation Process

CFD is a simulation software that used by engineer and analysts to predict the performance of liquids and gases. There are few steps in analyzing the fluid flow which are pre-processing, solver and post-processing. Figure 3.2 shows the steps of fluid flow fluent in ANSYS that need to be considered in a complete CFD simulation.



A	
1	Fluid Flow (Fluent)
2	Geometry ✓
3	Mesh ✓
4	Setup ✓
5	Solution ✓
6	Results ✓

Fluid Flow (Fluent)

Figure 3.2: Steps in Fluid Flow (Fluent)

### 3.4 Pre-processing of CFD Simulation

#### 3.4.1 Geometry Creating

Geometry creation is the first step in preprocessing process. The domain of geometry creation for drying chamber is started creating by its shape and size by using the ANSYS software. The geometry can consist of volumes, faces, edges and vertices. Fluid domain of solar drier that considered for analysis from journal by using Design Modeler in ANSYS Fluent software was shown in Figure 3.3.

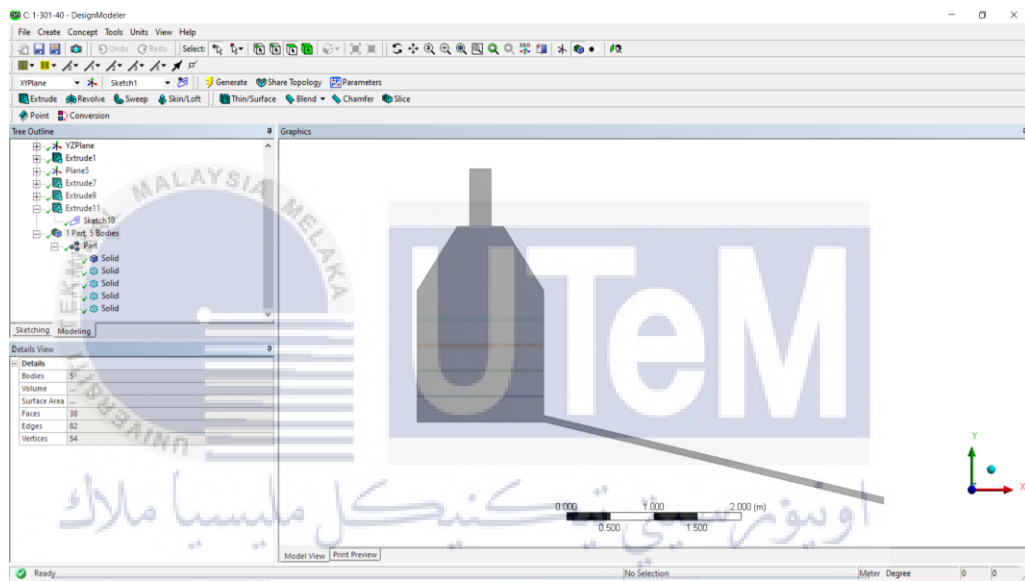


Figure 3.3: Computational Flow Domain for CFD Simulation

Figure 3.4 shows the full 3D schematic solar drier design in journal (Demissie et al, 2019). The domain of solar drier was sliced into two halves by taking the slices faces as symmetry planes as show in Appendix B to compute more efficiently. Structural supports on the drying chamber were excluded in the drawing as these components will not affected the simulation of air flow. The 3D drawing of modified design on solar collector was illustrate in Figure 3.5. As can be seen in the figure, the solar collector is modified by adding the insulator and glass on its structural system. Glass has good transmittance, high temperature capability and low transmittance. Besides that, insulator is added on the bottom of solar collector. These enhanced modifications on the solar collector can reduce the heat

losses from the solar collector to surrounding. Figure 3.6 shows the front view of drying chamber integrated with solar collector validated and enhancement on solar collector respectively, whereas Table 3.1 shows the summarized information on the dimension of both solar driers base on Figure 3.6.

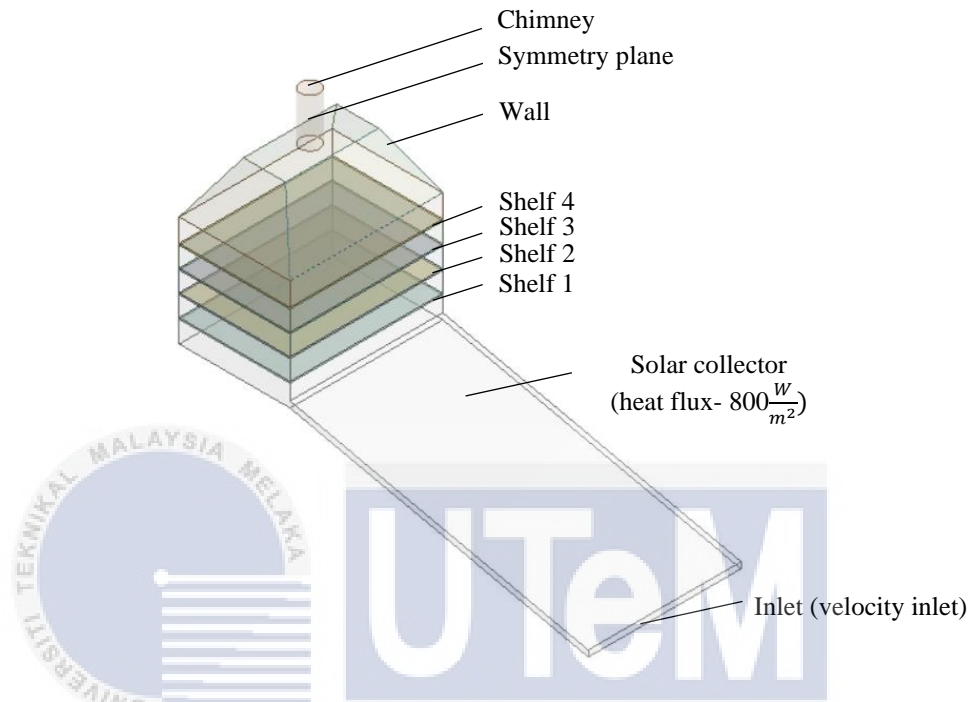


Figure 3.4: Full 3D schematic representation of various components of the solar drier in Ansys software

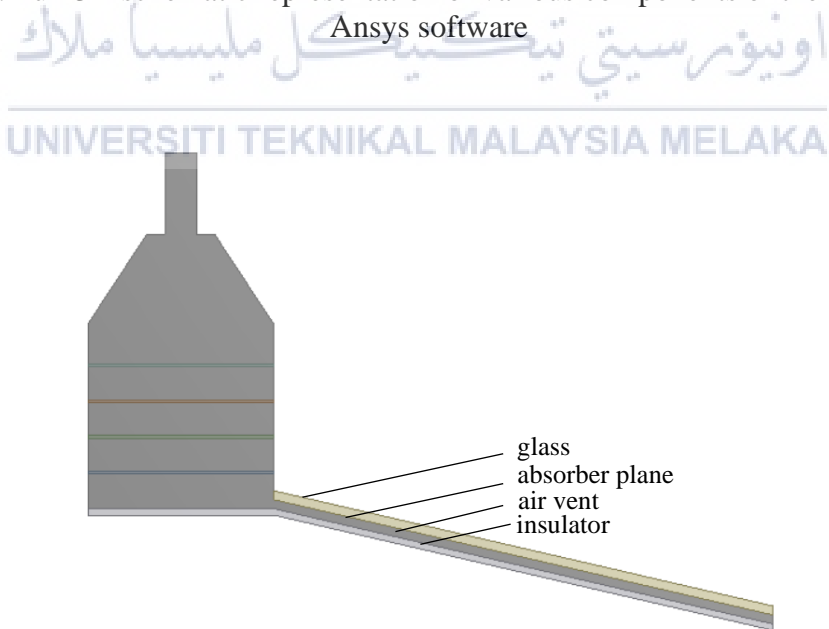
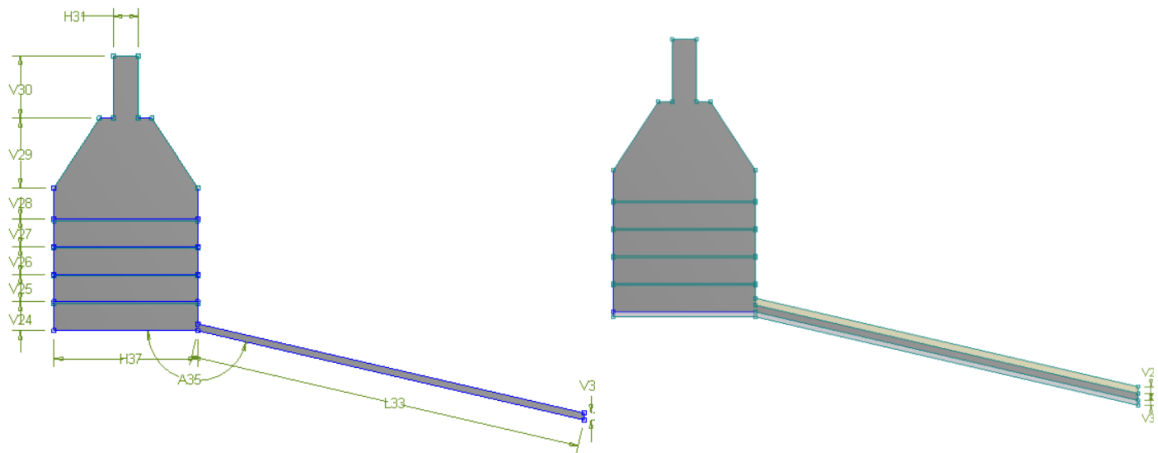


Figure 3.5: 3D Drawing of modified design on solar collector



(a) Solar Drier from Journal

(b) Modified Design on Solar Collector

Figure 3.6: (a) Front View of Drying Chamber integrated with Solar Collector from journal (b) Front View of Modified Design on Solar Collector

Table 3.1: Geometrical Parameters and Dimension of Solar Drier

Labels	Solar drier (a)	Solar drier (b)
H31		0.25 m
V30		0.63 m
V29		0.70 m
V28		0.31 m
V27		0.28 m
V26		0.28 m
V25		0.28 m
V24		0.29 m
V36		0.07 m
H37		1.45 m
L33		4.00 m
A35		167 °
V29	-	0.07 m
V30	-	0.05 m

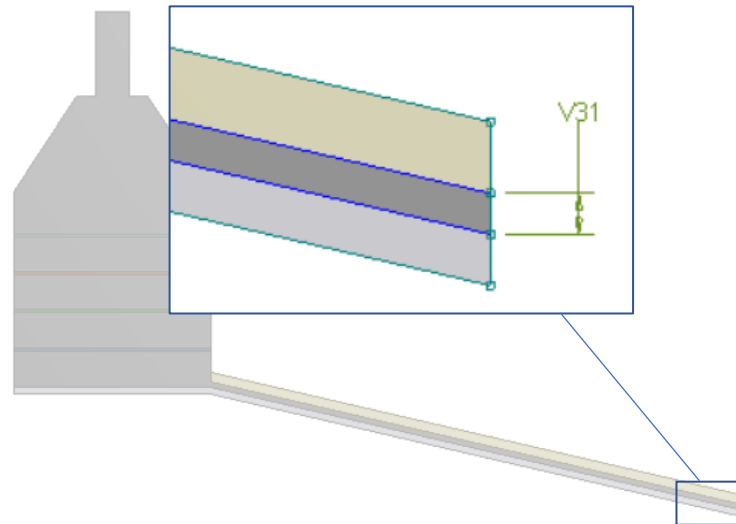
After redesign the solar collector, three different parameters were considered in the modified factor of drying chamber integrated with solar collector. First, the inlet area of air vent is a factor need to consider in the parameters. The area testing in this parameter is  $0.08\text{m}^2$ ,  $0.2\text{m}^2$  and  $0.3\text{m}^2$  as shown in Table 3.2. After simulated, one of the optimise design is chosen for the next step of testing which is different gap size between each rack shelves. The selected gap sizes are 0.2m, 0.5m and 0.2m with big gap shelf 0.5m in the middle of

drying chamber. The most uniform of temperature and air flow within the drying chamber will be chosen for the last simulation. Lastly, the testing parameter is the tilt angle of solar collector. 10°, 30° and 40° of tilt angle of solar collector is selected in the testing.

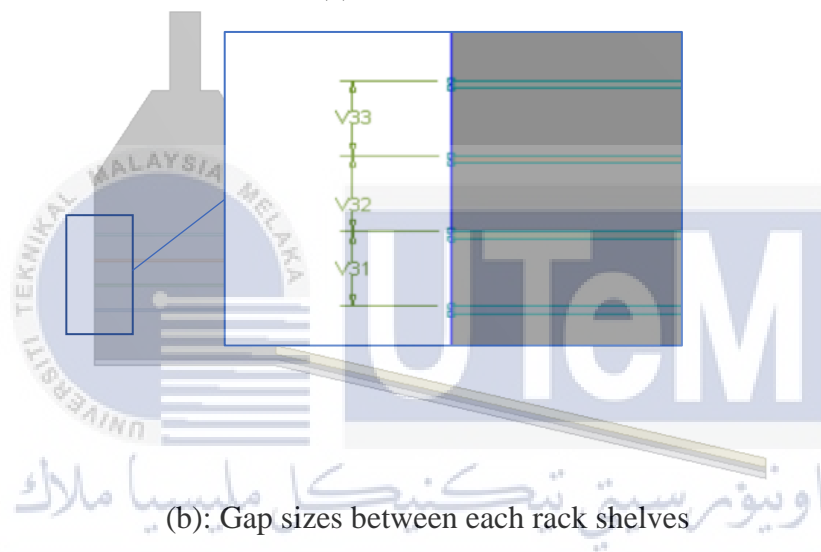
The purpose of reconsideration of these parameters is to ensure the uniformity drying throughout the drying chamber and find the most optimize design. Figure 3.7 shows the new parameters considered in the drying chamber integrated with solar collector at different inlet area, gap size between each rack shelves and tilt angle of solar collector respectively.

Table 3.2: Geometrical parameters considered in the drying chamber integrated with solar collector

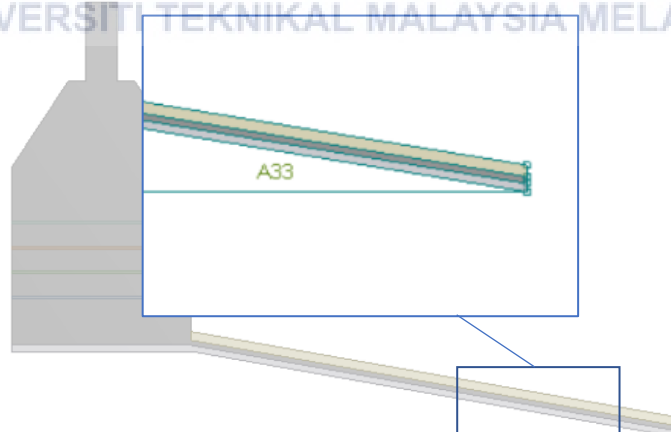
Parameter 1			
Parameter	a	b	c
Air inlet area	0.08 m <sup>2</sup>	0.2 m <sup>2</sup>	0.3 m <sup>2</sup>
Parameter 2			
Parameter	a	b	c
Gap between trays	0.2 m	0.25 m	0.2 m, big gap between shelf (0.5m)
Parameter 3			
Parameter	a	b	c
Tilt angle of solar collector	10°	30°	40°



(a): Air inlet area



(b): Gap sizes between each rack shelves



(c): Tilting angle of solar collector

Figure 3.7: Parameter considered at different (a) air inlet area, (b) gap size between each rack shelves, (c) tilting angle of solar collector

### 3.4.2 Domain Tags

After creating the geometry, the next step is the name selection to tags the boundary surface. Figures 3.8 and Figure 3.9 show the domain tags and named selection of the drying chamber integrated with solar collector validated and the enhance solar collector respectively.

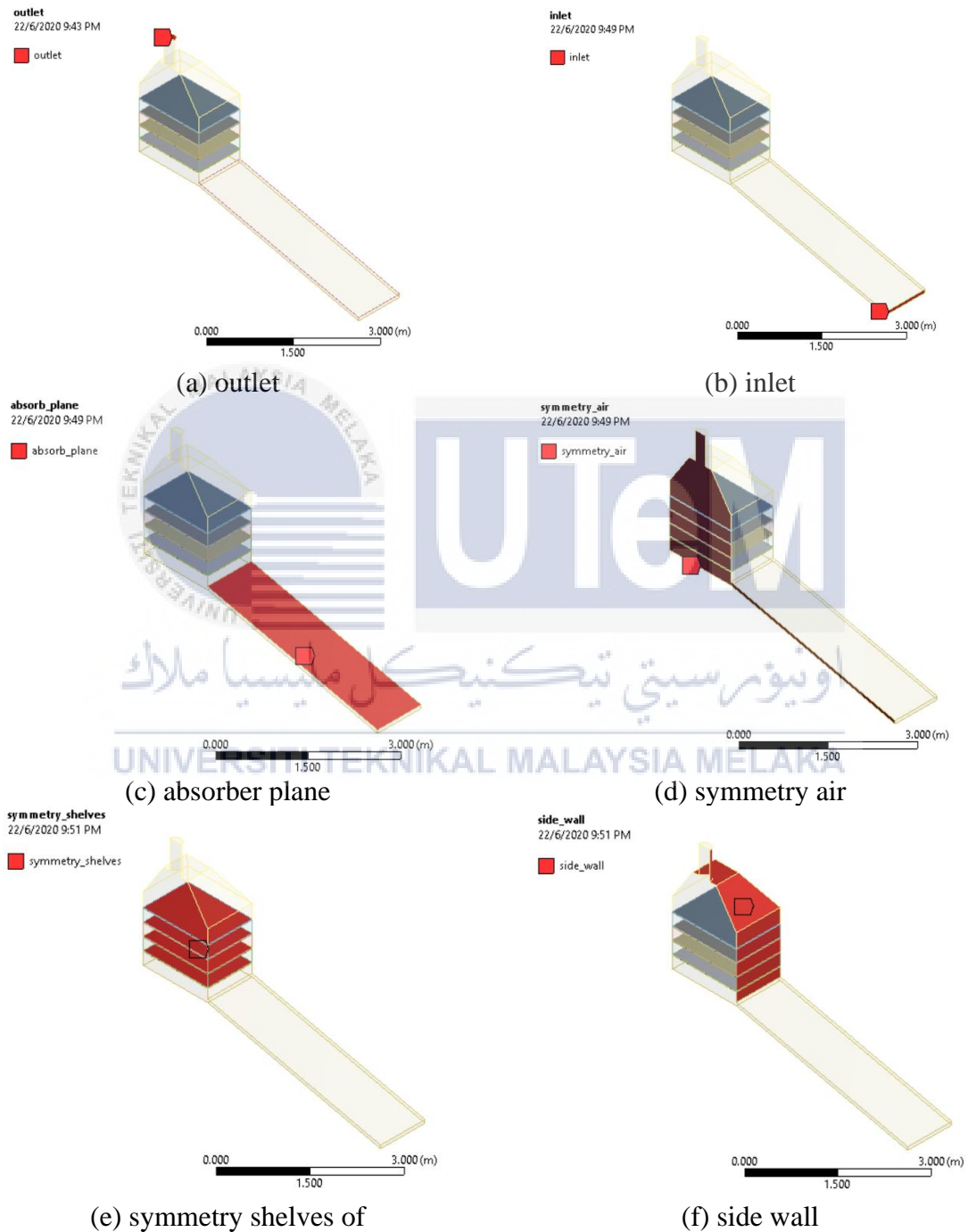


Figure 3.8: Domain Tags and Names Selection of the drying chamber integrated with solar collector from The Journal

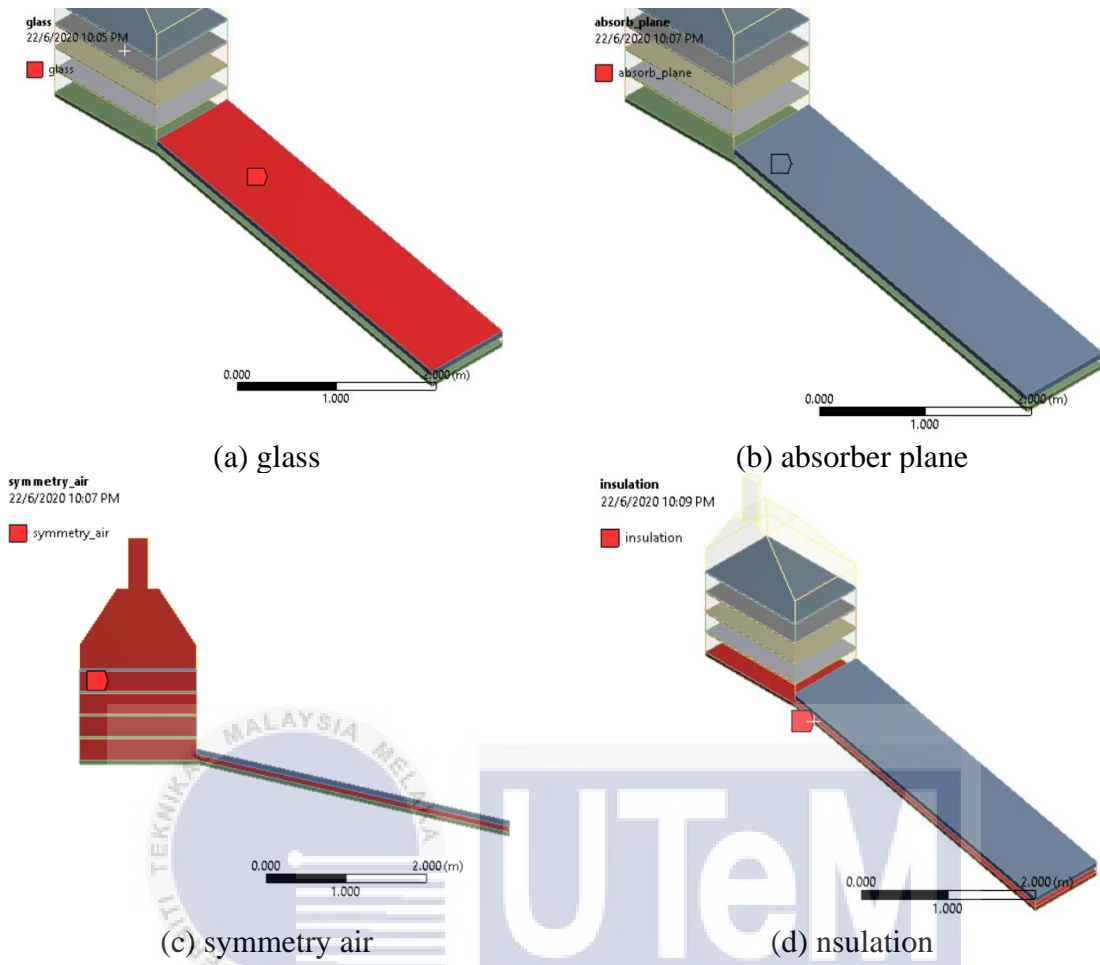


Figure 3.9: Domain Tags and Names Selection of the Enhance Solar Collector

### 3.4.3 Meshing

Mesh generation is one of the most important steps in simulating physics. It is the splitting of flow domains into smaller subdomain to analyze fluid flows. Accuracy of the solution will depend on the quality of mesh. The subdomains are known as elements or cells. A collection of all elements or cells is called mesh or grid. Meshing allows the creation of solution setup and to have an effective post-processing. The fluid domain of the system is identified and divided into smaller segments for mesh generation, grid generation and domain discretization step. A structured 3D block meshing generated on symmetric flow domain is shown in Figure 3.10.

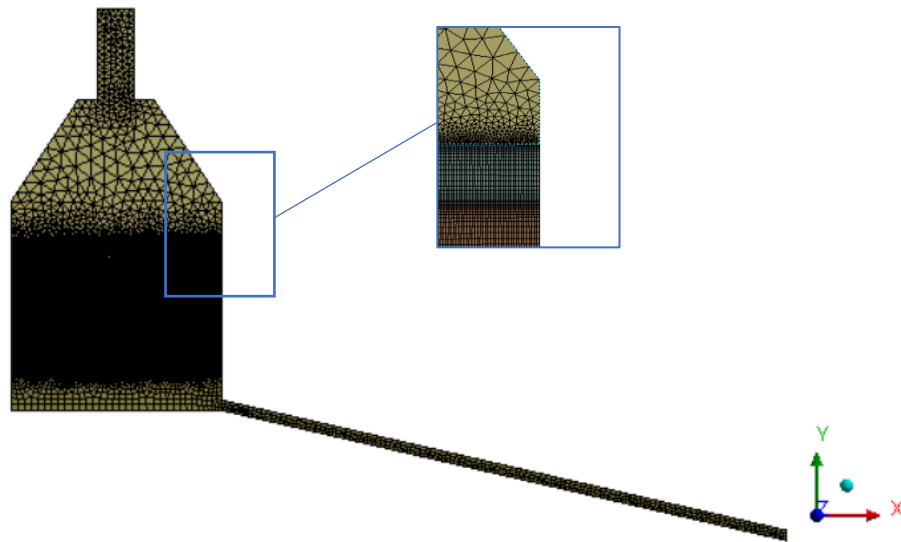


Figure 3.10: Meshing of drying chamber integrated with solar collector

Table 3.3 shows the grid independence test for drying chamber integrated with solar collector from journal and modified design on solar collector. Table 3.4 shows the meshing setup of solar drier validated.

Table 3.3: Parameters of Grid independence Test for Drying Chamber integrated with Solar Collector from Journal

<b>Grid independence test</b>				
<b>Solar Drier from Journal</b>				
<b>Parameters</b>	<b>Part solid</b>	<b>Symmetry shelves</b>		<b>All domains</b>
<b>Relevance center</b>				Fine
<b>Nodes</b>	924042	203040		1127082
<b>Element</b>	1291226	149544		1440770
<b>Used Advanced Size Function</b>				Proximity and Curvature
<b>Modified Design on Solar Collector</b>				
<b>Parameters</b>	<b>Part solid</b>	<b>Symmetry shelves</b>	<b>Part solid.1</b>	<b>All domains</b>
<b>Relevance center</b>				Fine
<b>Nodes</b>	1055645	219248	146544	1421437
<b>Element</b>	1557916	161280	107940	1827136
<b>Used Advanced Size Function</b>				Proximity and Curvature

Table 3.4: Mesh sizing parameters

Object Name	Mesh
State	Solved
<b>Display</b>	
Display Style	Body Color
<b>Defaults</b>	
Physics Preference	CFD
Solver Preference	Fluent
Relevance	0
<b>Sizing</b>	
Use Advanced Size Function	On: Proximity and Curvature
Relevance Center	Fine
Initial Size Seed	Active Assembly
Smoothing	Medium
Span Angle Center	Fine
Curvature Normal Angle	Default (18.0 °)
Min Size	Default (9.5799e-004 m)
Max Face Size	Default (9.5799e-002 m)
Max Size	Default (0.19160 m)
Growth Rate	Default (1.20)
Minimum Edge Length	2.e-002 m
<b>Inflation</b>	
Use Automatic nflation	None
Inflation Option	Smooth Transition.
Transition Ratio	0.272
Maximum Layers	2
Growth Rate	1.2
Inflation Algorithm	Pre
View Advanced Options	No

### 3.5 Solver of CFD Simulation

After the completion on pre-processing of CFD simulation, the mesh is exported to solver. The fluid material properties, flow physics model and boundary conditions of the drying chamber are set. The ANSYS software will solve the discretize governing equation.

### 3.5.1 Properties Materials

Based on the drying chamber integrated with solar collector studies, the material used in these simulations are air, copper, and aluminum. The properties of materials in solar drier validated and modified design on solar collector are as shown in Table 3.5 below.

Table 3.5: The properties of material used in CFD simulation

Material \ Properties	Density (kg/m <sup>3</sup> )	Specific Heat (J/kg.k)	Thermal Conductivity (W/m.k)
<b>Solar Drier Validated and Modified Design on Solar Collector</b>			
<b>Air</b>	1.225	1006.43	0.0242
<b>Copper</b>	8978	381	387.6
<b>Aluminum</b>	720	1255	0.16
<b>Modified Design on Solar Collector</b>			
<b>Glass</b>	2220	830	1.15
<b>Insulator</b>	10	830	0.1

### 3.5.2 Boundary Conditions

To properly define the CFD problem, boundary conditions plays an importance role in this simulation. The set-up of boundary condition is shown in Table 3.6.

Table 3.6: Boundary Conditions Set-up

Boundary	Type	Remark
<b>inlet</b>	velocity inlet	Velocity Magnitude: 3 m/s Temperature: 301K
<b>outlet</b>	pressure outlet	Gauge Pressure: 0 Pa
<b>bottom</b>	wall	
<b>absorber_plane</b>	wall	Heat Flux: 800 W/m <sup>2</sup>
<b>interior-part-solid</b>	interior	
<b>interior-symmetry_shelves</b>	interior	
<b>side_wall-part-solid</b>	wall	
<b>side wall-symmetry_trays</b>	wall	
<b>symmetry air</b>	symmetry	
<b>wall-part-solid</b>	wall	Heat Flux: 40 W/m <sup>2</sup>
<b>wall-part-solid-symmetry_shelves</b>	interior	
<b>wall-symmetry_shelves</b>	wall	

### 3.5.3 Turbulence Modelling

The model study in this project is realizable k-epsilon turbulence model with scalable wall functions (Demissie et al, 2019). Semi-empirical based on transport equation is used. Appropriate value of heat fluxes was applied on the wall of the flow domains.

### 3.5.4 Solution

The average temperature is measured in 2 hours. Table 3.7 shows the run calculation of the drying chamber integrated with solar collector in the simulation.

Table 3.7: Run Calculation of The Drying Chamber integrated with Solar Collector in The Simulation

Time Step Size (s)	144
Number of Time Steps	50
Max iterations/ Time Step	10
Reporting interval	1
Profile Update interval	1

### 3.6 Post-processing of CFD Simulation

In post-processing process, contour plots, vector plot, streamlines of the air velocity flow and data curve in the drying chamber integrated with solar collector were plot. in the simulation, it is performed by gradual increases in time step. From the results obtained, the performance of the drying chamber integrated with solar collector is evaluated and necessary modifications can be made to improve it.

## CHAPTER 4

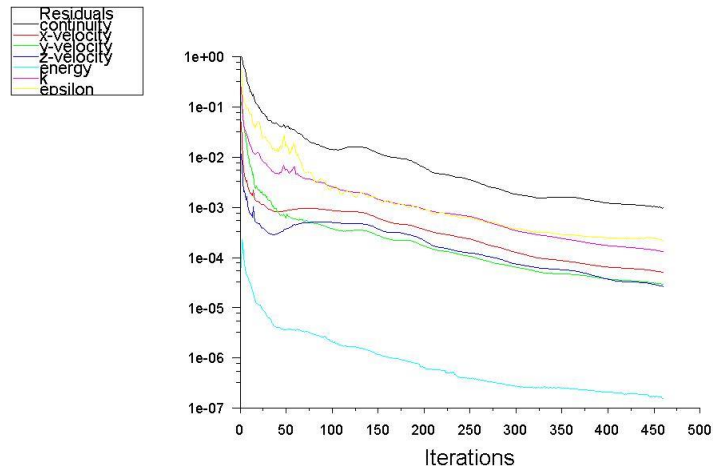
### RESULT ANALYSIS AND DISCUSSION

#### 4.1 Introduction

The methodology simulation of drying chamber integrated with solar collector by using CFD has been discussed in previous chapter. Demissie et al., (2018) has conducted a design, development and CFD modeling of indirect solar food dryer studies. The design dryer was designed using the combination of a solar collector unit, two columns of four rack shelves of drying chamber, chimney for the exhaust air, and a solar powered fan. The truncated pyramid geometry design of dryer outlet enables the minimization of precipitation of condensed water and additional heating of the drying air is possible at the exit. The temperature and velocity distribution within the drying chamber were predict using CFD through symmetric flow domain.

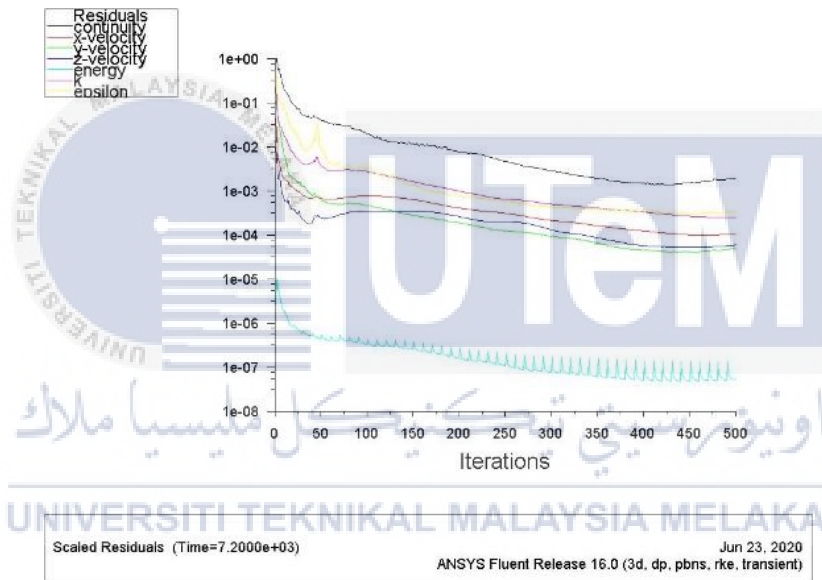
#### 4.2 Results of Convergence Solution

Figure 4.1 and 4.2, shows the graphs of convergence solution for the validation design in journal and modified design on solar collector. Besides that, Figure 4.3, 4.4 and 4.5 shows the graphs of convergence solution of different parameters considered in drying chamber integrated with solar collector based on difference variable such as inlet area, gap size between each rack shelves and tilt angle of solar collector respectively. The simulation run in transient state of condition. As shown, the values of convergence are  $1 \times 10^{-4}$  for energy equation.



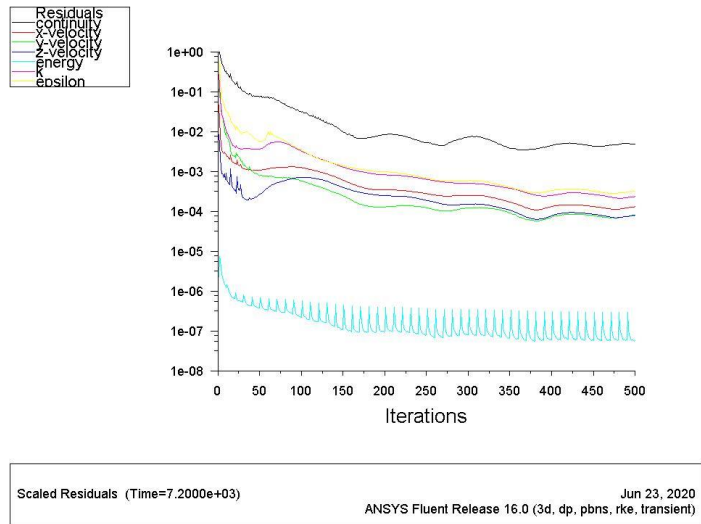
Scaled Residuals (Time=7.2000e+03) ANSYS Fluent Release 16.0 (3d, dp, pbns, rke, transient) Jun 23, 2020

Figure 4.1: Convergence Solution for Validation Design in Journal (Demissie et al, 2019)

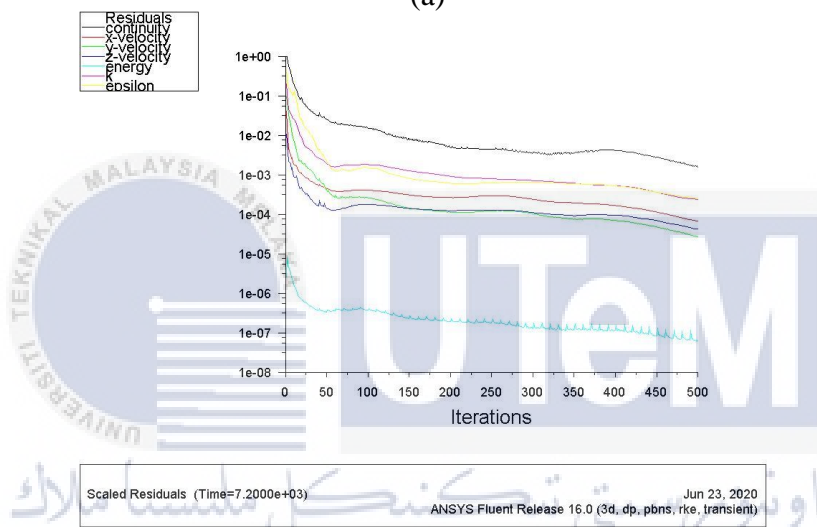


Scaled Residuals (Time=7.2000e+03) ANSYS Fluent Release 16.0 (3d, dp, pbns, rke, transient) Jun 23, 2020

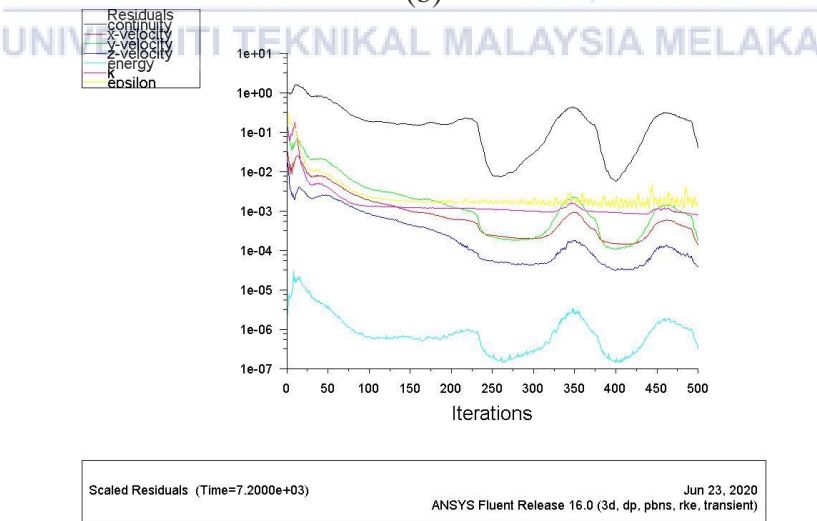
Figure 4.2: Convergence Solution for Modified Design of Solar Collector



(a)

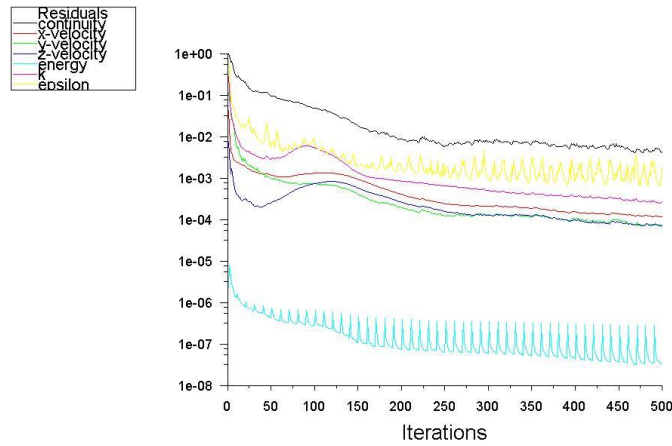


(b)



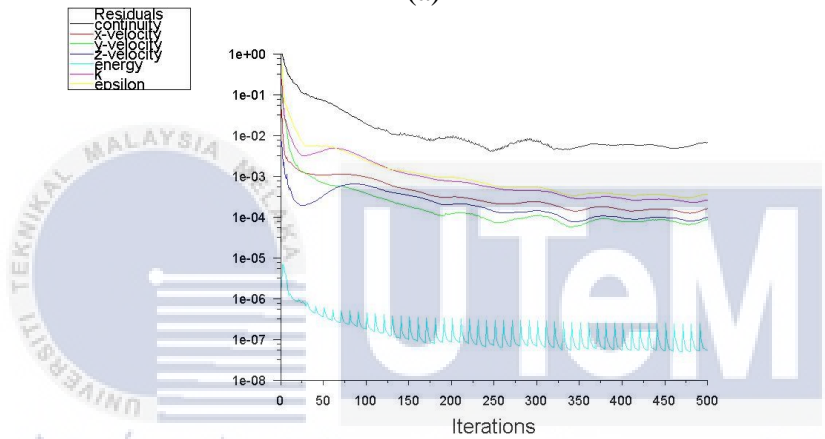
(c)

Figure 4.3: Convergence Solution for Parameter 1 at Different Area of Air Vent inlet (a), (b), (c)



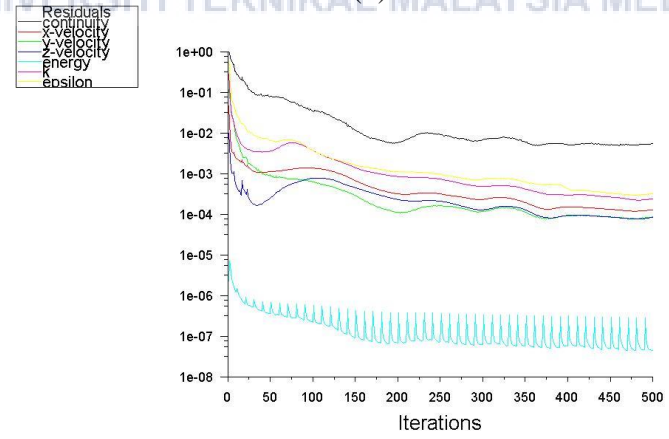
Scaled Residuals (Time=7.2000e+03) ANSYS Fluent Release 16.0 (3d, dp, pbns, rke, transient) Jun 23, 2020

(a)



Scaled Residuals (Time=7.2000e+03) ANSYS Fluent Release 16.0 (3d, dp, pbns, rke, transient) Jun 23, 2020

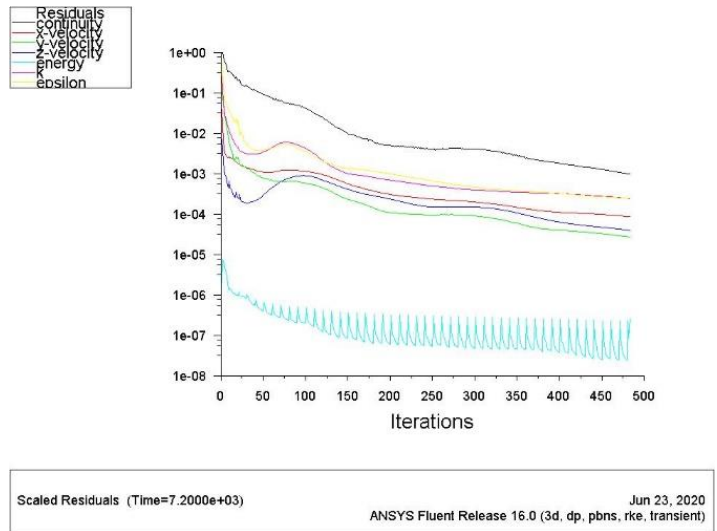
(b)



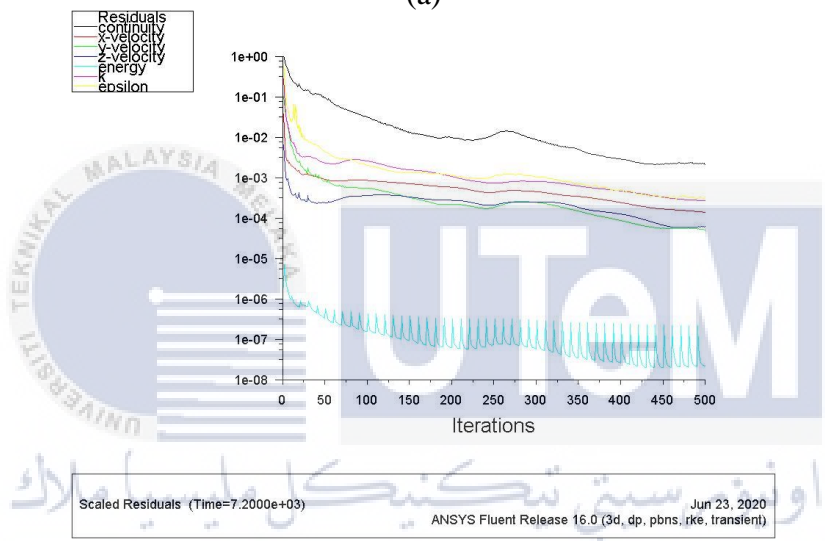
Scaled Residuals (Time=7.2000e+03) ANSYS Fluent Release 16.0 (3d, dp, pbns, rke, transient) Jun 23, 2020

(c)

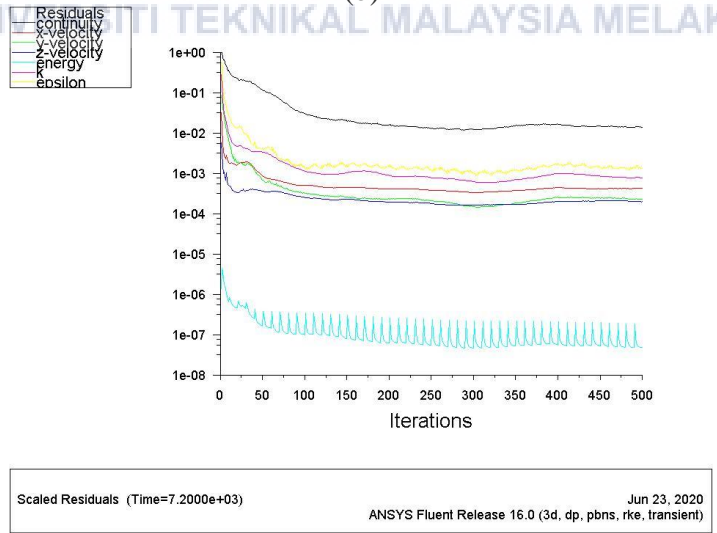
Figure 4.4: Convergence Solution of Parameter 2 at Different Gap Size between Rack Shelves (a), (b), (c)



(a)



(b)



(c)

Figure 4.5: Convergence Solution of Parameter 3 at Different Tilt Angle of Solar Collector Angle (a), (b), (c)

### 4.3 CFD Simulation Verification and Validation Results

#### 4.3.1 CFD Simulation Verification Results

The results from the simulation are compared with the simulation obtained from the literature study in the journal (Demissie et al., 2019) in order to ensure the steps and properties in simulating the drying chamber integrated with solar collector are correct. Figure 4.6 shows the comparison contour profile of total velocity distribution from the journal and with the results from the simulation. The results from the simulation are set with air velocity (3m/s) and air temperature (301K). Figure 4.7 shows the comparison of vector profile of air flow velocity distribution on the four rack shelves from the journal and with the results from the simulation.

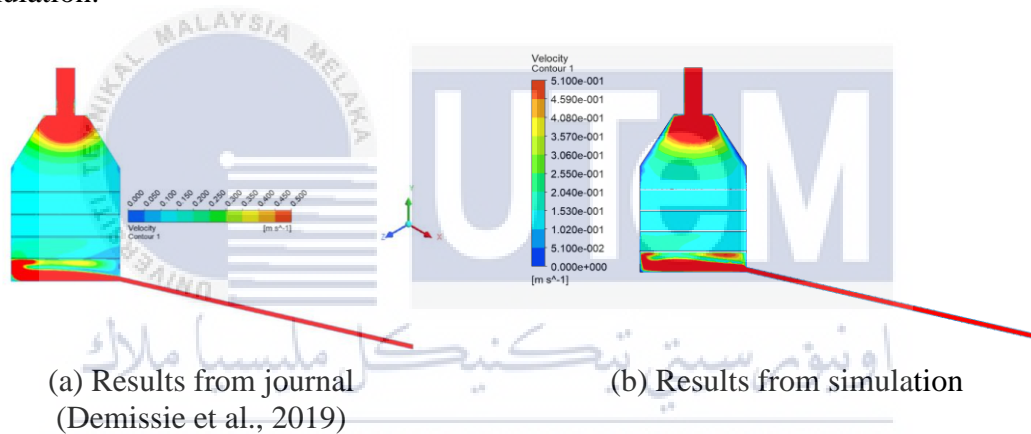


Figure 4.6: Validated Results of Contour Profile of total velocity distribution on the symmetry plane of the solar dryer.

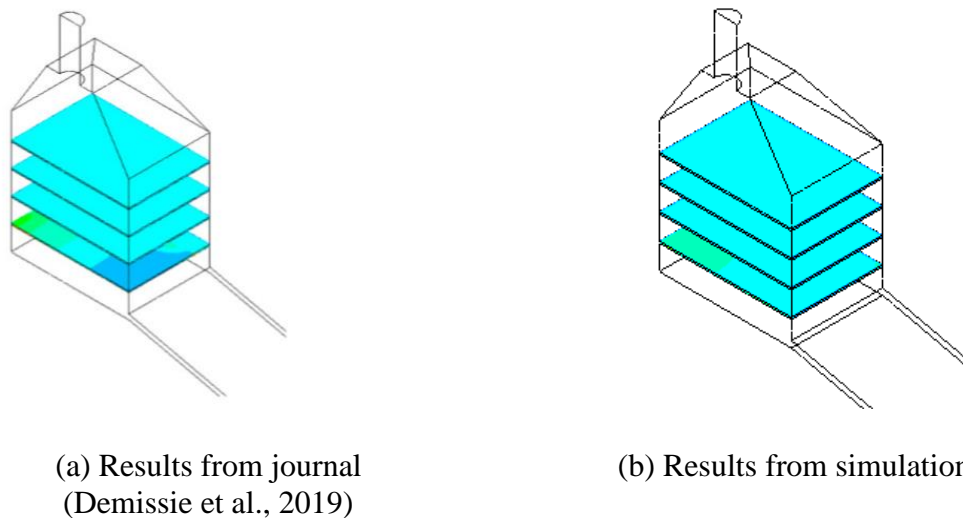


Figure 4.7: Validated Results of Contour Profile of air flow velocity distribution on the four rack shelves in 3D representation.

As can be seen clearly on Figure 4.6 and Figure 4.7, the contour plot of velocity on the symmetry plane and the four rack shelves of the drying chamber with solar collector from journal and simulation are almost similar. This can prove that the simulation's setting is correct. The more accuracy compares of the data as well as the percentage error will be discussed in Section 4.3.2, validation of results. Besides that, the results of correlation statistical analysis between the results of from journal and simulation are presented in Figure 4.8. As can be seen, the datapoints of simulation velocity in the journal and CFD simulation are tightly bunched together. It indicated a precise results and smaller standard deviation.

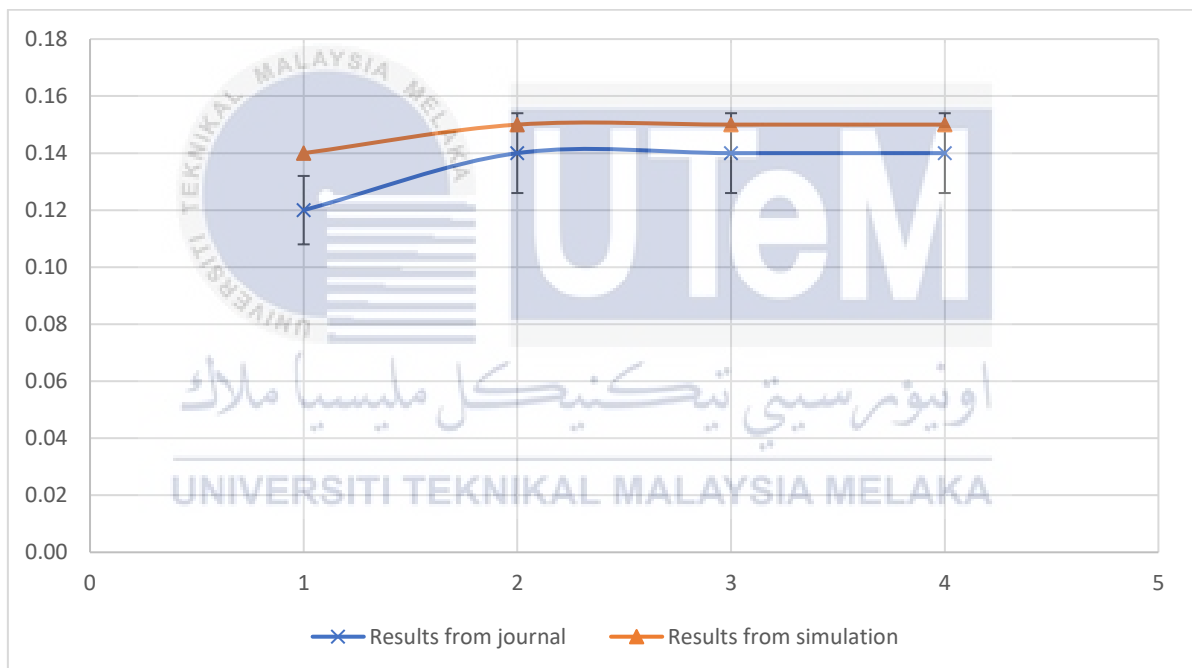
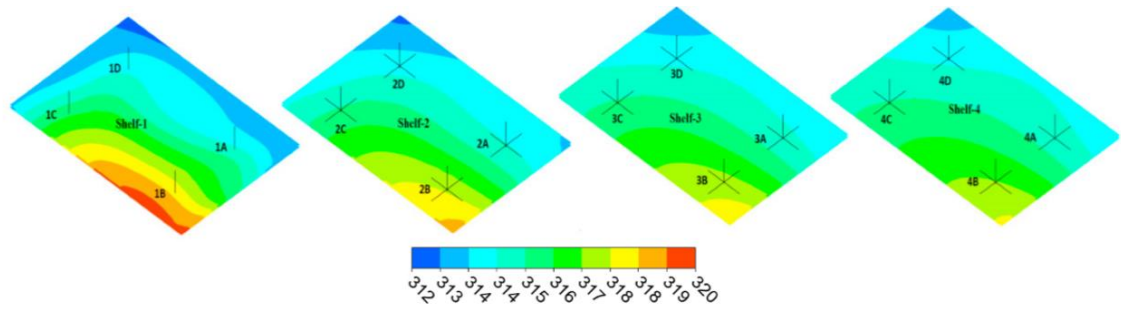
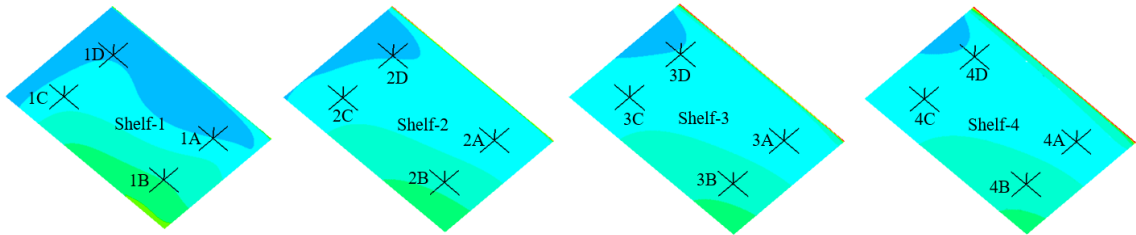


Figure 4.8: Comparison of the Result at four rack shelves of Simulation Velocity from the Journal and Simulation

Figure 4.9 shows the contour plot of temperature distribution within the drying chamber of the four rack shelves from the journal and with the results from the simulation. 4 points are tabulated on each rack shelves for getting the temperature data. The temperature distribution is all measured in Kelvin.



(a) Result from journal (Demissie et al., 2019)



(b) Result from simulation

Figure 4.9: Validated Results of Contour Profile of temperature distribution on the four rack shelves

The CFD simulation results are compared with two hours averaged temperature measurement on four points on each of the shelves rack. Figure 4.10 shows the comparison of the result of simulation temperature on four points on each of the rack shelves from the journal and simulation. It reported a good correlation between the simulation temperature from the journal and CFD velocity simulation as the simulation from the journal is directly proportional to the results in CFD simulation.

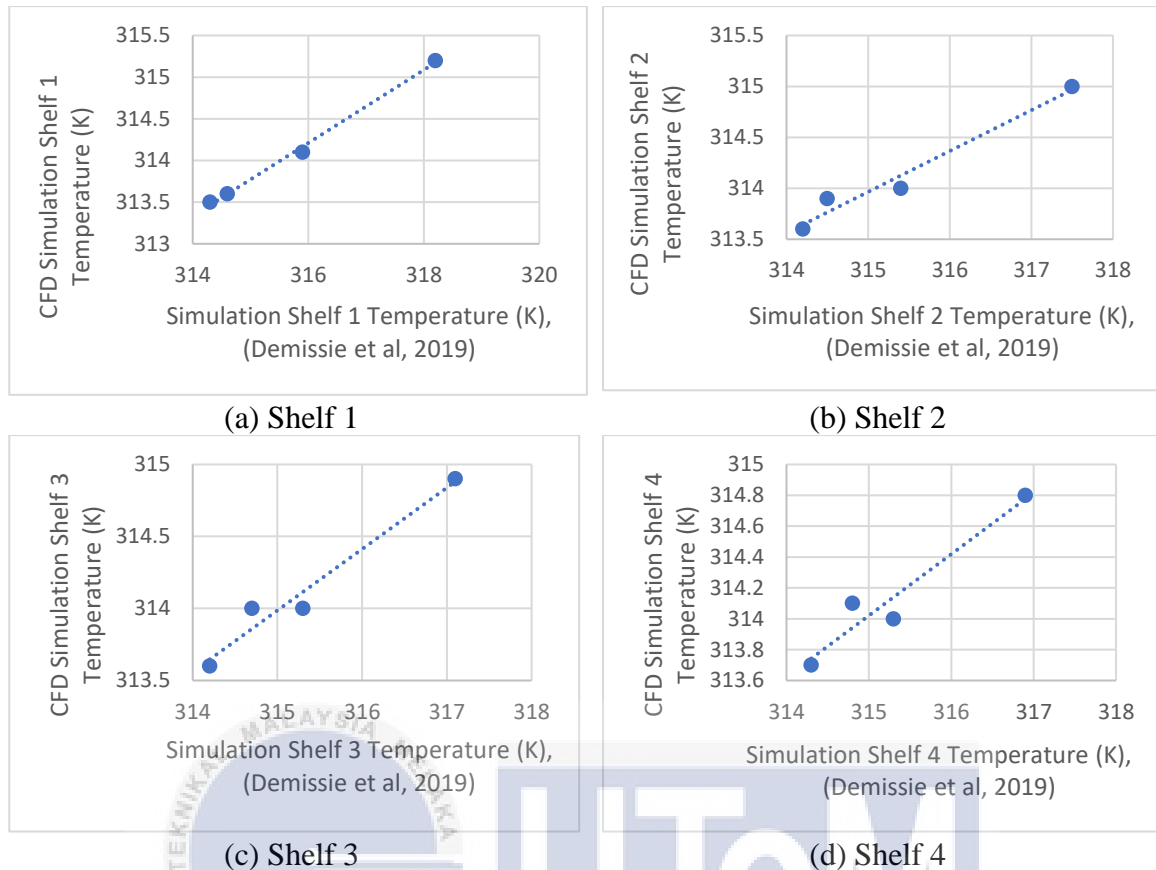
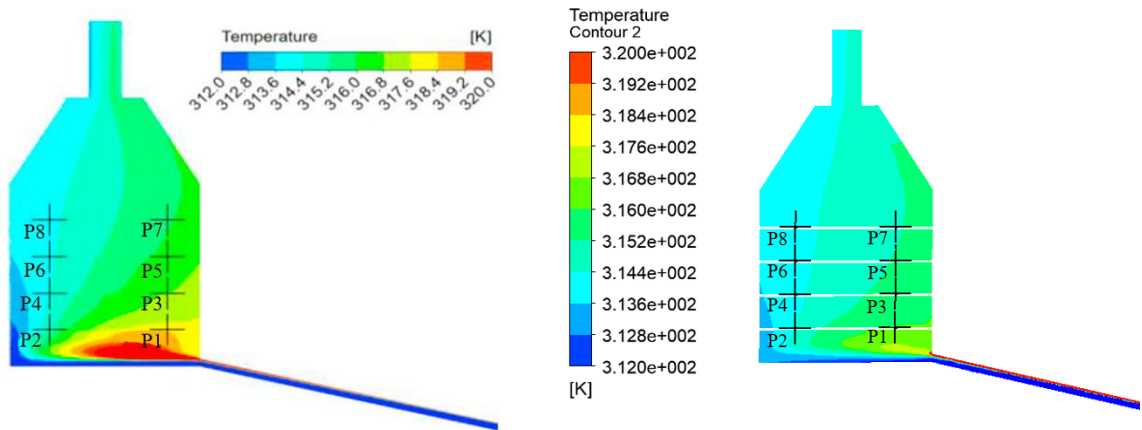


Figure 4.10: Comparison of The Result of Simulation Temperature on Four Points on Each of The Rack Shelves from The Journal and Simulation

Figure 4.11 shows the comparison of contour profile of temperature distribution on the symmetry plane from the journal and with the results from the simulation. Figure 4.12 shows the comparison of the result of simulation temperature on the symmetry plane of the drying chamber from the journal and simulation. As can be seen from the graph, the error bar shows the large overlap between result from journal and simulation as it indicates the results are almost likely to be significantly similar. Thus, it shows the high accuracy of results verification from journal and CFD simulation.



(a) Result from journal  
(Demissie et al., 2019)

(b) Result from simulation

Figure 4.11: Validated Results of Contour Profile of temperature distribution on the symmetry plane dividing the two halves of the drying chamber

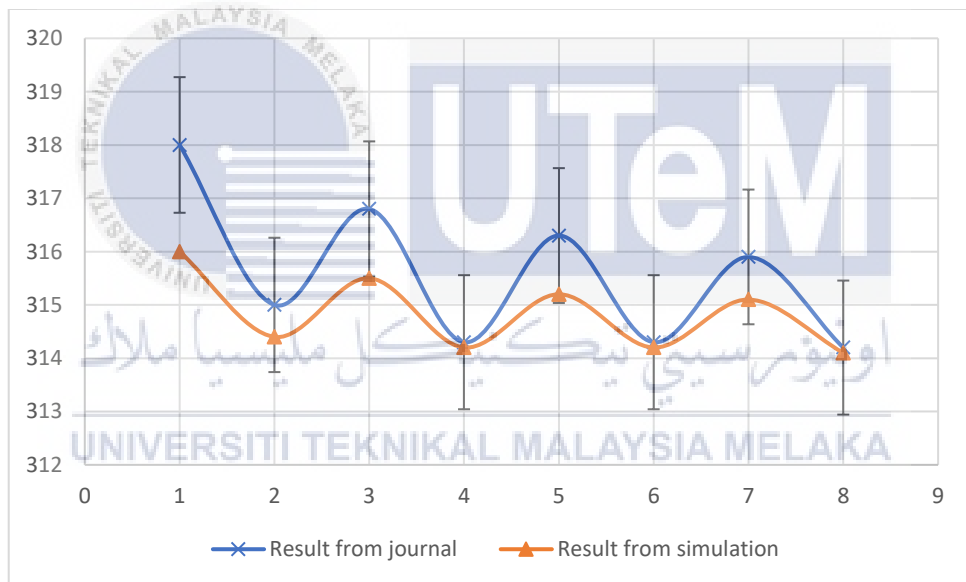


Figure 4.12: Comparison of the Result of Simulation Temperature Distribution on the symmetry plane of the drying chamber from the Journal and Simulation

Figure 4.13 shows the prediction of the streamline of the air velocity from inlet to outlet. The number of points used is 50. This result is obtained from the simulation by using ANSYS Fluent software.

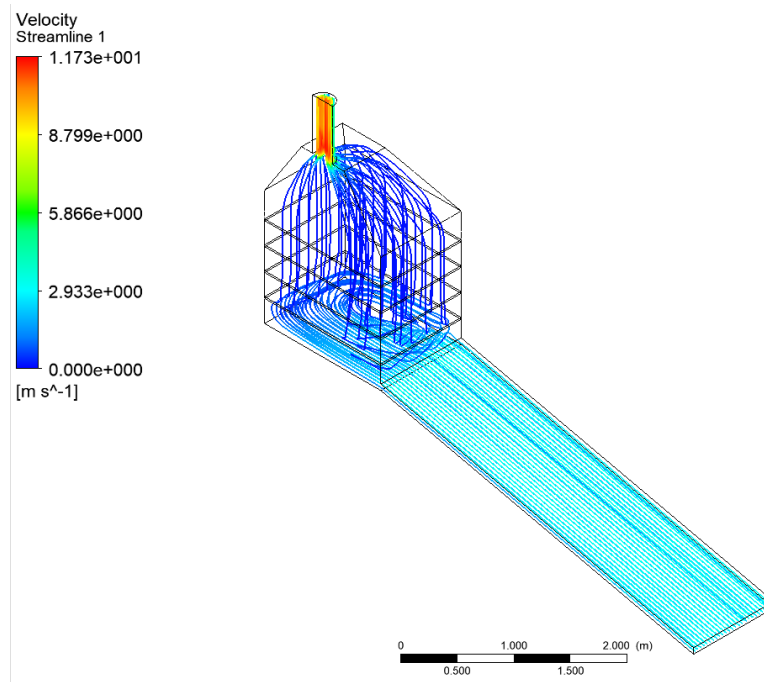


Figure 4.13 The analysis of streamline by using ANSYS Fluent

The prediction of the streamline of the air velocity from inlet to outlet shows in Figure 4.13. It analyzes that the velocity is higher at the bottom of the shelf rack as compare to the others shelves due to the cooling of air in the drying chamber. The inside of drying chamber is evolving in a steading operating temperature of 315 K.

### 4.3.2 CFD Simulation Validation Results

Table 4.1 and Table 4.2 shows the comparison of temperature distributions from the experiment and CFD modelling on each rack shelves from journal and CFD simulation and the comparison of temperature distributions from the experiment and CFD modelling on the symmetry plane from journal and CFD simulation respectively.

Table 4.1: Comparison Data Results of Air Temperature Distributions on each rack shelves between the experiment and CFD modelling from journal and CFD simulation.

Shelf Location	1				2				3				4				Avg
	1A	1B	1C	1D	2A	2B	2C	2D	3A	3B	3C	3D	4A	4B	4C	4D	
Experiment from journal	315.5	314.7	314.1	314.9	317	313.2	312.6	314.4	314.7	314.2	313.2	313.1	316.3	317	313.3	313.4	314.5
Simulation from journal	314.6	318.2	315.9	314.3	314.5	317.5	315.4	314.2	314.7	317.1	315.3	314.2	314.8	316.9	315.3	314.3	315.5
Difference between Experiment & Simulation in journal	0.9	3.5	1.8	0.6	2.5	4.3	2.8	0.2	0	2.9	2.1	1.1	1.5	0.1	2	0.9	1.7
Deviation between Experiment & Simulation in journal (%)	0.3	1.1	0.6	0.2	0.8	1.4	0.9	0.1	0.0	0.9	0.7	0.4	0.5	0.0	0.6	0.3	0.6
CFD Simulation	313.6	315.2	314.1	313.5	313.9	315.0	314.0	313.6	314.0	314.9	314.0	313.6	314.1	314.8	314.0	313.7	314.1
Difference between Experiment & CFD Simulation	1.9	0.5	0	1.4	3.1	1.8	1.4	0.8	0.7	0.7	0.8	0.5	2.2	2.2	0.7	0.3	1.2
Deviation between Experiment & CFD Simulation (%)	0.6	0.2	0.0	0.4	1.0	0.6	0.4	0.3	0.2	0.2	0.3	0.2	0.7	0.7	0.2	0.1	0.4

Table 4.2: Comparison Data Results of Temperature Distributions on symmetry plane between the experiment and CFD modelling from journal and CFD simulation.

Location	P1	P2	P3	P4	P5	P6	P7	P8	Avg
Experiment (Demissie et al, 2008)	314.2	314.4	313.9	313.6	312.9	313.9	313.4	313.7	313.8
Simulation (Demissie et al, 2008)	318.0	315.0	316.8	314.3	316.3	314.3	315.9	314.2	315.6
Difference between Experiment & Simulation in journal	3.8	0.6	2.9	0.7	3.4	0.4	2.5	0.5	1.9
Deviation between Experiment & Simulation in journal (%)	1.2	0.2	0.9	0.2	1.1	0.1	0.8	0.2	0.6
CFD Simulation	316	314.4	315.5	314.2	315.2	314.2	315.1	314.1	314.8
Difference between Experiment & CFD Simulation	1.8	0	1.6	0.6	2.3	0.3	1.7	0.4	1.1
Deviation between Experiment & CFD Simulation (%)	0.6	0.0	0.5	0.2	0.7	0.1	0.5	0.1	0.3

CFD simulation validate of results can be done by comparing the data obtain from experiment (Demissie et al., 2019) and CFD simulation. In the step of validation, it is importance to obtain the percentage error less than 5% to convince that the result obtained from simulation are correct. As can be seen from Table 4.1, the range between the difference of the experiment and CFD simulation on each rack shelves are 0 to 2.2, which indicates 0 to 0.7% deviation. Besides that, the smaller and largest difference between the experiment and CFD simulation in symmetry plane of the drying chamber in Table 4.2 is 0 and 2.3 respectively, which is 0 and 0.7% deviation. The deviation of validation result in the four selves rack and symmetry plane is both less than 5% which is only 0.7%. Besides that, the percentage deviation between experiment and CFD simulation is smaller than the simulation from journal. It shows that it is preferable on CFD simulation as compare to journal. The validation of results is successful in this CFD simulation.

## 4.4 CFD Modelling on Drying Chamber integrated with Solar Collector

### 4.4.1 Modified Design on Solar Collector

Figure 4.14 shows the contour plot temperature distribution and velocity distribution of modified design of solar collector respectively.

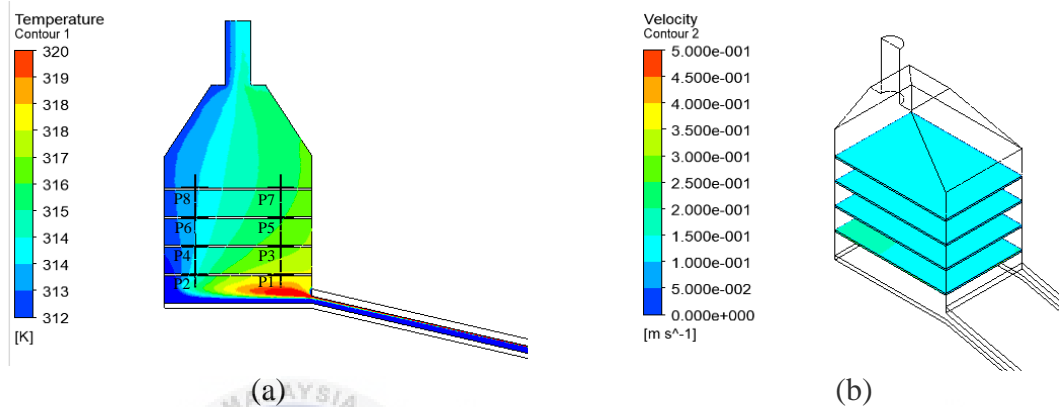


Figure 4.14: Contour Plot of Modified Design of Solar Collector

Table 4.3 and 4.4 shows the temperature and velocity distributions on the symmetry plane and four rack shelves of the modified design of solar collector respectively. As shown in the Figure 4.14 and Table 4.3, the adding of glass and insulation has significantly improve the temperature and prevent the heat losses from drying chamber to surrounding. The mean temperature distribution in the drying chamber has increase from 314.8K to 315.1K.

Table 4.3: Temperature Distributions on the symmetry plane of the Modified Enhancement on Solar Collector

Location	P1	P2	P3	P4	P5	P6	P7	P8	Avg
Temperature(K)	317.7	314.1	316.5	313.7	315.9	313.5	315.7	313.5	315.1

Table 4.4: Velocity Distributions on four rack shelves of Modified Design of Solar Collector

Design Plane	Velocity (m/s)				
	1	2	3	4	Avg
Temperature(K)	0.1450	0.1448	0.1448	0.1448	0.1449

#### 4.4.2 Parameter 1: Different Area of Air Vent Inlet

Figure 4.15 shows the contour plot of temperature distribution of the drying chamber integrated with solar collector at different area of air vent inlet (a), (b), (c).

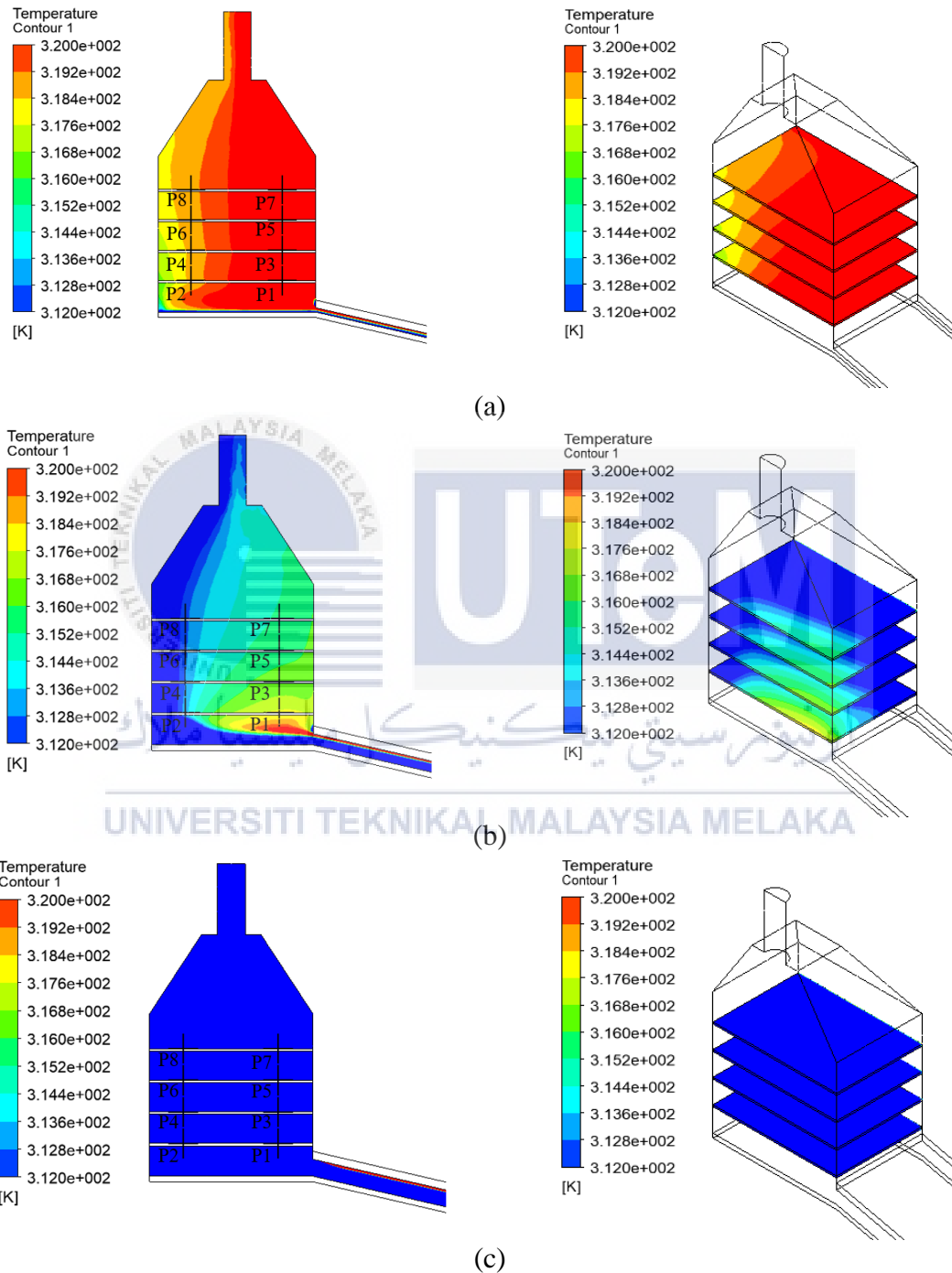


Figure 4.15: Contour Plot of Temperature Distribution at Different Area of Air Vent inlet (a), (b), (c)

Figure 4.16 shows the contour plot of velocity distribution in the drying chamber integrated with solar collector at different air inlet area (a), (b), (c) respectively.

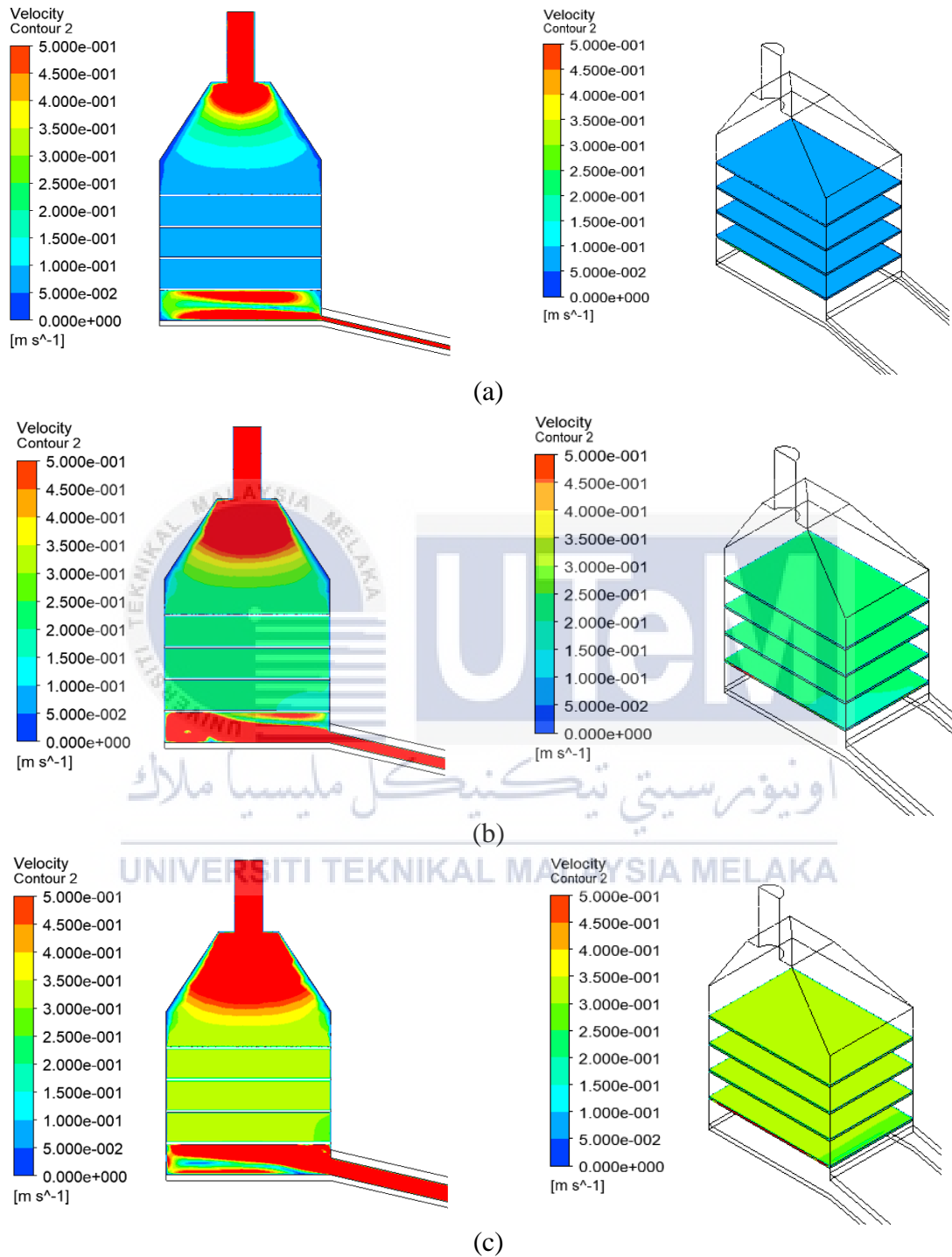


Figure 4.16: Contour Plot of Velocity Distribution at Different Air Inlet Area (a), (b), (c)

Table 4.5 and Table 4.6 shows the temperature distributions on the symmetry plane and four rack shelves of the parameter 1 at different air inlet area (a), (b), (c). Figure 4.17 and Figure 4.18 shows the predicted graph temperature and velocity distribution by CFD simulation of Parameter 1 against 8 points located on the symmetry plane and 4 rack shelves.

Table 4.5: Temperature Distributions on the symmetry plane of Parameter 1 at different air inlet area (a), (b), (c)

Location	P1	P2	P3	P4	P5	P6	P7	P8	Avg
(a)	321.4	318.6	321.4	318.6	321.3	318.9	321.3	319.0	320.1
(b)	317.8	313.2	316.4	312.8	315.7	312.6	315.3	312.5	314.5
(c)	308.3	305.3	308.1	305.3	308.1	305.3	308.1	305.3	306.7

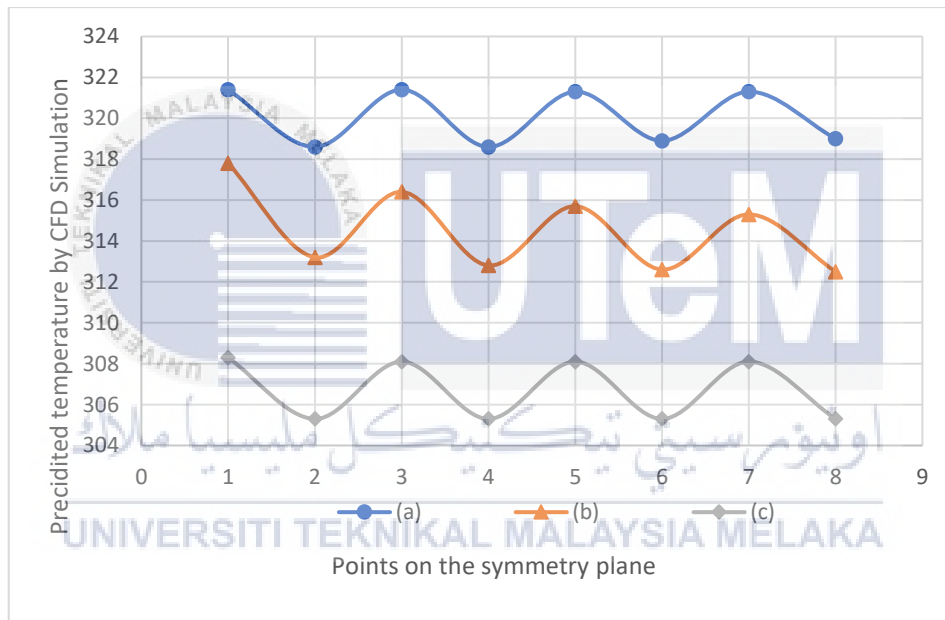


Figure 4.17: Predicted Temperature by CFD Simulation of Parameter 1 against 8 points located on the symmetry plane.

Table 4.6: Velocity Distributions on the four rack shelves of the Parameter 1 at different air inlet area (a), (b), (c)

Design Plane	Velocity (m/s)				
	1	2	3	4	Avg
(a)	0.0829	0.0828	0.0828	0.0827	0.0828
(b)	0.2070	0.2069	0.2069	0.2068	0.2069
(c)	0.3102	0.3104	0.3104	0.3102	0.3103

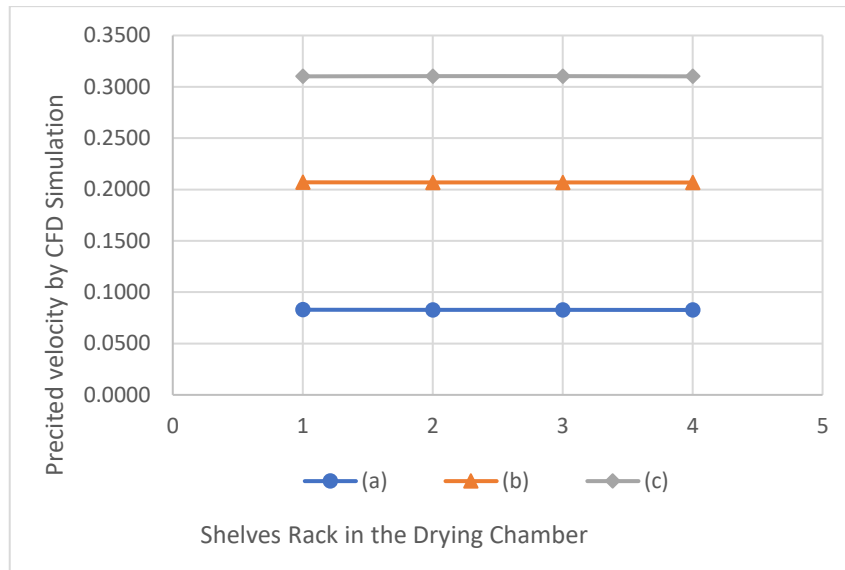


Figure 4.18: Predicted Air Velocity by CFD Simulation of Parameter 1 against the four rack shelves

All the design is different with the air inlet area, which is  $0.08\text{m}^2$ ,  $0.2\text{m}^2$  and  $0.3\text{m}^2$ . Although, the velocity profiles for all the designs are reasonable and considered uniform in Figure 4.18, the temperature distribution on the symmetry plane are different for the inlet area of drying chamber integrated with solar collector. The parameter (a) in Figure 4.17 with the inlet area of  $0.08\text{m}^2$  shows the highest temperature among the rest of the inlet area. The temperature range is between 318 K to 322 K is suitable for agriculture food to be dried. Parameter 1 (a) is selected to continue improve with the temperature and velocity work.

#### 4.4.3 Parameter 2: Different Gap Size Between Each Rack Shelves

Figure 4.19 shows the contour plot of temperature distribution in the drying chamber integrated with solar collector at different gap size between the rack shelves (a), (b), (c).

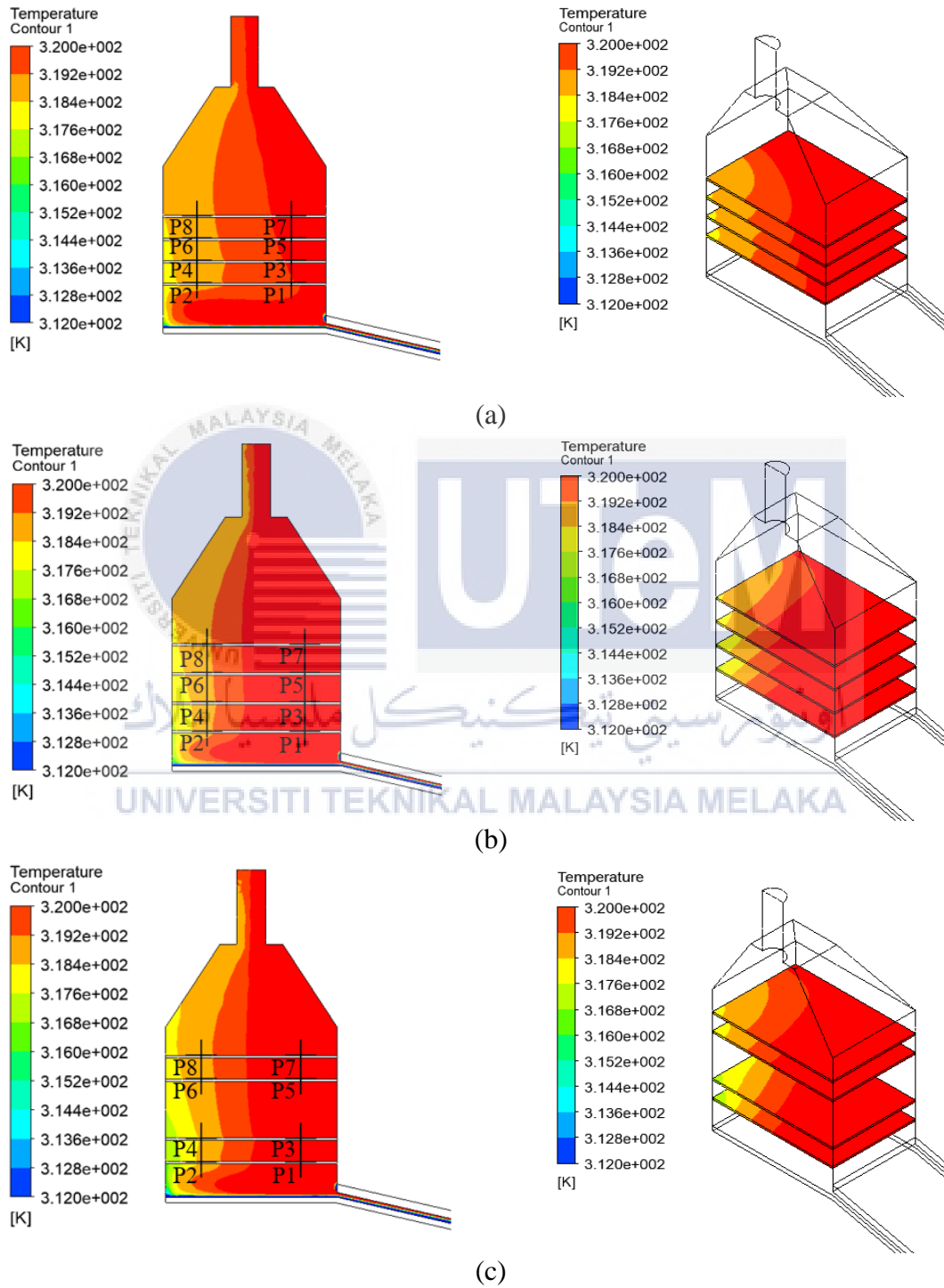


Figure 4.19: Contour Plot of Temperature Distribution at Different Gap Size between Each Rack Shelves (a), (b), (c)

Figure 4.20 shows the contour plot of velocity distribution in the drying chamber integrated with solar collector at different gap size between the rack shelves (a), (b), (c) respectively.

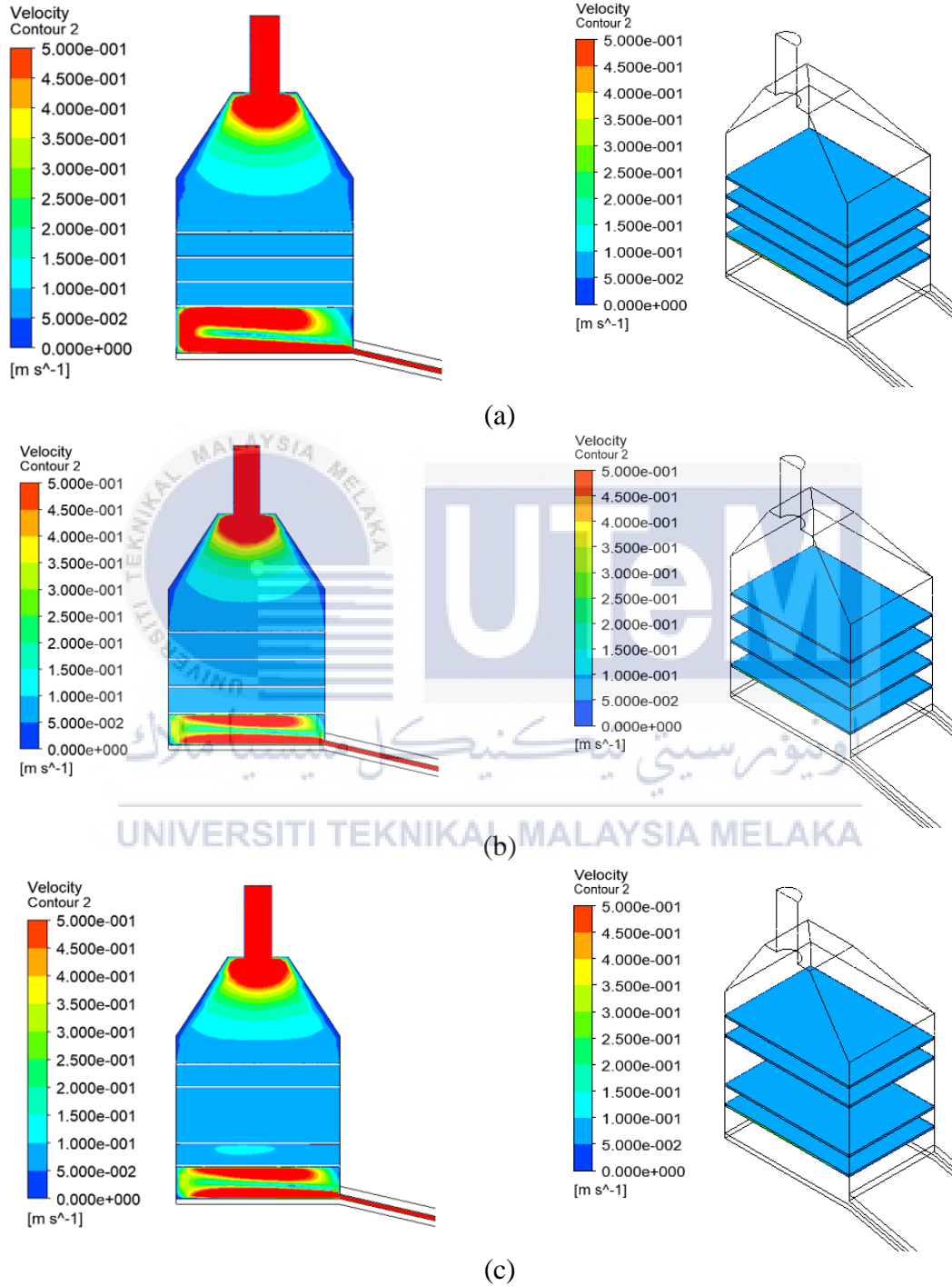


Figure 4.20: Contour Plot of velocity distribution at different gap size between each rack shelves (a), (b), (c)

Table 4.7 and Table 4.8 shows the temperature distributions on the symmetry plane of the Parameter 2 at different gap size (a), (b), (c). Figure 4.21 and Figure 4.22 shows the predicted graph temperature and velocity distribution by CFD simulation of Parameter 2 against 8 points located on the symmetry plane and 4 rack shelves respectively.

Table 4.7: Temperature Distributions on the symmetry plane of Parameter 2 at different gap size between each rack shelves (a), (b), (c)

Location	P1	P2	P3	P4	P5	P6	P7	P8	Avg
(a)	319.9	318.8	320.1	318.7	320.1	318.8	320.2	318.9	319.4
(b)	321.5	319.0	321.4	318.9	321.4	319.0	321.4	319.1	320.2
(c)	321.0	318.6	321.0	318.5	321.0	318.9	321.0	318.9	319.9

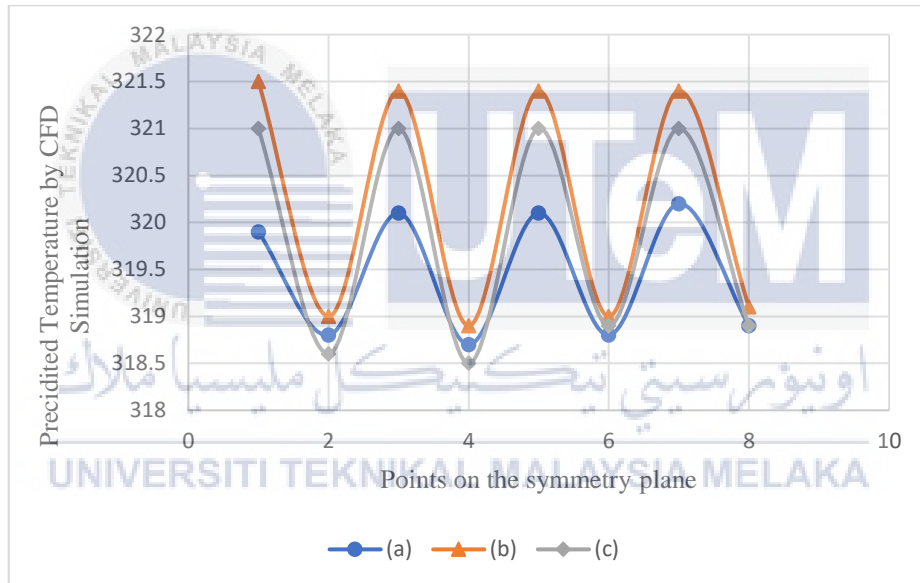


Figure 4.21: Predicted Temperature by CFD Simulation of Parameter 2 against 8 points located on the symmetry plane.

Table 4.8: Velocity Distributions on the four rack shelves of the Parameter 2 at different gap size between each rack shelves (a), (b), (c)

Design Plane	Velocity (m/s)				
	1	2	3	4	Avg
(a)	0.0829	0.0828	0.0828	0.0827	0.0828
(b)	0.0828	0.0828	0.0828	0.0827	0.0828
(c)	0.0829	0.0828	0.0828	0.0827	0.0828

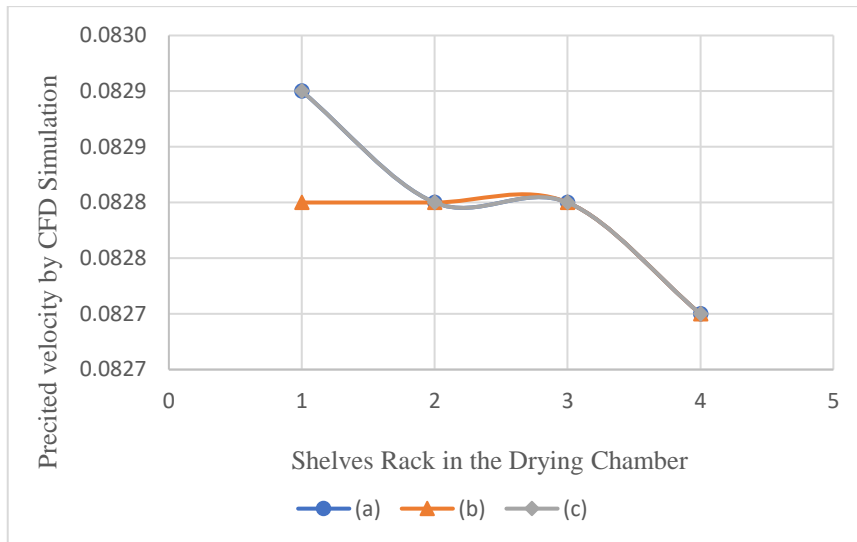


Figure 4.22: Predicted Air Velocity by CFD Simulation of Parameter 2 against the four shelves rack in the drying chamber

The inlet area of all the design of drying chamber are fixed at a constant dimension which is  $0.08\text{m}^2$ . As shown in Figure 4.21, it is clearly displayed that the most uniformity distribution of temperature of all the design are parameter (a) with 0.2m of gap size between the shelves rack. From Table 4.8, it also shown that the velocity only shows a small discrepancy on each rack shelf.

#### 4.4.4 Parameter 3: Difference Tilt Angle of Solar Collector

Figure 4.23 shows the contour plot of temperature distribution in the drying chamber integrated with solar collector at different tilt angle of solar collector (a), (b), (c).

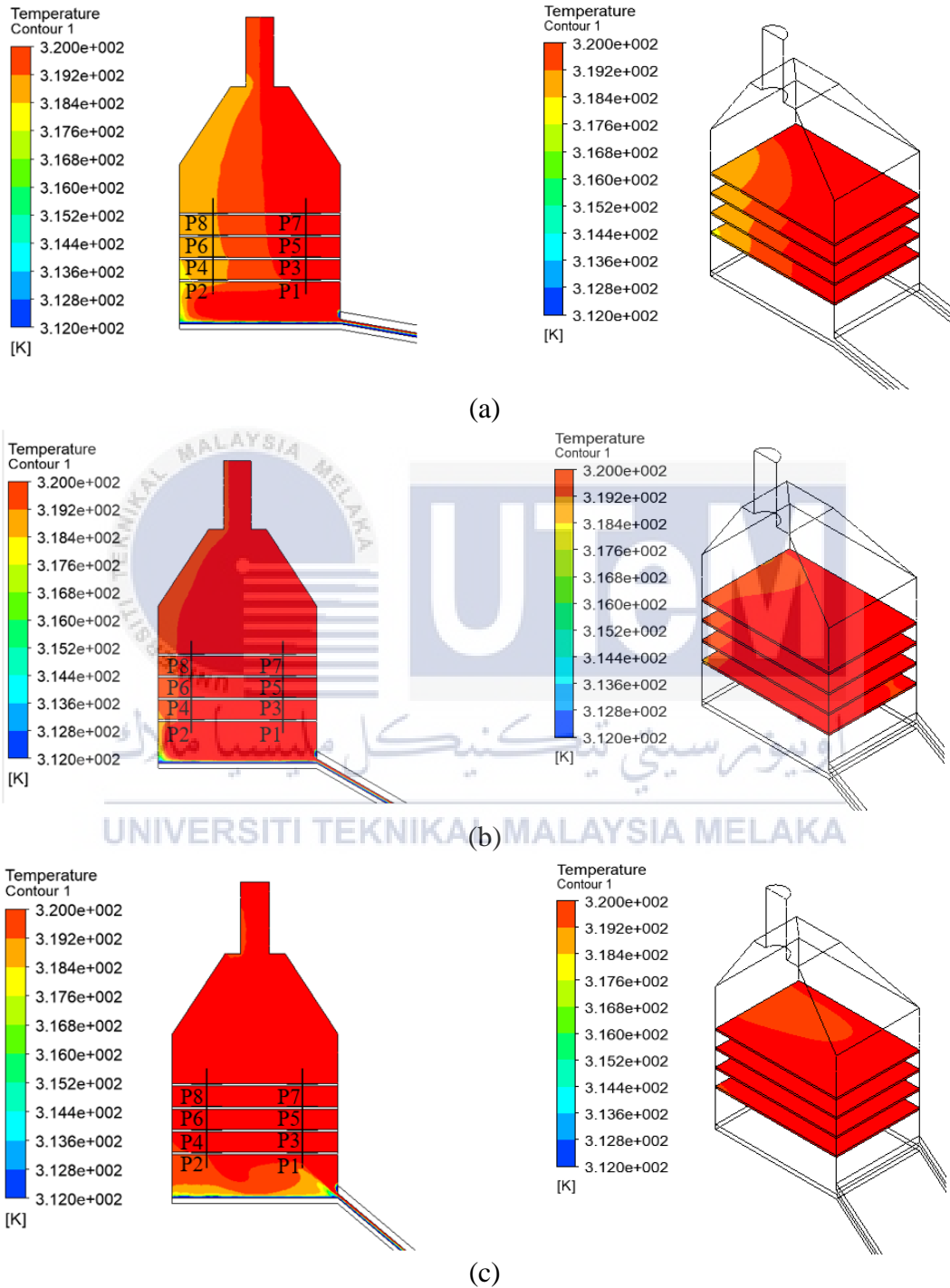


Figure 4.23: Contour Plot of temperature distribution on Parameter 3 of Drying Chamber integrated with Solar Collector at different Angle (a), (b), (c)

Figure 4.24 shows the contour plot of velocity distribution in the drying chamber integrated with solar collector at different solar collector angle (a), (b), (c) respectively.

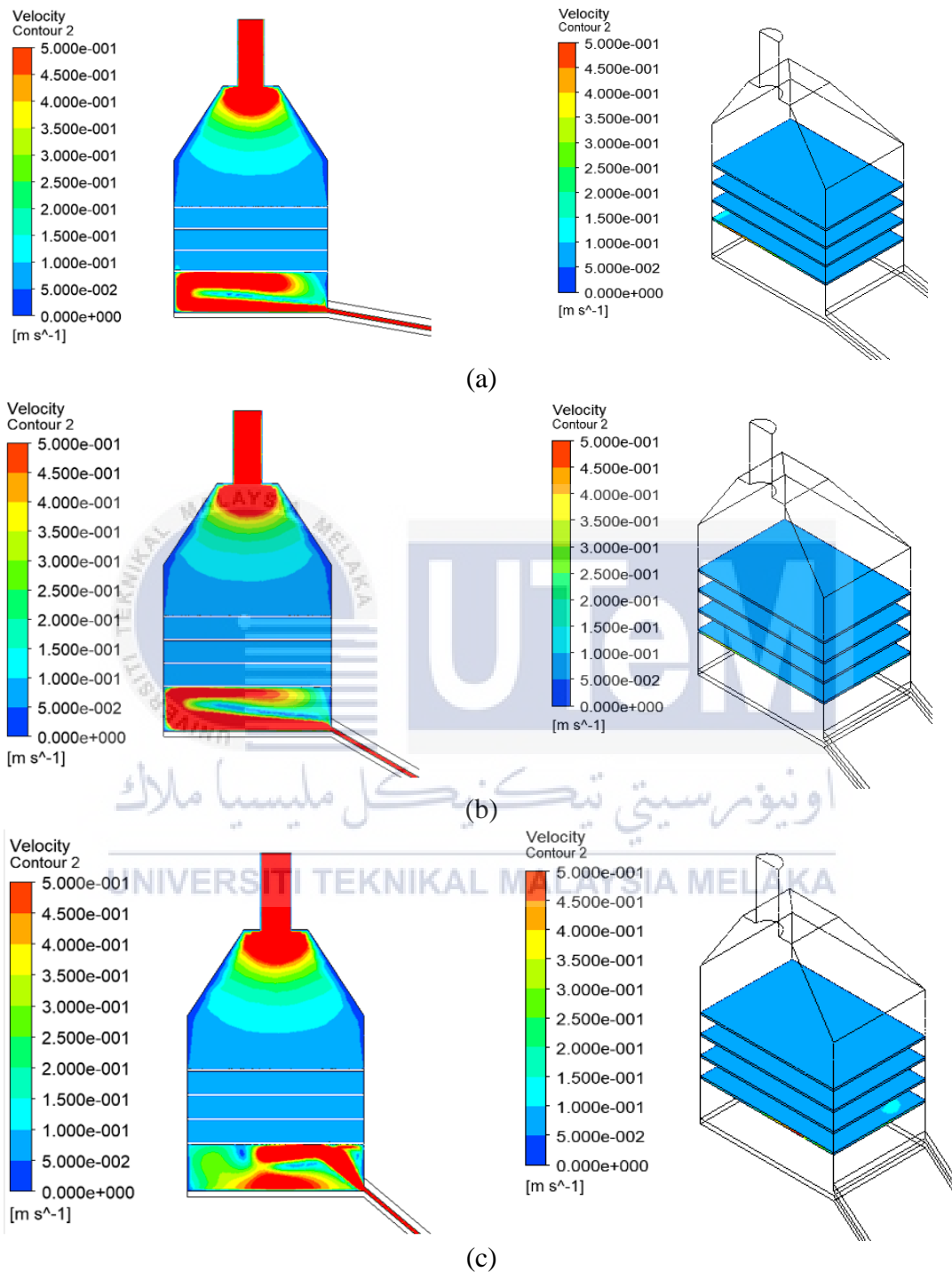


Figure 4.24: Contour Plot of velocity distribution on Parameter 3 of Drying Chamber integrated with Solar Collector at different tilt angle of solar collector (a), (b), (c)

Table 4.9 and Table 4.10 shows the temperature distributions on the symmetry plane of the parameter 3 at different solar collector angle (a), (b), (c). Figure 4.27 and Figure 4.28 shows the predicted graph temperature and velocity distribution by CFD simulation of Design 3 against 8 points located on the symmetry plane and the four rack shelves respectively.

Table 4.9: Temperature Distributions on the symmetry plane of the Parameter 3 at different tilt angle of solar collector (a), (b), (c)

Location	P1	P2	P3	P4	P5	P6	P7	P8	Avg
(a)	320.3	318.9	320.1	318.9	320.4	319.1	320.4	319.1	320.3
(b)	321.4	320.7	321.3	320.4	321.3	320.4	321.2	320.4	321.4
(c)	322.3	320.1	322.4	320.3	322.4	320.3	322.3	320.3	322.3

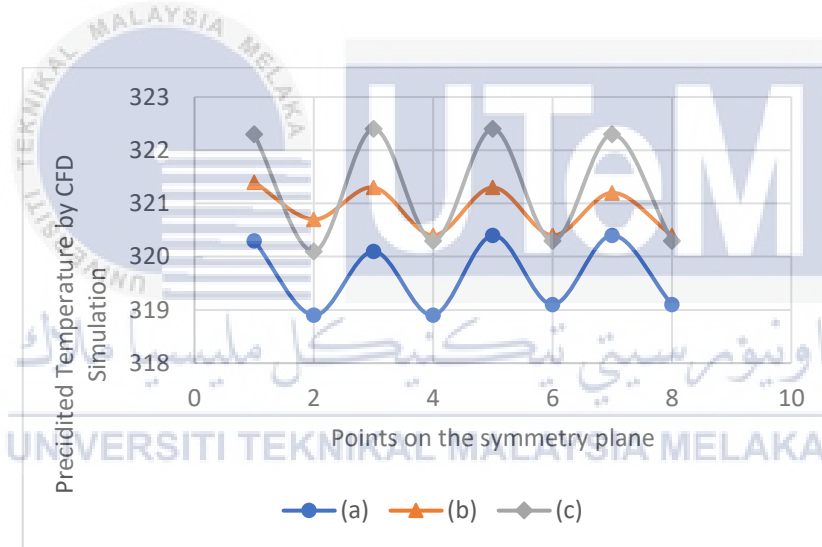


Figure 4.25: Predicted Temperature by CFD Simulation of Parameter 3 against 8 points located on the symmetry plane.

Table 4.10: Velocity Distributions on the symmetry plane of the Parameter 3 at different tilt angle of solar collector (a), (b), (c)

Design Plane	Velocity (m/s)				
	1	2	3	4	Avg
(a)	0.0829	0.0828	0.0828	0.0827	0.0828
(b)	0.0829	0.0828	0.0828	0.0827	0.0828
(c)	0.0821	0.0828	0.0828	0.0827	0.0826

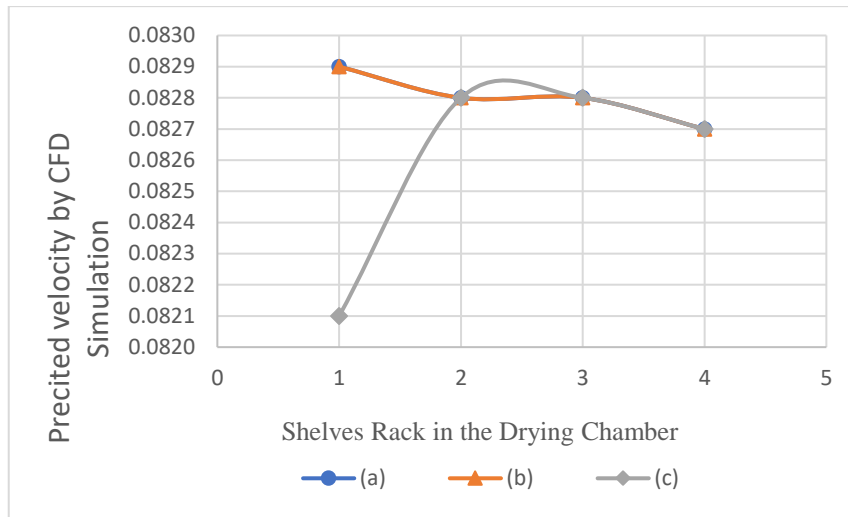


Figure 4.26: Predicted Air Velocity by CFD Simulation of Parameter 3 against the four shelves rack

Figure 4.25 shows the graph comparing the temperature distributions for the drying chambers integrated with solar collector simulated with difference angle of solar collector which is 10 °, 30 ° and 40 °. The maximum average temperature along the symmetry plane of the drying chamber is only 1 K. From Figure 4.25 and Figure 4.26, parameter 3 (b) shows more stable and uniform air temperature and velocities distribution compare to other designs of drying chamber.

#### 4.5 The Best Configurations of the Trays

Last but not least, based on the data obtained from the CFD simulation as tabulated in Table 4.5, 4.6, 4.7, 4.8, 4.9 and 4.10 it can be concluded that the design with the best configurations is with  $0.08\text{m}^2$  of air inlet area,  $0.2\text{m}$  of gap size between each rack shelves and  $30^\circ$  of tilt solar collector angle. This design had achieved uniformity in terms of velocity and temperature distribution simultaneously. Therefore, the propose parameter for the best performance in term uniformity distribution is design 3 (b) which shown in Figure 4.27.

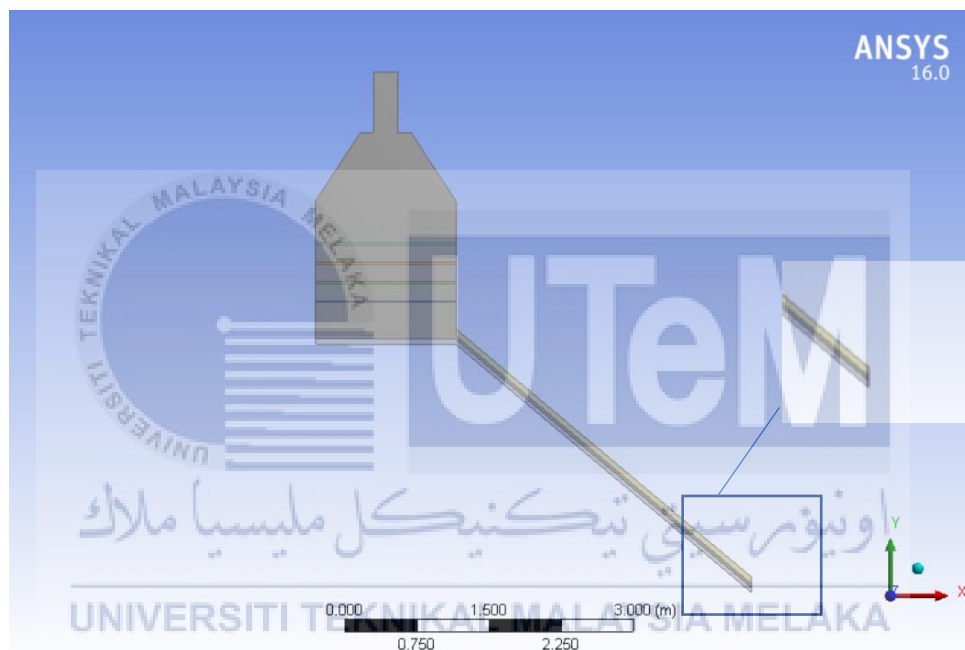


Figure 4.27: Propose Design for The Best Performance in Term Uniformity Distribution

## CHAPTER 5

### CONCLUSION AND RECOMMENDATIONS

#### 5.1 Conclusion

Overall, this project had achieved satisfied simulation results with a uniformity temperature and air flow velocity distribution in the drying chamber integrated with solar collector. Transient- state 3D CFD simulations are conducted in this project. The validation of results was done by comparing the velocity and temperature distributions from the experimental data in journal. The comparison is able to show that the steps in simulating the solar drier are correct. Based on the verification and validation results, it shows that the maximum velocities are observed in the solar collector and at the chimney. Besides, as can be seen in the temperature contour plot, the symmetry plane exhibits higher temperature at the bottom of drying chamber and distributed more evenly at the outlet of chimney. To achieve objective; to propose a design of drying chamber integrated with solar collector. Three different parameters are considered in the design to improve the weakness of solar drier in the journal studies. The best configuration on parameter in the modified design of drying chamber integrated with solar collector are 0.08m<sup>2</sup> air vent inlet area, 0.2m gap size between each rack shelves and 30 ° of tilt solar collector angle. The mean temperature and velocity obtain in the CFD simulation are 320.4K and 0.08m/s respectively. In order to achieve objective i: to investigate the temperature and velocity distribution in the drying chamber integrated solar collector, the temperature and velocity distribution at the symmetry plane of drying chamber integrated with solar collector are studies. Lastly objective ii; to

investigate the temperature and velocity distribution on each level of shelf trays within the drying chamber; the expected results on each rack shelves were discussed in Chapter 4.

## 5.2 Recommendation for Future Work

As recommendation, there are several suggestions that can be included for the improvement of air flow and temperature distribution in drying chamber for the future work. First, it is recommended to resize the dimension of drying chamber. it is one of the parameters that should be consider in the CFD simulation. Besides that, the solar collector is suggested to design in an adjustable and flexible angle to ensure the best fit based on solar elevation. This is because the tilt angle of solar collector will depend on the latitude based on different region. Lastly, the actual drying chamber integrated with solar collector should be developed for agriculture product for experiment purpose to validate the simulation data.



## REFERENCES

A. Nakayama, F. Kuwahara, Algebraic model for thermal dispersion heat flux within porous media, *AIChE J.* 51 (2005) 2859–2864.

Abdenouri, N., Zoukit, A., Elferouali, H., Salhi, I., & Doubabi, S. (2018). Mathematical modeling of an innovative hybrid solar-gas dryer. *Proceedings of 21th International Drying Symposium*. doi: 10.4995/ids2018.2018.7523

Abdullah, A. L., Misha, S., Tamaldin, N., Rosli, M., & Sachit, F. (2020). Theoretical study and indoor experimental validation of performance of the new photovoltaic thermal solar collector (PVT) based water system. *Case Studies in Thermal Engineering*, 18, 100595. doi:10.1016/j.csite.2020.100595

Aissa, W., El-Sallak, M., & Elhakem, A. (2014). Performance of solar dryer chamber used for convective drying of sponge-cotton. *Thermal Science*, 18(suppl.2), 451–462. doi: 10.2298/tsci110710084a

Al-Busoul, M. (2017). Design of Fruits Solar Energy Dryer under Climatic Condition in Jordan. *Journal of Power and Energy Engineering*, 05(02), pp.123-137.

Al-Neama, Maytham & Farkas, I. (2018). Utilization of Solar Air Collectors for Product's Drying Processes. *The Journal of Scientific and Engineering Research*. 5. 40-56.

Alqadhi, Ahmed & Misha, Suhaimi & Mohd Rosli, Mohd Afzanizam & Akop, Mohd Zaid. (2017). Design and simulation of an optimized mixed mode solar dryer integrated with desiccant material. *International Journal of Mechanical & Mechatronics Engineering*. 17.

Ambesange, N.A., & S.K., N.K. (2017). *Analysis of Flow Through Solar Dryer Duct Using CFD*.

A. O. Dissa, H. Desmorieux, J. Bathiebo, and J. Koulidiati, “Convective drying characteristics of Amelie mango (*Mangifera Indica* L. cv. ‘Amelie’) with correction for shrinkage,” *J. Food Eng.*, vol. 88, no. 4, pp. 429–437, Oct. 2008.

Arinze E.A., J.S. Sokhansanj, G.J. Schoenu and F.G. Trauttmansdorff. (1996). Experimental evaluation, simulation and optimization of a commercial heated-air batch hay drier: Part 1, drier functional performance, product quality, and economic analysis of drying. *Journal of Agricultural Engineering Research*, 63, 301-314

Boughali, S, Benmoussa, H, Bouchekima, B, Mennouch, D, Bouguettaia, H, Bechki, D. Crop drying by indirect active hybrid solar-electrical dryer in the eastern Algerian Septentrional Sahara. *Solar Energy* 2009; 83(12): 2223-2232. DOI: <https://doi.org/10.1016/j.solener.2009.09.006>.

Belloulid, M.O., Hamdi, H, Mandi, L, Ouazzani, N., Solar drying of wastewater sludge: a case study in Marrakesh, Morocco. *Environmental Technology (United Kingdom)* 2018; 1–7. DOI: 10.1080/09593330.2017.1421713.

B. Yesilata and M. A. Aktacir, “A simple moisture transfer model for drying of sliced foods,” *Appl. Therm. Eng.*, vol. 29, no. 4, pp. 748–752, Mar. 2009.

Caparanga, A. R., Reyes, R. A. L., Rivas, R. L., Vera, F. C. D., Retnasamy, V., & Aris, H. (2017). Effects of air temperature and velocity on the drying kinetics and product particle size of starch from arrowroot (*Maranta arundinacea*). *EPJ Web of Conferences*, 162, 01084. doi: 10.1051/epjconf/201716201084

Cengel, Y.A. (1998). Fundamentals of thermal radiation. Heat transfer: A practical approach (pp. 561-604). Boston, Mass: WBC McGraw-Hill.

Chabane, F., Bensahal, D., Brima, A., & Moumami, N. (2019). Solar drying of drying agricultural product (Apricot). *Mathematical Modelling of Engineering Problems*, 6(1), 92–98. doi: 10.18280/mmep.060112

Chegg.com. (2009). Retrieved from <https://www.chegg.com/homework-help/definitions/transient-period-31>.

Christian, C. Milioli & Fernando E. Milioli. (2009). On the statistical steady state gas-solid flow in a riser as predicted through a two-fluid simulation. *Thermal and Fluids Engineering Laboratory EESC - School of Engineering of São Carlos, USP - University of São Paulo Av. Trabalhador São-Carlense, 400, 13566-590 São Carlos, SP, Brazil.*

C. Lamnatou, E. Papanicolaou, V. Belessiotis, and N. Kyriakis, “Conjugate Heat and Mass Transfer from a Drying Rectangular Cylinder in Confined Air Flow,” *Numer. Heat Transf. Part A Appl.*, vol. 56, no. 5, pp. 379-405, 2009.

Cyprien. (2013). Steady State VS Transient State FE Analysis. Retrieved from <http://feaforall.com/steady-vs-transient-state-fea-analysis/>

Demissie, P., Hayelom, M., Kassaye, A., Hailesilassie, A., Gebrehiwot, M., & Vanierschot, M. (2019). Design, development and CFD modeling of indirect solar food dryer. *Energy Procedia*, 158, 1128–1134. doi: 10.1016/j.egypro.2019.01.278

Dina, S. F., Ambarita, H., Napitupulu, F. H., & Kawai, H. (2015). Study on effectiveness of continuous solar dryer integrated with desiccant thermal storage for drying cocoa beans. *Case Studies in Thermal Engineering*, 5, 32–40. doi: 10.1016/j.csite.2014.11.003

G. E. Page, “Factors influencing the Maximum Rates of Air Drying Shelled Corn in Thin Layers,” Purdue University, 1949.

Garbs, M. (2015) ‘Pinch Analysis and Process integration: a User Guide on Process integration for the Efficient Use of Energy’, *Journal of Cleaner Production*, 110, p. 203. doi: 10.1016/j.jclepro.2015.10.003.

Gary (June 8, 2008). Solar Collector Glazing Materials. Build it Solar. Retrieved from <https://www.builditsolar.com/Projects/SpaceHeating/Glazing.htm#:~:text=Glass%20is%20a%20good%20glazing,IR%20reduces%20heat%20loss%2C%20strong>. [Accessed 12 June 2020].

Gedeon, M. (2018, June). Thermal emissivity and radiative heat transfer. Technical Tidbits, 114. Retrieved from <https://materion.com/-/media/files/alloy/newsletters/technical-tidbits/issue-no-114-thermal-emissivity-and-radiative-heat-transfer.pdf> [Accessed 31 May 2020].

Gomez, M. A. D., Velasco, C. A. G., Ratkovich, N., & Daza, J. C. G. (2018). Numerical Analysis of a Convective Drying Chamber from Drying Air Velocity and Temperature Perspective. *Proceedings of the 3rd World Congress on Momentum, Heat and Mass Transfer*. doi: 10.11159/icmfht18.134

Ikem, I. A., Ibeh, M. I., & John, U. (2017). Estimating the efficiency of okra drying mixed-mode solar dryer. *International Journal of Engineering Research*, 6(5), 250. doi: 10.5958/2319-6890.2017.00013.7

Iranmanesh, M., Akhijahani, H. S., & Jahromi, M. S. B. (2019). CFD modeling and evaluation the performance of a solar cabinet dryer equipped with evacuated tube solar collector and thermal storage system. *Renewable Energy*, 145, 1192–1213. doi: 10.1016/j.renene.2019.06.038.

Jain, A., Sharma, M., Kumar, A., Sharma, A., & Palamanit, A. (2018). Computational fluid dynamics simulation and energy analysis of domestic direct-type multi-shelf solar dryer. *Journal of Thermal Analysis and Calorimetry*, 136(1), 173–184. doi: 10.1007/s10973-018-7973-5

Jayas D.S. & J.S. Sokhansanj. (1989). *Thin layer drying of barley at low temperatures*. Canadian Agricultural Engineering, 31, 21–23

Kalogirou, Soteris. “The Potential of Solar industrial Process Heat Applications.” *Applied Energy*, vol. 76, no. 4, 2003, pp. 337–361., doi:10.1016/s0306-2619(02)00176-9.

Kalogirou, S. A. (2014). Solar Energy Collectors. *Solar Energy Engineering*, 125–220. doi: 10.1016/b978-0-12-397270-5.00003-0

Kerr, W. L. (2013). Food Drying and Evaporation Processing Operations. *Handbook of Farm, Dairy and Food Machinery Engineering*, 317–354. doi: 10.1016/b978-0-12-385881-8.00012-4

Lucas, J. (2015, May 19). What is the first law of thermodynamics? Retrieved from <https://www.livescience.com/50881-first-law-thermodynamics.html>. [Accessed 31 May 2020].

M.A. Delele, A. Schenk, H. Ramon, B.M. Nicolai, P. Verboven, Evaluation of a chicory root cold store humidification system using computational fluid dynamics, *J. Food Eng.* 94 (2009) 110–121. doi:10.1016/j.jfoodeng.2009.03.004.

M.A. Delele, Engineering design of spraying systems for horticultural applications using computational fluid dynamics, *Status Publ.* (2009) 220.

M. A. Karim and M. N. A. Hawlader, “Mathematical modelling and experimental investigation of tropical fruits drying,” *nt. J. Heat Mass Transf.*, vol. 48, no. 23–24, pp. 4914–4925, Nov. 2005

Mat, Sohif, et al. (2018). Development and Performance Analysis of New Solar Dryer with Continuous and intermittent Ventilation. *Jurnal Kejuruteraan*, vol. SI1, no. 3, 2018, pp. 1–8., doi:10.17576/jkukm-2018-si1(3)-01.

Misha, S., Abdullah, A. L., Tamaldin, N., Rosli, M., & Sachit, F. (2019). Simulation CFD and experimental investigation of PVT water system under natural Malaysian weather conditions. *Energy Reports*. doi:10.1016/j.egy.2019.11.162

Misha, S., Mat, S., Ruslan, M. H., Sopian, K., & Salleh, E. (2013). The Prediction of Drying Uniformity in Tray Dryer System using CFD Simulation. *International Journal of Machine Learning and Computing*, 3(5), 419–423. doi: 10.7763/ijmlc.2013.v3.352

M. P. Cano and J. Barta, *Handbook of Fruits and Fruit Processing*, 1st ed. Hoboken, NJ: Blackwell Publishing, 2006.

Natalia, S. V., Mauricio, C., Hugo, A. M.-C., & Hugo, F. L. (2018). Drying Uniformity

Analysis in a Tray Dryer: An Experimental and Simulation Approach. *Advance Journal of Food Science and Technology*, 15(SPL), 233–238. doi: 10.19026/ajfst.14.5901

Ndukwu M.C. (2009) “Effect of Drying Temperature and Drying Air Velocity on the Drying Rate and Drying Constant of Cocoa Bean” *Agricultural Engineering International: the CIGR Ejournal*. Manuscript 1091. Vol. XI.

Nicholas Musembi Maundu, Kosgei Sam Kiptoo, Kiprop Eliud, Dickson Kindole, and Yuichi Nakajo, “Air-flow Distribution Study and Performance Analysis of a Natural Convection Solar Dryer.” *American Journal of Energy Research*, vol. 5, no. 1 (2017): 12-22. doi: 10.12691/ajer-5-1-2.

Odewole, M. M., Sunmonu, M. O., Oyeniya, S. K., & Adesoye, O. A. (2017). Computational fluid dynamics (CFD) simulation of hot air flow pattern in cabinet drying of osmo-pretreated green bell pepper. *Nigerian Journal of Technological Research*, 12(1), 36. doi: 10.4314/njtr.v12i1.7

Oluwasanmi, Alonge & Obayopo, S. (2019). Computational fluid dynamics and experimental analysis of direct solar dryer for fish. *Agricultural Engineering International: The CIGR e-journal*. 21. 108-117.

P.D. Tegenaw, M.G. Gebrehiwot, M. Vanierschot, Design and CFD Modeling of a Solar Food Drier, n: EuroDrying, 6th European Drying Conference, 2017: pp. 183–184.

Pirasteh, G., Saidur, R., Rahman, S.M.A. & Rahim, N.A. 2014. A review on development of solar drying applications. *Renewable and Sustainable Energy Reviews* 31: 133-148.

Prakash, Om, and Anil Kumar. “Historical Review and Recent Trends in Solar Drying Systems.” *International Journal of Green Energy*, vol. 10, no. 7, Sept. 2013, pp. 690–738., doi:10.1080/15435075.2012.727113.

Rahman, M. M., Mustayen, A. G. M. B., Mekhilef, S., & Saidur, R. (2015). The Optimization of Solar Drying of Grain by Using a Genetic Algorithm. *International Journal of Green Energy*, 12(12), 1222–1231. doi: 10.1080/15435075.2014.890106

Reddy, R. M., Reddy, E. S., Maheswari, C. U., & Reddy, K. K. (2018). CFD and experimental analysis of solar crop dryer with waste heat recovery system of exhaust gas from diesel engine. *OP Conference Series: Earth and Environmental Science*, 164, 012010. doi: 10.1088/1755-1315/164/1/012010

Sabarez, H. and Food, C. (2016) Drying of Food Materials, Reference Module in Food Science. Elsevier. doi: 10.1016/B978-0-08-100596-5.03416-8.

Samantha, H (2016). *Development of a system model for an indirect passive solar dryer with experimental validation* (master's thesis). Kate Gleason College of Engineering, Rochester Institute of Technology, New York, USA.

Seiedlou, S., H.R. Ghasemzadeh, N. Hamdami, F. Talati and M. Moghaddam, 2010. Convective drying of apple: mathematical modeling and determination of some quality parameters. *International Journal of Agriculture and Biology*, 12: 171–178.

Sharafeldin, M.a., and Gyula Gróf. “Evacuated Tube Solar Collector Performance Using CeO<sub>2</sub>/Water Nanofluid.” *Journal of Cleaner Production*, vol. 185, 2018, pp. 347–356., doi:10.1016/j.jclepro.2018.03.054

Sotocinal, S.A. (1992). *Design and testing of a natural convection solar fish dryer* (Master's thesis). McGill University, Montreal, Canada.

Tarigan, E. (2018). Mathematical modeling and simulation of a solar agricultural dryer with back-up biomass burner and thermal storage. *Case Studies in Thermal Engineering*, 12, 149–165. doi: 10.1016/j.csite.2018.04.012

Tegenaw, P. D., Gebrehiwot, M. G., & Vanierschot, M. (2019). On the comparison between computational fluid dynamics (CFD) and lumped capacitance modeling for the simulation of transient heat transfer in solar dryers. *Solar Energy*, 184, 417–425. doi: 10.1016/j.solener.2019.04.024

T. L. Bergman, A. S. Lavine, F. P. Incropera, and D. P. Dewitt, *Fundamentals of Heat and Mass Transfer*, 7th ed. John Wiley & Sons, 2011.

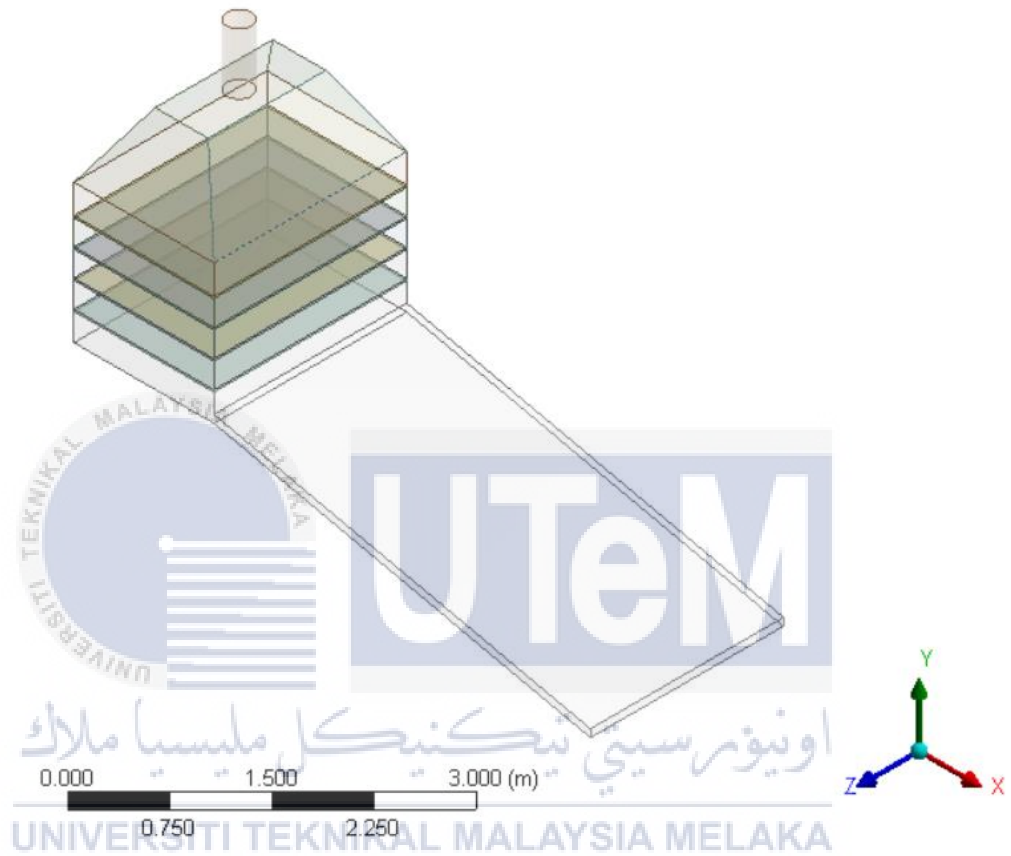
Y. Amanlou, A. Zomorodian, Applying CFD for designing a new fruit cabinet dryer, *J. Food Eng.* 101 (2010) 8–15

Yunus, Y. M., & Al-Kayiem, H. H. (2013). Simulation of Hybrid Solar Dryer. *OP Conference Series: Earth and Environmental Science*, 16, 012143. doi: 10.1088/1755-1315/16/1/012143

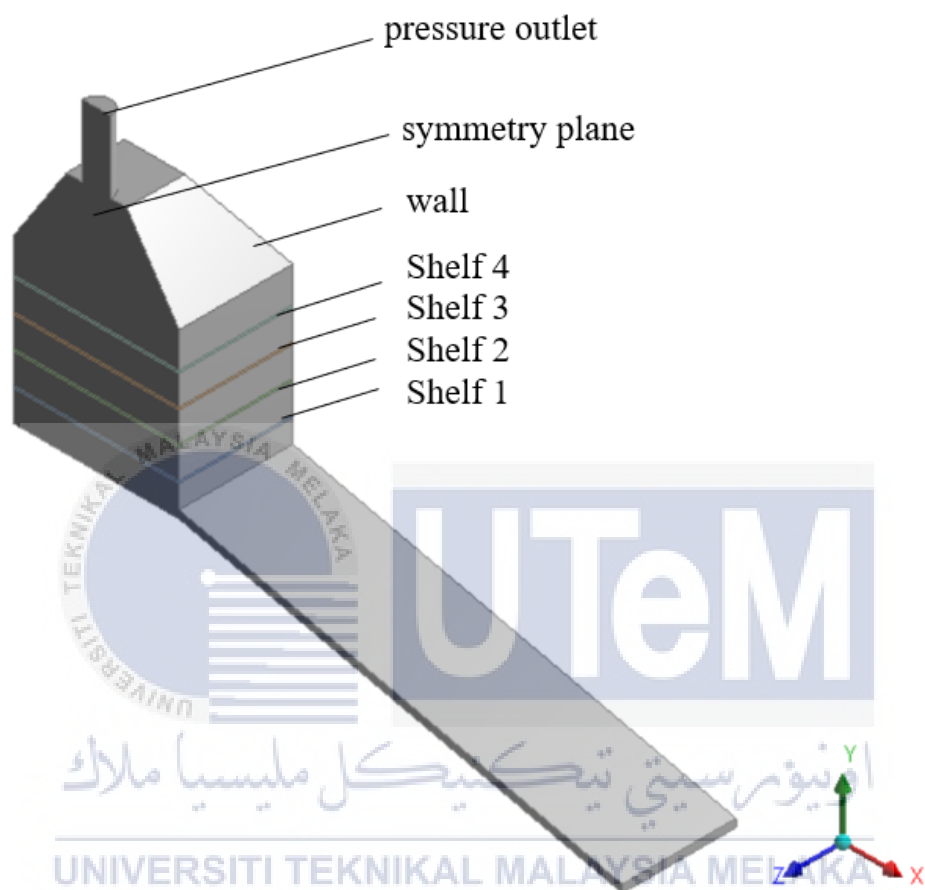
Zoukit, Ahmed, et al. “Mathematical Modeling of an innovative Hybrid Solar-Gas Dryer.”

*Journal of Energy Systems*, 2018, pp. 260–275., doi:10.30521/jes.457647.

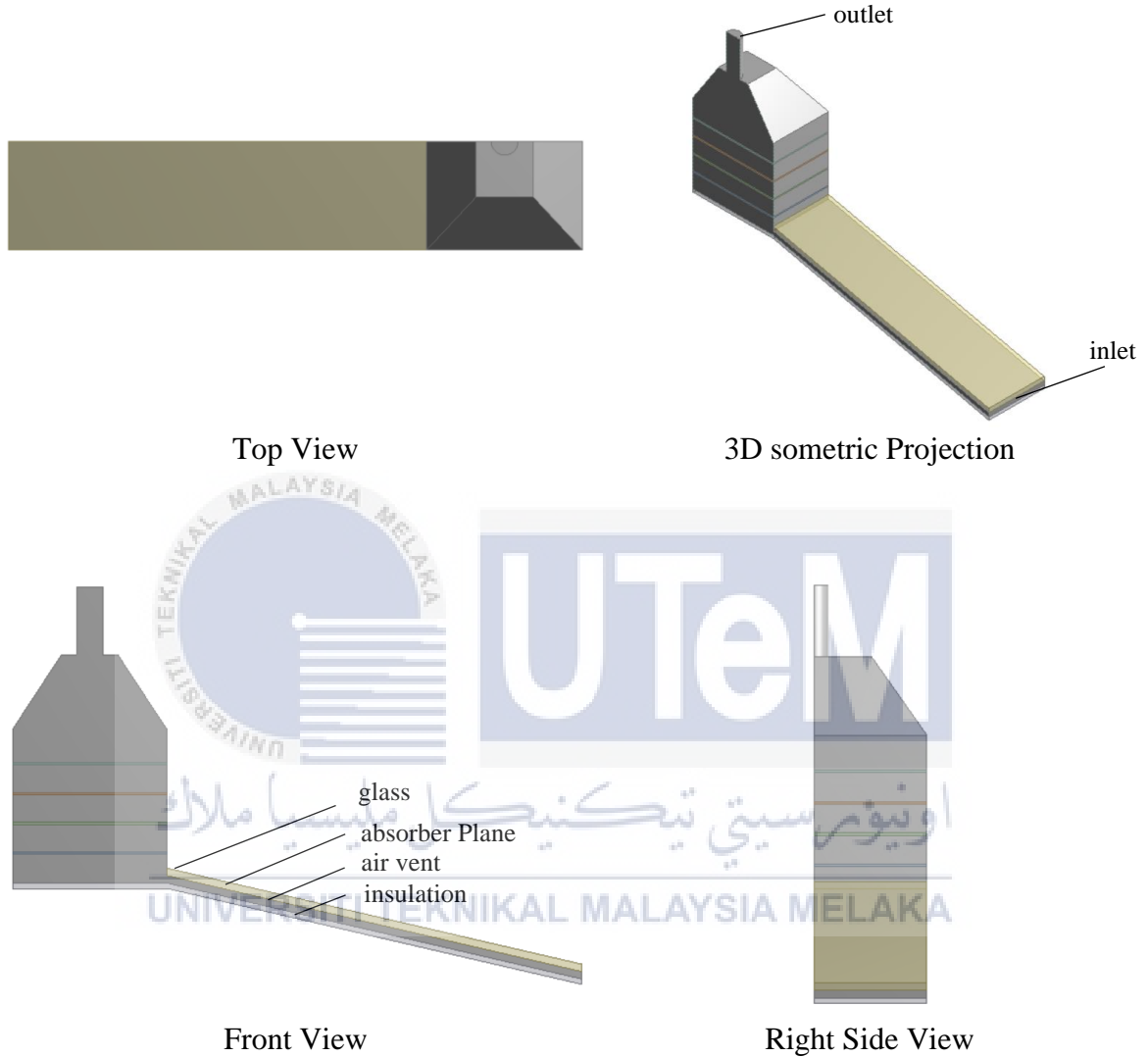
**APPENDIX A: Full 3D Schematic Diagram of Solar Collector Integrated with Solar Collector**



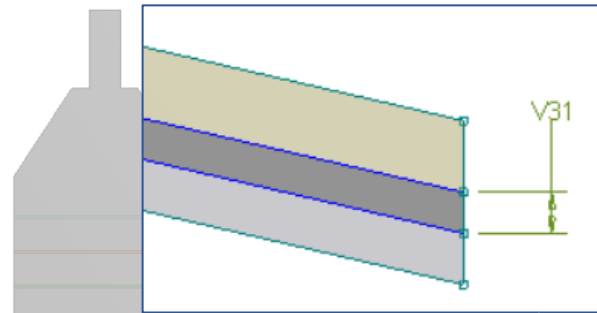
## APPENDIX B: Full 3D Schematic Diagram of Solar Collector Integrated with Solar Collector



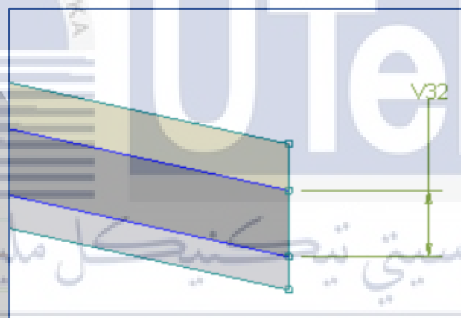
### APPENDIX C: 3D Drawing of Modified Design on Solar Collector



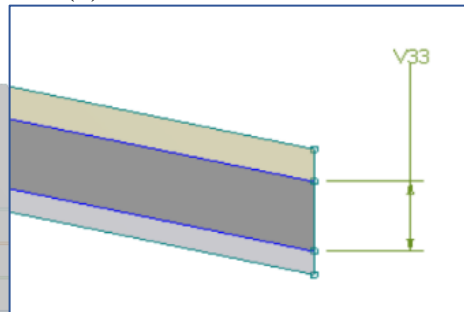
**APPENDIX D: Parameter considered in Drying Chamber Integrated with Solar Collector at different air inlet area (a), (b), (c)**



(a): inlet area =0.08 m<sup>2</sup>

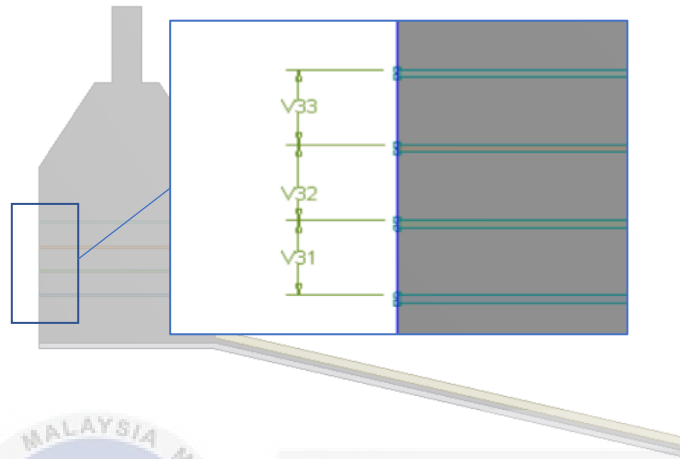


(b): inlet area =0.20 m<sup>2</sup>

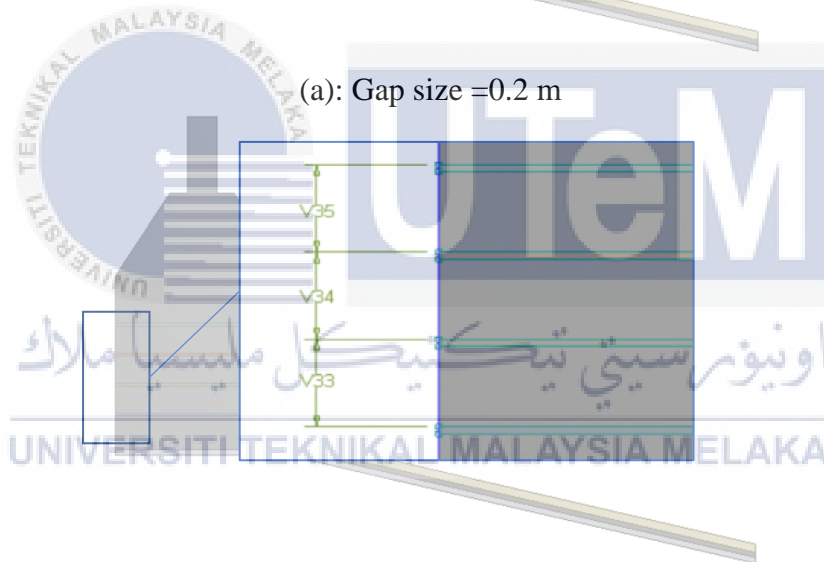


(c): inlet area =0.30 m<sup>2</sup>

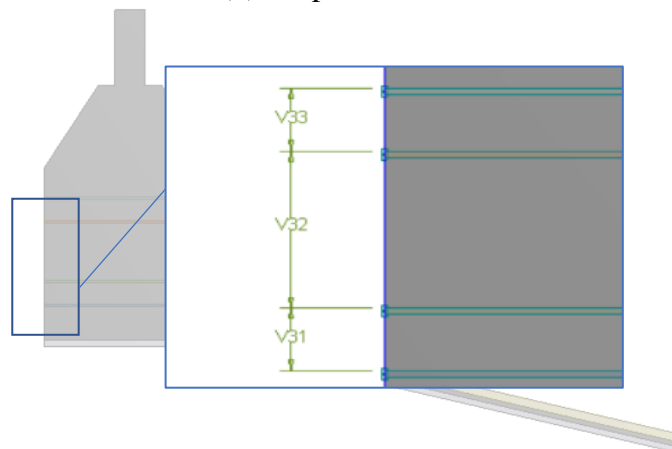
**APPENDIX E: Parameter considered in Drying Chamber Integrated with Solar Collector at different gap size (a), (b), (c)**



(a): Gap size =0.2 m

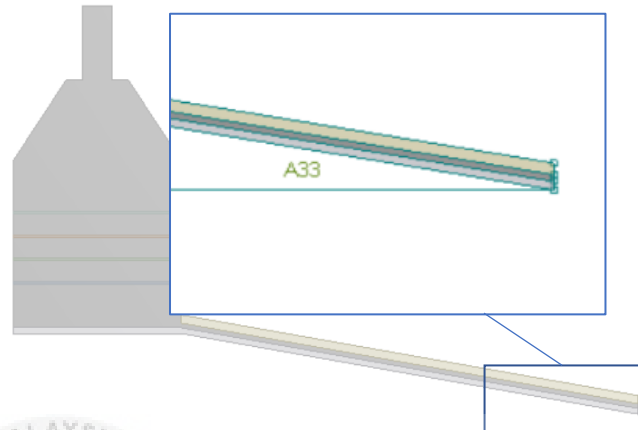


(b): Gap size =0.25 m

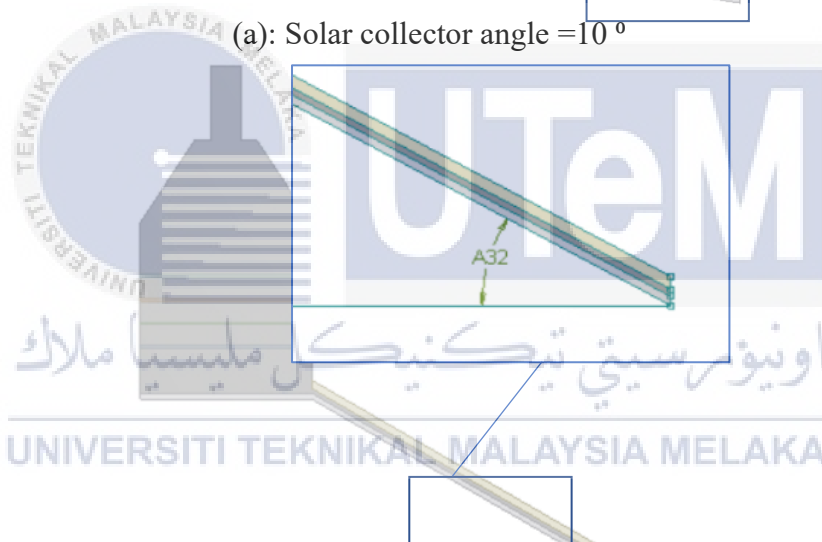


(c): Gap size =0.2m, big gap between tray =0.5m

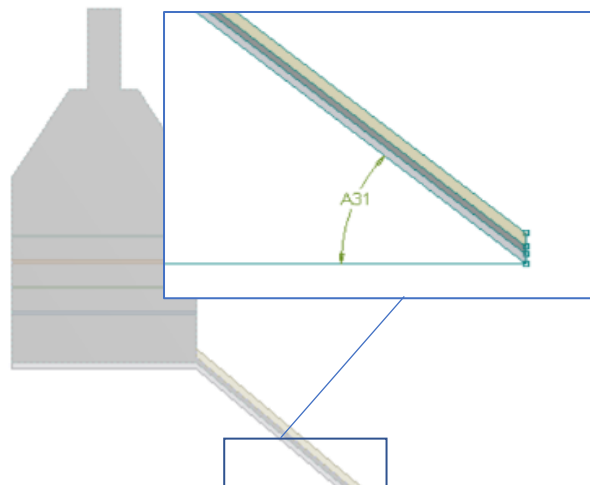
**APPENDIX F: Parameter considered in Drying Chamber Integrated with Solar Collector at Different Solar Collector Angle (a), (b), (c)**



(a): Solar collector angle =  $10^{\circ}$

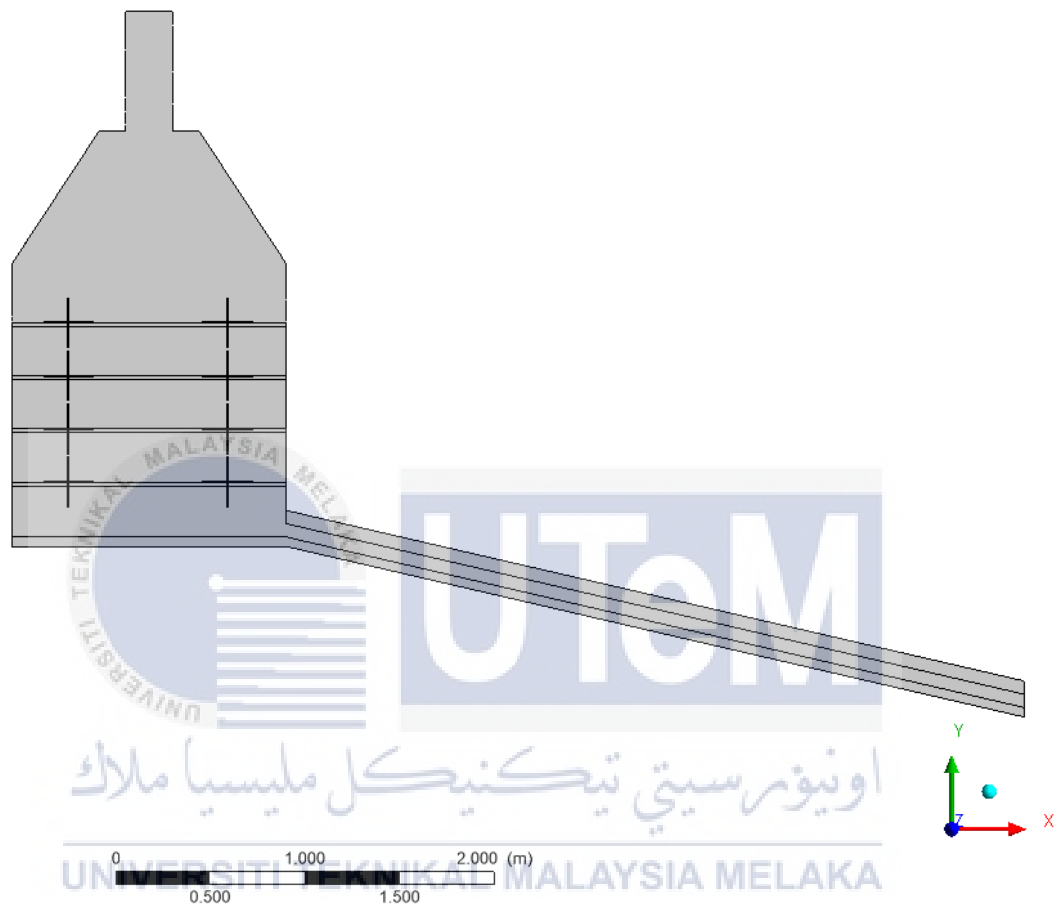


(b): Solar collector angle =  $30^{\circ}$

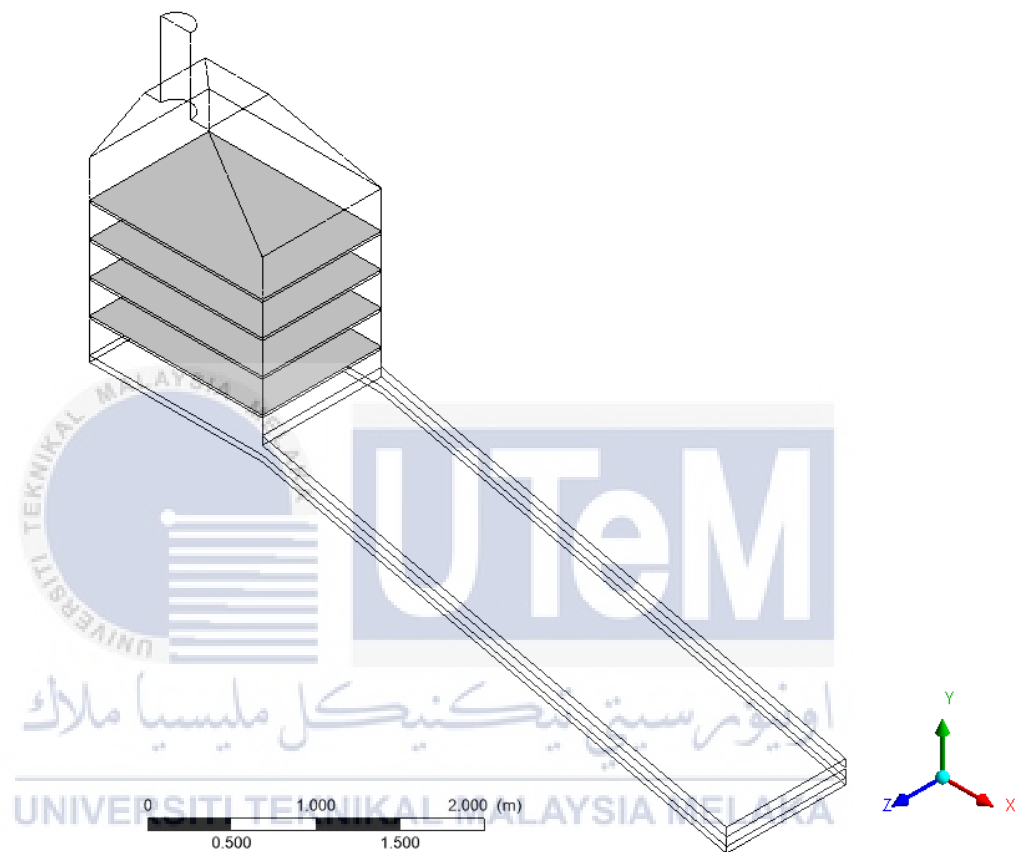


(c): Solar collector angle =  $40^{\circ}$

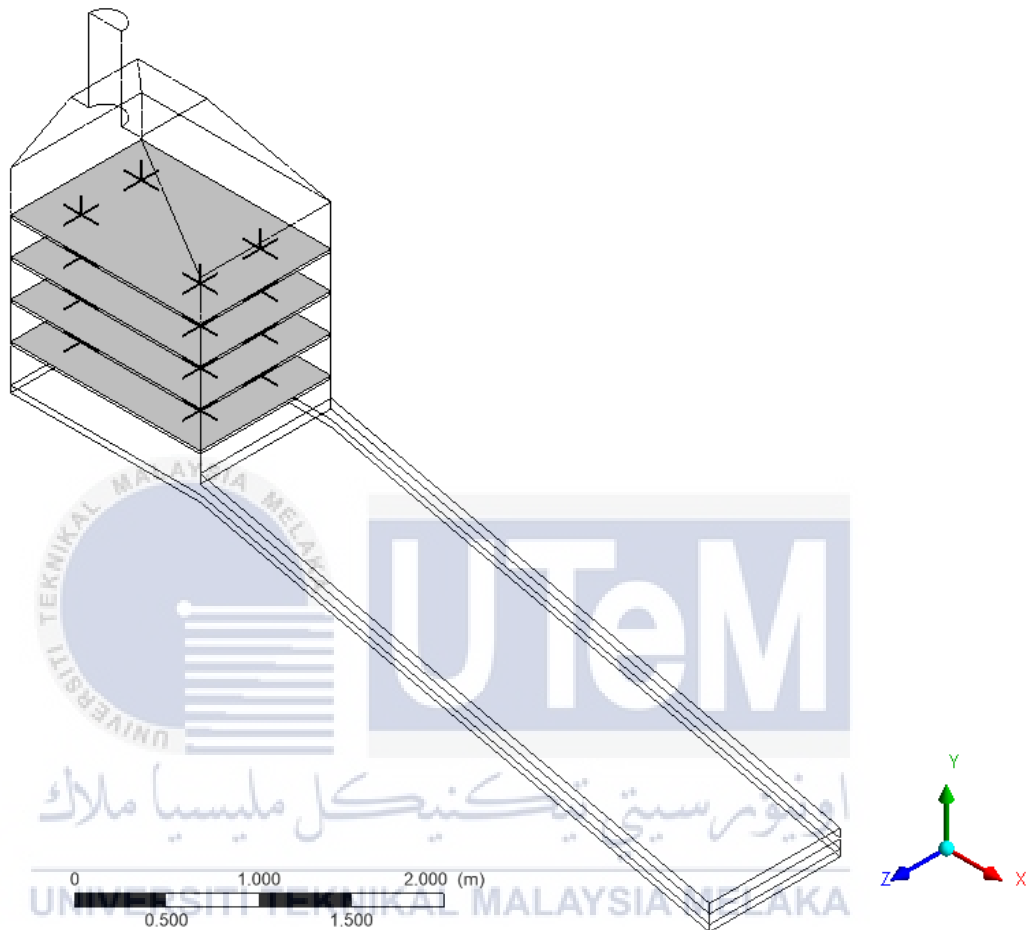
**APPENDIX G: 8 Points on the Symmetry Plane within Drying Chamber Integrated with Solar Collector**



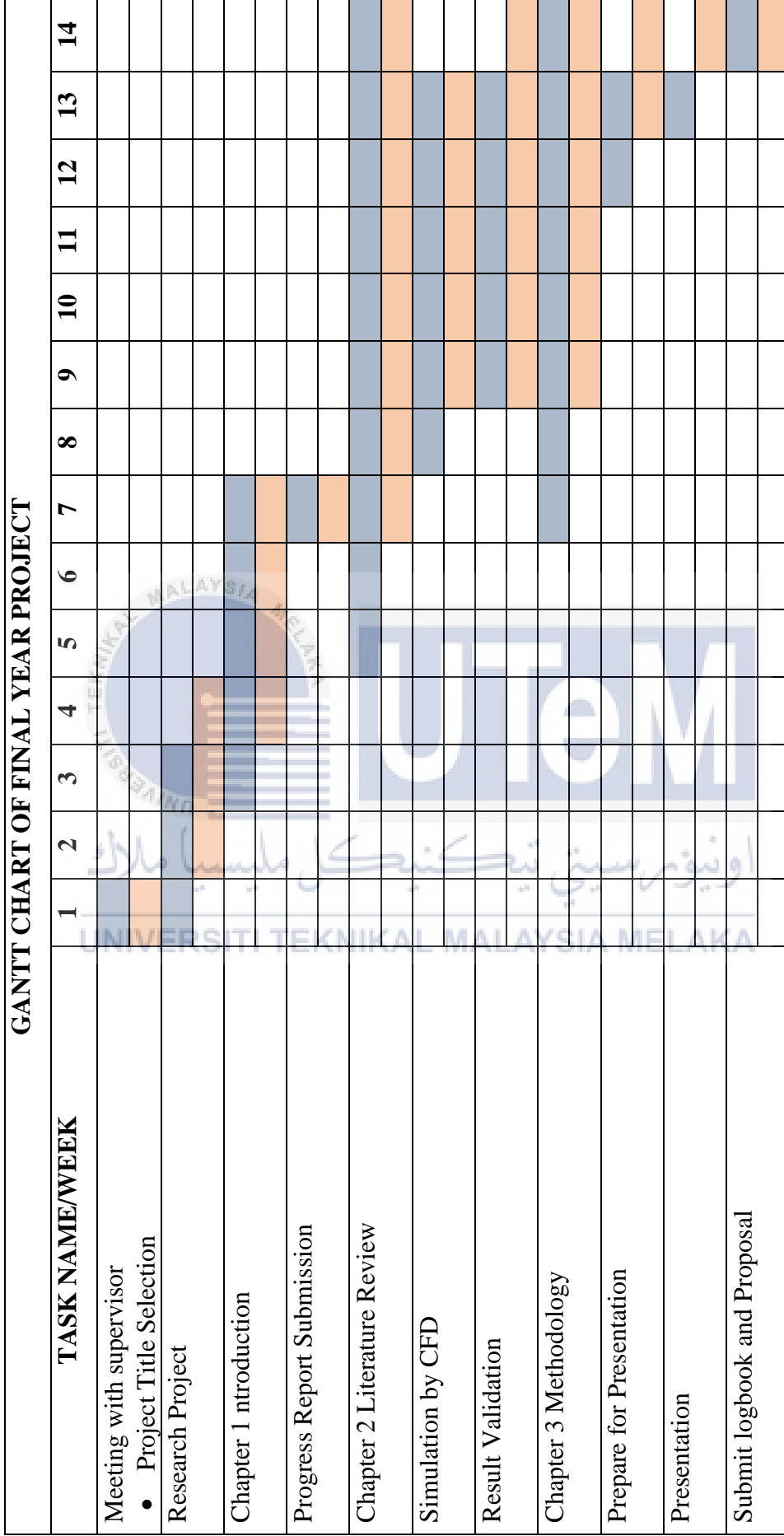
## APPENDIX H: 4 Rack Shelves Studies in Drying Chamber Integrated with Solar Collector



**APPENDIX I: 4 Points on Each Rack Shelves in Drying Chamber Integrated with Solar Collector**



**APPENDIX J: GANTT CHART OF FINAL YEAR PROJECT I**



**APPENDIX K: GANTT CHART OF FINAL YEAR PROJECT II**

